Friedrich-Schiller-Universität Jena
Physikalisch-Astronomische Fakultät

Thüringer Landessternwarte Tautenburg


# The Mass Dependence of Planet Formation: A Radial-Velocity Survey for Extrasolar Planets around F and Ap Stars

**DISSERTATION**

zur Erlangung des akademischen Grades
doctor rerum naturalium (Dr. rer. nat.)

vorgelegt dem Rat der Physikalisch-Astronomischen Fakultät
der Friedrich-Schiller-Universität Jena

von Dipl.-Phys. Michael Hartmann
geb. am 01.10.1980 in Halle (Saale)

| | |
|---|---|
| **Name:** | Michael Hartmann |
| **Geboren:** | 01.10.1980 in Halle (Saale) |
| **1. Gutachter:** | Prof. Dr. Artie P. Hatzes<br>Thüringer Landessternwarte Tautenburg |
| **2. Gutachter:** | Prof. Dr. Ulrich Heber<br>Dr. Karl Remeis-Sternwarte Bamberg |
| **3. Gutachter:** | Prof. Dr. Ansgar Reiners<br>Georg-August-Universität Göttingen |
| Tag der Disputation: | 24.10.2019 |

Für meine Eltern

und in Erinnerung an meine Großeltern

Hildegard & Walter Nitsche

*"I think music is about our internal life.*
*It's part of the way people touch each other.*
*That's very precious to me.*
*And astronomy is, in a sense, the very opposite thing.*
*Instead of looking inwards, you are looking out, to things beyond our grasp."*

(Brian May)

*"Astronomers, like burglars and jazz musicians, operate best at night."*

(Miles Kington)

# Contents

**Abstract** ix

**Zusammenfassung** xi

**1 Introduction** 1

**2 Detection methods** 5
2.1 Radial-velocity technique . . . . . 5
2.2 Transit method . . . . . 6
2.3 Astrometry . . . . . 7
2.4 Pulsar timing . . . . . 8

**3 Data acquisition** 11
3.1 The F-star survey in the northern hemisphere . . . . . 11
3.1.1 The TLS Coudé Échelle Spectrograph . . . . . 11
3.1.2 Target selection . . . . . 12
3.1.3 Observations . . . . . 13
3.1.4 Data reduction . . . . . 14
3.2 The Ap-star survey in the southern hemisphere . . . . . 16
3.2.1 The HARPS spectrograph . . . . . 16
3.2.2 Target selection . . . . . 17
3.2.3 Observations . . . . . 18
3.2.4 Data reduction . . . . . 18

**4 Radial-velocity determination** 19
4.1 Iodine-cell technique . . . . . 19
4.2 Cross-correlation technique . . . . . 22
4.3 HARPS-TERRA – A least-squares template-matching method . . . . 23

**5 Analysis of radial-velocity data** 25
5.1 Tests for variability and trends . . . . . 25
5.2 Periodogram analysis . . . . . 25
5.3 Keplerian orbital solutions . . . . . 28

**6 Results and discussion** **29**
6.1 The F-star survey in the northern hemisphere . . . . . 29
6.1.1 Spectroscopic binaries with orbit . . . . . 29
6.1.2 Spectroscopic binaries without orbit . . . . . 45
6.1.3 Sub-stellar companions . . . . . 51
6.1.4 Concluding remarks . . . . . 60
6.2 The Ap-star survey in the southern hemisphere . . . . . 64
6.2.1 Spectroscopic binaries with orbit . . . . . 64
6.2.2 Spectroscopic binaries without orbit . . . . . 81
6.2.3 Rotational modulation . . . . . 87
6.2.4 Concluding remarks . . . . . 93

**7 Outlook** **97**

**Bibliography** **99**

**Appendix A: Target lists** **107**

**Danksagung** **113**

**Ehrenwörtliche Erklärung** **115**

# Abstract

Most radial-velocity (RV) planet search programs are focused on solar-type stars with spectral types F8–K0 that cover only a small range in stellar mass (0.8–1.2 $M_{\odot}$). As a result, our knowledge on how the stellar mass influences the frequency and properties of giant planets is very limited.

The present study deals with the question if there is a correlation between the planet occurrence rate and the stellar mass. This will give information on processes that are crucial for the formation of giant planets.

The main emphasis of this work was to perform spectroscopic observations to carry out a systematic search for sub-stellar and – as a by-product – stellar companions around stars more massive than the Sun. Therefore, I monitored a sample of 155 F-type main-sequence stars with the 2.0-meter Alfred Jensch Telescope of the Thüringer Landessternwarte Tautenburg (TLS) and its high-resolution Tautenburg Coudé Échelle Spectrograph (TCES). An iodine absorption cell placed in the optical light path provided the wavelength reference for precise stellar RV measurements.

In addition, I investigated 62 chemically peculiar A-type (Ap) stars with the HARPS spectrograph at the 3.6-meter telescope at the European Southern Observatory (La Silla, Chile). The RVs were obtained using two different methods: the cross-correlation function (CCF) with a binary mask, which is implemented in the HARPS Data Reduction Software, and a new software tool called HARPS-TERRA, which is based on a least-squares template-matching approach.

For the F-star survey, I find 24 (16%) spectroscopic binaries. Moreover, this sample contains six stars with planets. Three of them were published by other authors, and three were detected in the framework of this program. The planet frequency of F stars (4%) is less than expected from theoretical studies and contrary to observations based on giant stars.

For the Ap-star survey, I find 17 (27%) spectroscopic binaries. Almost all Ap stars show large RV variations most likely connected to stellar rotation via abundance spots. Thus, it is very difficult to extract any other signal due to planetary companions. Only in one case, the RV data obtained with the CCF method contain a signal, which cannot be assigned to the rotation period or its harmonics. This might be a possible planetary companion.

# Zusammenfassung

Die meisten Programme zur Suche nach extrasolaren Planeten mittels Radialgeschwindigkeitsmessungen (*engl. radial velocity*, kurz RV) konzentrieren sich auf Spektraltypen von F8–K0, die nur einen engen stellaren Massenbereich (0.8–1.2 $M_{\odot}$) umfassen. Demzufolge ist unser Wissen über den Einfluss der stellaren Masse auf Häufigkeit und Eigenschaften von Gasplaneten sehr begrenzt.

Die vorliegende Studie beschäftigt sich mit der Frage, ob es einen Zusammenhang zwischen Planetenhäufigkeit und Sternmasse gibt? Dies wird Aufschluss über Prozesse geben, die entscheidend für die Entstehung von Gasplaneten sind.

Der Schwerpunkt dieser Arbeit liegt auf der Durchführung spektroskopischer Beobachtungen zwecks systematischer Suche nach substellaren und – als Nebenprodukt – stellaren Begleitern um Sterne, die massereicher als die Sonne sind. Daher habe ich eine Stichprobe von 155 Hauptreihensternen des Spektraltyps F mit dem 2.0-m-Alfred-Jensch-Teleskop der Thüringer Landessternwarte Tautenburg (TLS) und dem hochauflösenden Tautenburger Coudé-Échelle-Spektrographen (TCES) beobachtet. Eine Iodabsorptionszelle im Strahlengang diente der Wellenlängenkalibration für die präzisen stellaren RV-Messungen.

Zusätzlich habe ich 62 chemisch auffällige (*engl. peculiar*) A-Sterne (Ap-Sterne) mit dem HARPS-Spektrographen des 3.6-m-Teleskops der Europäischen Südsternwarte (La Silla, Chile) untersucht. Die RVs wurden mit zwei unterschiedlichen Methoden bestimmt: zum einen mittels Kreuzkorrelationsfunktion (*engl. cross-correlation function*, kurz CCF) mit einer binären Maske, die in der HARPS-Datenreduktionssoftware implementiert ist, und zum anderen mit dem neuentwickelten Programm HARPS-TERRA, welches auf dem Ansatz basiert, die beobachteten Spektren an eine Vorlage anzupassen.

In der Stichprobe der F-Sterne finde ich 24 (16%) spektroskopische Doppelsterne. Weiterhin sind darin sechs Sterne mit einem Planeten enthalten. Drei von diesen wurden bereits durch andere Autoren veröffentlicht, die drei anderen wurden im Rahmen dieser Arbeit entdeckt. Die Planetenhäufigkeit bei F-Sternen (4%) ist geringer als von theoretischen Studien erwartet und steht im Widerspruch zu auf Riesensternen basierenden Beobachtungen.

In der Stichprobe der Ap-Sterne finde ich 17 (27%) spektroskopische Doppelsterne. Fast alle Ap-Sterne zeigen grosse RV-Variationen, die höchstwahrscheinlich im ursächlichen Zusammenhang mit stellarer Rotation durch Elementanreicherung stehen. Dadurch ist es sehr schwierig, irgendein anderes Signal zu extrahieren, welches von planetaren Begleitern verursacht wird. Nur in einem Fall enthalten die mit der CCF-Methode bestimmen RV-Daten ein Signal, das nicht der Rotationsperiode oder ihren Harmonischen zugeordnet werden kann. Dies könnte ein möglicher planetarer Begleiter sein.

# 1 Introduction

To date, about 4000[1] extrasolar planets (exoplanets) or planet candidates have been discovered in orbit around other stars. While many of them were found by means of the transit method with ground-based facilities (WASP, HAT, etc.) as well as space-based satellite missions (*CoRoT* and *Kepler*), the first exoplanets were identified by a second very successful technique: the radial-velocity (RV) or Doppler method, which has led to the detection of about 800[1] exoplanets in circa 600[1] planetary systems. Also, this method is obligatory to confirm transit planet candidates.

Most RV planet search surveys are focussing on solar-type stars spanning only a small range in stellar mass (0.8–1.2 $M_{\odot}$) covered by the spectral types F8–K0 because these stars have plenty of narrow absorption lines, allowing precise RV measurements, and show only little activity. Nonetheless, some programs have extended their planet searches also to less massive M dwarfs (e.g., Bonfils et al. 2005; Butler et al. 2006; Endl et al. 2006; Reiners et al. 2018; Sarkis et al. 2018).

In addition, there are quite a few RV surveys monitoring more massive, evolved giants: the Lick Observatory survey of G and K giants using the Hamilton spectrograph (Frink et al. 2001, 2002; Reffert et al. 2006; Mitchell et al. 2013; Trifonov et al. 2014), the FEROS survey at the European Southern Observatory (ESO) at La Silla (Setiawan et al. 2003, 2005), the survey at Okayama Observatory with the HIDES spectrograph (Sato et al. 2003, 2007, 2008a,b, 2010, 2012), the Tautenburg Observatory Planet Search (TOPS) at the Thüringer Landessternwarte (TLS; Hatzes et al. 2005, 2006; Döllinger et al. 2007, 2009a,b), the Penn State Torun planet search with the Hobby–Eberly Telescope at McDonald Observatory (Niedzielski et al. 2007, 2009a,b; Gettel et al. 2012a,b), the planet search at Bohyunsan Observatory using the BOES spectrograph (Han et al. 2010; Lee et al. 2012a,b, 2013) as well as the EXoPlanets aRound Evolved StarS (EXPRESS) survey employing FEROS at the La Silla Observatory and FECH/CHIRON at the Cerro Tololo Inter-American Observatory (Jones et al. 2011, 2013, 2014, 2015a,b). Johnson et al. (2010a) also observed a sample of subgiants at Lick Observatory.

On the other hand, more massive main-sequence (MS) stars of spectral types A–F have been almost ignored in RV surveys so far. These earlier spectral types are hotter and rotate faster, hence their spectra have fewer and broader absorption lines. As a consequence, RV measurements are less precise, making the detection of planetary companions more difficult. Beside the current doctoral work, which revealed already two published planet discoveries (see Guenther et al. 2009; Hartmann et al. 2010), there is only one other RV survey dedicated to A–F-type MS stars using the ELODIE fiber-fed échelle spectrograph on the 1.93 m telescope at the Observatoire de Haute-Provence (France) and the HARPS spectrograph on the ESO 3.6 m telescope at La Silla (Chile). Several papers on this survey appeared within the series *"Extrasolar planets and brown dwarfs around AF-type stars"* (e.g., Galland et al. 2005a,b, 2006; Borgniet et al. 2014, 2017).

[1] According to the Extrasolar Planets Encyclopaedia (http://exoplanet.eu; Schneider et al. 2011) as of March 2019.

As a result, our knowledge on how planet formation, especially the frequency and properties of planets, depends on the stellar mass – the stellar key parameter that determines the entire physics of a star – is still very limited.

The most widely accepted model for giant planet formation is the core accretion scenario. Here, a solid core is formed first by collisional accumulation of planetesimals. Later, when the core reaches a critical mass of $\gtrsim 10\ M_\oplus$, it starts to capture gas to slowly grow a hydrostatic low-mass atmosphere, finally leading to a phase of runaway gas accretion to form an extended gaseous envelope around it. In support of this model, it has been observationally established that solar-like MS planet-hosting stars are more metal-rich than stars without planets (so-called planet–metallicity correlation; e.g., Santos et al. 2004; Fischer & Valenti 2005).

On the basis of this giant planet formation model, several theoretical studies have been made to predict the planet frequency. The most commonly used models are those from Kennedy & Kenyon (2008). Calculations by these authors suggest that gas giant formation around more massive stars is more likely than around less massive stars. They provide a linearly rising probability $P_{\rm GG}$ for stars with masses between 0.4 and 3 $M_\odot$ that a given star hosts at least one gas giant planet. To match the results with observations, they applied a normalization to 6% for solar-mass stars to the models. Therefore, the predicted planet occurrence rate of their baseline model is 1% for 0.4 $M_\odot$ stars and 10% for 1.5 $M_\odot$ stars (see Figure 1.1).

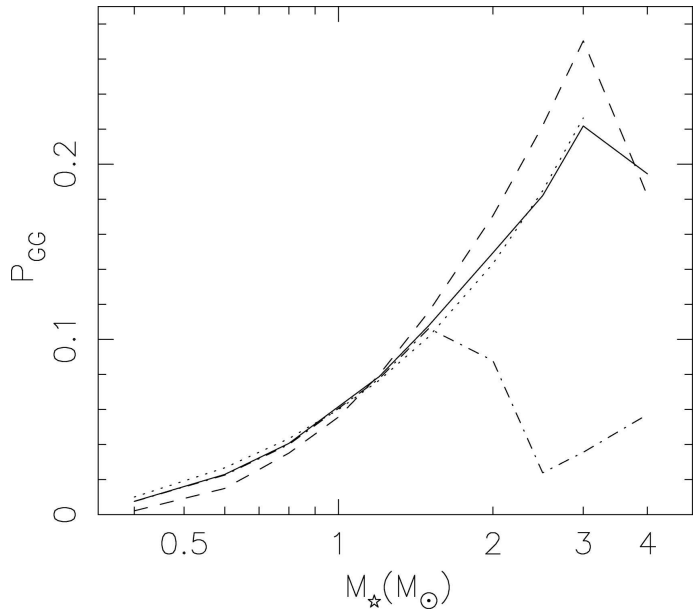


**Figure 1.1:** Probability $P_{\rm GG}$ of a star harboring at least one gas giant planet as a function of stellar mass for the baseline model (solid line), a model with $\delta = 1$ and $M_{\rm core} = 5\,M_\oplus$ (dashed line) and a fitted line of constant slope $P_{\rm GG} = 0.20\,M_\star - 0.06$ (dotted line). For comparison, the dot-dashed line illustrates a model with $a_{\rm snow} \propto 2.7\,M_\star^2$, similar to the main model of Ida & Lin (2005). All curves are normalized to 6% at $1\,M_\odot$ via a straight line fit. (Figure from Kennedy & Kenyon 2008)

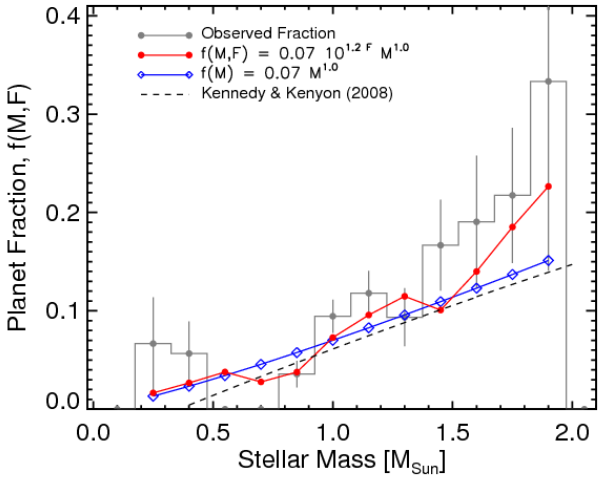


**Figure 1.2:** Planet fraction ($f = N_{\rm planets}/N_{\rm stars}$) as a function of mass for the observed stellar sample (grey histogram). The red filled circles describe the calculated planet fraction according to the given formula for the masses ($M$) and metallicities ($F \equiv$ [Fe/H]) of the stars in each histogram bin. The blue open diamonds describe the calculated planet fraction for [Fe/H] = 0. The dashed line shows the theoretical predictions by Kennedy & Kenyon (2008) for solar metallicity. (Figure from Johnson et al. 2010b)

Contrary to that result, an analysis by Kornet et al. (2006), who investigated the influence of the stellar mass on the evolution of the protoplanetary disk, in particular on the redistribution of solids in the disk, shows that the percentage of stars with massive planets decreases with increasing stellar mass at least from 0.5 to 4 $M_{\odot}$.

From the observational point of view, the planet frequency of intermediate-mass evolved stars varies between $\sim$9% (Johnson et al. 2007) and $\sim$26% (Bowler et al. 2010). A further analysis by Johnson et al. (2010b) provided an empirical relationship between the planet occurrence rate and the stellar mass and metallicity (Figure 1.2). They found a significant increase of the planet frequency with the stellar mass. This increase is partly due to a rise in the average stellar metallicity for the higher-mass stars (red filled circles); but when considering only the dependence on the stellar mass ([Fe/H] = 0), the planet fraction rises almost linearly (blue open diamonds) and resembles the theoretical predictions of Kennedy & Kenyon (2008) pretty well. While the sample of Johnson et al. (2010b) contained stars with masses up to 1.9 $M_{\odot}$, the Lick survey of 373 giant stars covered masses up to 5 $M_{\odot}$ (Reffert et al. 2015), extending the mass regime to even higher stellar masses. In their study, Reffert et al. (2015) confirmed the increase of the planet occurrence rate within the mass range from 1.0 to 1.9 $M_{\odot}$, found a maximum at 1.9 $M_{\odot}$ and noticed a sharp drop for masses larger than 2.5 to 3.0 $M_{\odot}$ (Figure 1.3). However, comparing the planet occurrence rates of their secure planets (i.e., without their planet candidates) in the mass regime of 1.0 to 1.9 $M_{\odot}$ with Johnson et al. (2010b), their values are markedly lower.

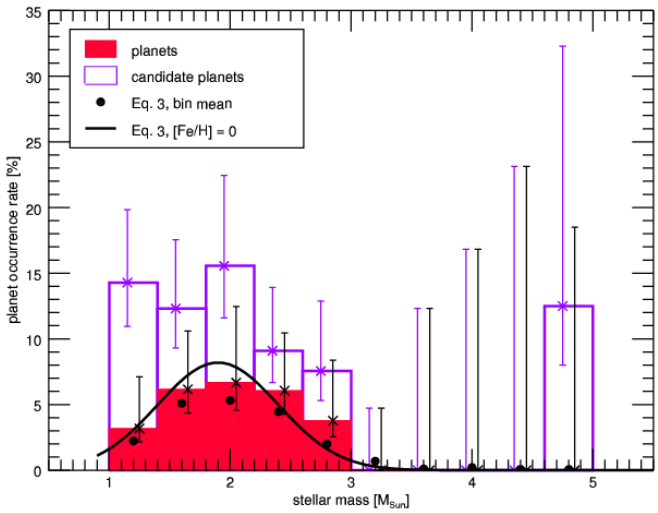


**Figure 1.3:** Planet occurrence rate as a function of stellar mass of 373 G and K giants of the Lick survey. The solid line represents the best-fit Gaussian distribution for [Fe/H] = 0. The black dots correspond to the same model, but the mean metallicity of each mass bin is taken into account. (Figure from Reffert et al. 2015)

One part of the present work represents one of the first comprehensive high-precision RV surveys of F-type MS stars, while the other part is indeed the first such survey of chemically peculiar A-type (Ap) stars to search for extrasolar planets and brown dwarfs. The main goal is to investigate the frequency of planets around MS stars more massive than the Sun and whether there is a correlation between the planet occurrence rate and the stellar mass, as predicted by the theories of Kennedy & Kenyon (2008) and the observations of evolved giants and subgiants by Bowler et al. (2010), Johnson et al. (2010b) and Reffert et al. (2015).

# 2 Detection methods

Several observational techniques have been utilized for the detection of extrasolar planets, each of them with specific strengths and weaknesses and sensitive to different regions in the parameter space of planetary properties. In this section, I will introduce some of the most important methods in detail. Apart from techniques like microlensing and direct imaging, which have resulted in some detections in recent years, but suffer from the low number of discoveries and the lack of essential orbital parameters (period, eccentricity), I will concentrate on detection methods that provide these parameters in almost all cases, namely the radial-velocity method and the transit method, the two most successful methods, but also astrometry and pulsar timing.

## 2.1 Radial-velocity technique

This method is very successful in finding extrasolar planets. During the last two decades, radial-velocity measurements have led to the discovery of several hundreds of planets. The principle of this technique, which only allows astronomers to make indirect detections, is quite simple: If a star is orbited by a companion, both celestial bodies are moving around their common center of mass. Consequently, also the star is moving sometimes towards to or away from the observer on Earth. This velocity component along the line of sight is called the radial velocity (RV or $v_\mathrm{r}$) and can be measured spectroscopically. Because of the Doppler effect, the stellar spectrum including its spectral lines is blue- or red-shifted. The wavelength shift $\Delta\lambda$ of the emitted light of wavelength $\lambda$ is directly correlated to the RV of the star:

$$\frac{\Delta\lambda}{\lambda} = \frac{v_\mathrm{r}}{c}, \tag{2.1}$$

as long as $v_\mathrm{r} \ll c$, where $c$ is the speed of light.

A companion on a Keplerian orbit around a star thus produces a variation of the stellar RV, which follows the equation:

$$v_\mathrm{r}(t) = \gamma + K[e\cos\omega + \cos(\nu + \omega)]. \tag{2.2}$$

The RV curve is described by six orbital parameters: the eccentricity $e$, the longitude of periastron $\omega$, the amplitude (sometimes referred to as semi-amplitude) $K$ as well as the period $P$ and the time of periastron passage $T_0$, which are both covered by the true anomaly $\nu$, and finally, the RV offset $\gamma$ (RV of the center of mass of the system; I will assign $RV_0$ for this offset when analyzing relative RVs). By taking RV measurements over a long timespan, it is possible to determine the orbital parameters of a companion by fitting an RV curve to the data. The RV, however, is just a one-dimensional component of a three-dimensional motion in space. From RV measurements alone, there is no information available about the exact orientation of the Kepler ellipse, i.e., the other two orbital parameters (longitude of the ascending

node $\Omega$ and inclination $i$, the angle between projected and true orbital plane) cannot be derived.

The companion mass is obtained from these parameters using the so-called mass function:

$$f(m_1, m_2, i) = \frac{(m_2 \sin i)^3}{(m_1 + m_2)^2} = \frac{P}{2\pi G} \left( K\sqrt{1-e^2} \right)^3 , \tag{2.3}$$

where $m_1$ and $m_2$ are the masses of the star and the companion, respectively, and $G$ being the gravitational constant. The right-hand side of this equation can be calculated using the derived orbital parameters, but the cubic equation for $m_2$ on the left-hand side cannot be solved without a known inclination $i$. Reformulating Equation (2.3) and assuming $i = 90°$, i.e., an orbital plane viewed edge-on, results in a minimum companion mass:

$$m_{2_{\min}} \simeq m_2 \sin i = K\sqrt{1-e^2} \cdot \sqrt[3]{(m_1 + m_2)^2 \frac{P}{2\pi G}} . \tag{2.4}$$

Taking also into account that $m_2 \ll m_1$ (i.e., $m_1 + m_2 \approx m_1$) for small planets leads to:

$$m_{2_{\min}} = m_2 \sin i \approx K\sqrt{1-e^2} \cdot \sqrt[3]{m_1^2 \frac{P}{2\pi G}} . \tag{2.5}$$

In consequence, the true companion mass $m_2$ is by a factor of $\sim \frac{1}{\sin i}$ higher than the minimum mass $m_{2_{\min}}$. Note that the relation $m_{2_{\min}} = m_2 \sin i$ is strictly valid only when the approximation $m_2 \ll m_1$ can be applied. For stellar as well as for brown-dwarf and giant-planet companions, however, this approximation is not valid anymore. In such cases, it is recommended to use Equation (2.4) and solve for $m_{2_{\min}}$ iteratively starting with $m_{2_{\min}}$ derived from Equation (2.5).

For randomly orientated orbits, the probability $p$ that $i$ is smaller than a certain threshold $i_0$ is given by:

$$p(i \leq i_0) = 1 - \cos i_0. \tag{2.6}$$

This technique is well-suited for the search of short-period, high-mass planets. A disadvantage of this method is that the inclination $i$, the angle between projected and true orbital plane, is unknown; therefore, only a minimum mass of the companion can be determined.

## 2.2 Transit method

The basic idea of this method is to photometrically measure changes in the brightness of a star caused by an orbiting planetary companion crossing the stellar disk of its host star. However, a transit only occurs if the orbital plane is oriented in such a way that the following geometric condition is fulfilled:

$$a \cos i \leq R_\star + R_\mathrm{p}. \tag{2.7}$$

Here, $a$ is the semi-major axis of the planetary orbit, $R_\mathrm{p}$ and $R_\star$ are the radii of the star and the planet, respectively. For randomly oriented orbits, the probability $p_\mathrm{trans}$ for a transit (considering also the assumption $R_\mathrm{p} \ll R_\star$) then follows:

$$p_\mathrm{trans} = \frac{R_\star + R_\mathrm{p}}{a} \approx \frac{R_\star}{a}. \tag{2.8}$$

During the eclipse, the planet blocks a part of the stellar light, resulting in a dip in the light curve. Assuming an uniformly illuminated stellar disk and treating the planet as a black disk, the relative change of the measured flux $F$ is equal to the ratio of the blocking area compared to the area of the stellar disk:

$$\frac{\Delta F}{F} = \frac{A_\mathrm{p}}{A_\star} = \left(\frac{R_\mathrm{p}}{R_\star}\right)^2, \tag{2.9}$$

with $A_\mathrm{p}$ and $A_\star$ denoting the planetary and stellar areas, respectively. For example, a Jupiter-sized planet moving in front of a solar-like star would cause a relative brightness dip of $\approx 1\%$, while an Earth-sized object would show a dip of only $8.4 \times 10^{-5}$. From Equation (2.9) follows that the planetary radius can be determined if the stellar radius is known.

Furthermore, the transit duration $t_\mathrm{transit}$ can be obtained from the light curve. For circular orbits, it is given by:

$$t_\mathrm{transit} = \frac{P}{\pi} \arcsin\left(\frac{\sqrt{(R_\star + R_\mathrm{p})^2 - a^2 \cos^2 i}}{a}\right). \tag{2.10}$$

If $a \gg R_\star \gg R_\mathrm{p}$, Equation (2.10) simplifies itself to:

$$t_\mathrm{transit} \approx \frac{P}{\pi} \sqrt{\left(\frac{R_\star}{a}\right)^2 - \cos^2 i}. \tag{2.11}$$

In our Solar System, observed from outside, a transit of the Earth would last about 13 hours, while a Jupiter transit would take even 30 hours.

A light curve with a transit-like dip needs further investigations to confirm the planetary origin because there are other possible events that can lead to false positives, such as grazing eclipsing binaries, background binaries, eclipsing brown dwarfs or stellar activity (e.g., flares or starspots). Thus, RV measurements are essential as well as the accurate determination of the stellar parameters. The combination of both the transit and the RV method allows us to obtain the true companion mass and – together with the stellar radius – the density of the companion.

## 2.3 Astrometry

This technique also makes use of the motion of the star around the common center of mass in a star–planet system. In contrast to the RV method, not the motion along

the line of sight is measured, but the motion projected on the sky. The semi-major axis of the depicted ellipse is visible under the angle:

$$\alpha \approx \tan\alpha = \frac{M_\mathrm{p}}{M_\star} \cdot \frac{a}{d}. \tag{2.12}$$

If the semi-major axis $a$ and the distance to the star $d$ are expressed in astronomical units (AU) and parsecs (pc), respectively, the angular semi-major axis $\alpha$ is obtained in arcseconds ($''$). With $a$ known from RV measurements, $d$ derived from the parallax and the stellar mass $M_\star$ determined from spectral analysis, the true companion mass $M_\mathrm{p}$ can directly be calculated. This is a substantial advantage in comparison with the RV method alone, allowing the inclination $i$ of the orbital plane to be measured.

The Sun observed from a distance of 10 pc would show an astrometric signal of about 500 $\mu$as caused by Jupiter; in contrast, the Earth would generate an amplitude of only 0.3 $\mu$as. It impressively demonstrates the astrometric precision needed to detect Jupiter- or even Earth-like planets in orbit around other stars.

Being more sensitive to long-period companions, this method is primarily suitable for detecting massive companions at large orbital distances around stars in the solar neighborhood. In consequence, such surveys require very long timeframes.

## 2.4 Pulsar timing

In this case, the indirect detection of extrasolar planets happens in principle similar to the RV method. Instead of measuring Doppler shifts of lines in a spectrum, one measures the time-of-arrival variations of the radio pulses, which are generated by the reflex motion of a pulsar due to the presence of a planetary companion. For a circular orbit and a pulsar mass of 1.35 $M_\odot$, the amplitude of the timing residuals $\tau$ due to a planetary companion is:

$$\tau = 1.2\,\mathrm{ms} \left(\frac{m_\mathrm{p}}{M_\oplus}\right) \left(\frac{P}{\mathrm{yr}}\right)^{\frac{2}{3}} \sin i. \tag{2.13}$$

The first extrasolar system with planetary-mass bodies was found by this method orbiting the 6.2-millisecond pulsar PSR B1257+12 (Wolszczan & Frail 1992). Initially, the existence of two planets with orbital periods of 66.6 and 98.2 days (close to a 3:2 orbital resonance) was verified. Further observations revealed the presence of a third, Moon-mass object in a 25.34-day orbit (Wolszczan 1994) and possibly a fourth, Saturn-mass companion ($\sim$95 $M_\oplus$) with $P \sim 170$ years at an orbital separation of $\sim$35 AU (Wolszczan 1997). Later, Wolszczan et al. (2000) could provide somewhat stricter constraints on the orbit of the outer planet, allowing circular orbits ranging from 6 AU for a 0.05 $M_\oplus$ object to 29 AU for a 81 $M_\oplus$ planet (assuming $i = 90°$). The 3:2 orbital resonance between planets B and C leads to accurately predictable periodic perturbations of the two orbits. Because these mutual gravitational interactions between the two planets depend on their masses, it is possible to

deduce the true masses and orbital inclinations of planets B and C from modeling the timing data. The most recent orbital parameters of this system are listed in Table 2.1 (Konacki & Wolszczan 2003).

**Table 2.1:** Parameters of the PSR B1257+12 planetary system (Konacki & Wolszczan 2003).

| Parameter | Planet A | Planet B | Planet C |
|---|---|---|---|
| Orbital period $P$ (days) | $25.262 \pm 0.003$ | $66.5419 \pm 0.0001$ | $98.2114 \pm 0.0002$ |
| Semi-major axis $a$ (AU) | 0.19 | 0.36 | 0.46 |
| Eccentricity $e$ | 0.0 | $0.0186 \pm 0.0002$ | $0.0252 \pm 0.0002$ |
| Planet mass $m_{\rm p}$ ($M_\oplus$) | $0.020 \pm 0.002$ | $4.3 \pm 0.2$ | $3.9 \pm 0.2$ |
| Longitude of periastron $\omega$ (°) | 0.0 | $250.4 \pm 0.6$ | $108.3 \pm 0.5$ |
| Epoch of periastron $T_0$ (MJD) | $49765.1 \pm 0.2$ | $49768.1 \pm 0.1$ | $49766.5 \pm 0.1$ |
| Inclination $i$ (solution 1) (°) | ... | $53 \pm 4$ | $47 \pm 3$ |
| Inclination $i$ (solution 2) (°) | ... | $127 \pm 4$ | $133 \pm 3$ |

A further example for a pulsar planet is the companion to the binary system PSR B1620−26. The binary consists of a millisecond pulsar and a white dwarf in a 191-day orbit (Thorsett et al. 1999) and is orbited by a low-mass body, which was initially identified by Arzoumanian et al. (1996) as 10–30 $M_{\rm Jup}$ object at a separation of $a \sim 35$–60 AU and $P \sim 100$ years. Later, additional measurements led to a mass of $2.5 \pm 1.0$ $M_{\rm Jup}$ and a semi-major axis of 23 AU (Sigurdsson et al. 2003).

10

# 3 Data acquisition

## 3.1 The F-star survey in the northern hemisphere

### 3.1.1 The TLS Coudé Échelle Spectrograph

The 2.0-meter Alfred Jensch Telescope (AJT) of the Thüringer Landessternwarte Tautenburg (TLS) is a multi-purpose telescope (Figure 3.1). Beside the Fraunhofer Telescope of the Wendelstein Observatory (commissioning in 2012), it is the biggest optical telescope in Germany. The AJT can be used in three different configurations: the Schmidt mode for imaging and photometry, the nasmyth mode for low-resolution spectroscopy of faint objects and the coudé mode for high-resolution spectroscopy of bright stars. It is worth mentioning that with its 1.34-meter aperture, the AJT is the largest Schmidt camera in the world.

**Figure 3.1:** The 2.0-meter Alfred Jensch Telescope of the Thüringer Landessternwarte Tautenburg (Photo: Christian Högner).

In the framework of this thesis, I used the telescope in coudé mode. The spherical primary mirror, 2 m in diameter, has a focal length of 4 m. An over-deformed secondary mirror is installed in this configuration to lengthen the focal length to an effective value of 92 m. The high-resolution Tautenburg Coudé Échelle Spectrograph (TCES), situated in a temperature-stabilized room (coudé room) in the cellar of the dome building, is optically coupled to the telescope by means of five flat mirrors. All mirrors are made of a glass-ceramic material ("SITALL"), which practically shows no deformation with temperature changes. Four of the deflection mirrors have been silvered to maximize the throughput. In contrast, the primary, secondary and first deflection mirror are aluminized since they are directly exposed to the outside air during observations, which would destroy the silver coating rapidly.

The optical light path of the spectrograph is visualized in Figure 3.2. The incoming light enters the spectrograph through the entrance slit. Note that an iodine cell can be moved into the optical path in front of the slit to measure RVs very precisely. Inside the spectrograph, an $f/46$ collimator of 6900 mm focal length is used to produce a parallel light beam of 150 mm in diameter, which is directed to the dispersing element, an échelle grating with 31.6 grooves per mm and a blaze

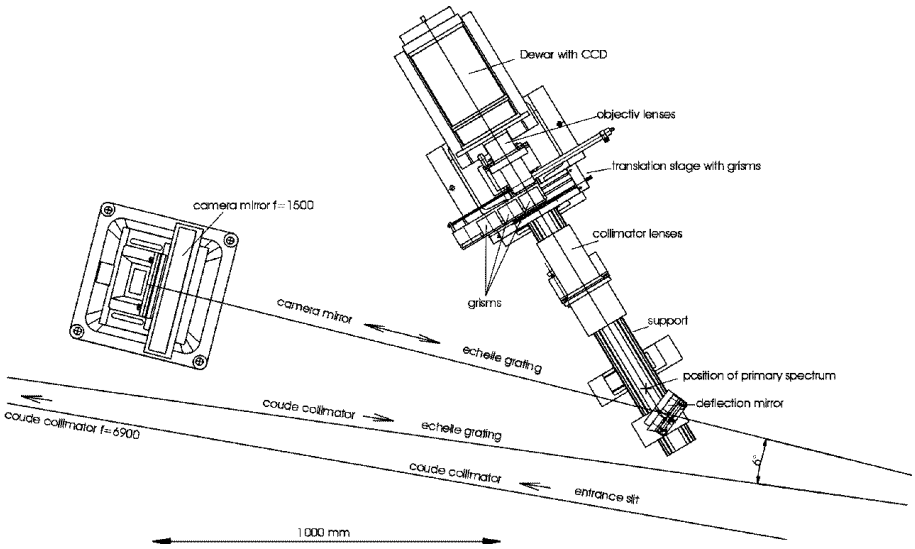


**Figure 3.2:** Construction drawing of the Tautenburg Coudé Échelle Spectrograph (TCES). The light path is as follows: (1) entrance slit (*outside the image to the bottom right*), (2) collimator (*outside left*), (3) échelle grating (*outside right*), (4) camera mirror, (5) deflection mirror, (6) collimator lenses, (7) grism, (8) objectiv lenses (9) CCD detector (Credit: TLS).

angle of 65°. The grating is used with a grating angle of $67\overset{\circ}{.}5$ to ensure that the maximum of the blaze function lies on the center of the detector.

Subsequently, the light passes a camera mirror (focal length of 1500 mm) and a deflection mirror and is collimated again to enter the cross-disperser. Three different grisms (UV, VIS, IR) are available for the cross-dispersion. These can be changed by remote control from the observing room within a few seconds. The spectrum is finally created by an $f/3$ camera lens of 450 mm focal length onto a $2\mathrm{k} \times 2\mathrm{k}$ CCD chip with 13.5 $\mu$m pixels.

For my observations, I adjusted the slit width to 0.52 mm corresponding to $1\overset{''}{.}2$ on the sky and resulting in a resolving power of $R = \lambda/\Delta\lambda = 64\,000$. Furthermore, I used the visual (VIS) grism to cover the wavelength range of 4700–7400 Å (corresponding to spectral orders 122–77).

### 3.1.2 Target selection

The goal of this survey is to investigate main-sequence (MS) stars more massive than the Sun that still have a sufficient number of narrow enough spectral lines, allowing precise RV measurements to detect giant planets and brown dwarfs. This directly translates into stars of spectral types F2–F9, which have masses of 1.0–1.7 $M_\odot$.

The sample of stars to be monitored with the AJT was selected fulfilling further criteria. First, given the geographic latitude of $\approx +51°$ at TLS, only stars with declinations $\delta \gtrsim 0°$ were chosen to ensure the visibility over at least a few months per year. In addition, the targets should be evenly distributed in right ascension

because observing times were allocated regularly to this project every 1–2 months. Second, merely the brightest stars were selected (visual magnitudes of $V \lesssim 7.1$) in order to obtain spectra with adequate signal-to-noise ratios (S/N) in relatively short integration times. In this way, it was possible to observe a statistically significant sample ($> 100$ stars). Third, since the RV precision is proportional to the projected rotational velocity $v \sin i$, only stars with $v \sin i \lesssim 40$ km s$^{-1}$ were considered in this survey; and fourth, known short-period spectroscopic binaries were excluded from the sample, but long-period spectroscopic and visual binaries were not.

The final target list for the TLS survey consisted of 155 F-type MS stars. The star names and their basic physical parameters are provided in Appendix A (Table A.1). Holmberg et al. (2007) derived stellar masses for almost all of the program stars. The corresponding mass distribution is given in Figure 3.3 and shows a mean and median value of 1.30 $M_{\odot}$.

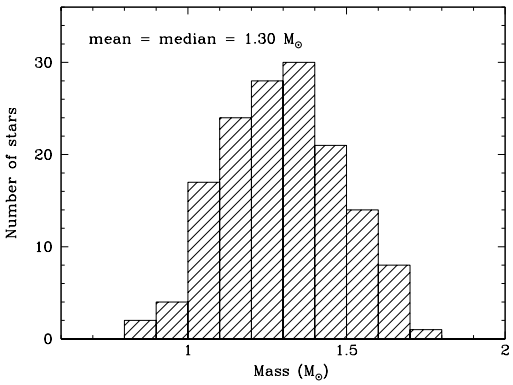


**Figure 3.3:** Histogram of the stellar masses of the F-star sample. The masses are taken from Holmberg et al. (2007).

### 3.1.3 Observations

I initiated the observations for the F-star survey in April 2006. Some objects in this monitoring were also part of former programs, so there were already several spectra acquired before. For the most part, the observations were carried out by myself. At least one week every 1–2 months was allocated to that program, resulting in 50–100 nights per year.

The exposure times were chosen according to the brightness of the star as well as the weather and seeing conditions, aiming for a S/N of $\sim 100$, but not exceeding 30 minutes. In this way, changes in the barycentric velocity over the exposure time were kept lower than the expected individual RV error. Typically, two consecutive spectra were taken for the very bright stars with only a few minutes integration time ($\lesssim 5$ min), otherwise only one spectrum for the fainter stars. In case of a cloudy sky or bad seeing, this was handled differently by observing each star two times in a row to reduce the expected larger RV error by averaging both RV measurements. The same was applied to stars with larger intrinsic RV errors.

### 3.1.4 Data reduction

The reduction of the raw CCD frames, i.e., the correction of the occurring image errors and the extraction of one-dimensional spectra from the two-dimensional images and the following wavelength calibration were done by means of the IRAF astronomical software package (*"Image Reduction and Analysis Facility"*). The required steps and calibration frames are described in the following:

1. **Bias subtraction:** Each CCD frame contains an offset, the so-called bias, to avoid problems with the analog-to-digital converter (ADC) in view of low count rates when reading out the chip (possible negative count rates due to the read-out noise). Therefore, a little charge (bias) is added by the electronics to the signal during the read-out process, which has to be subtracted from each CCD image. This addional charge can be measured by taking bias frames of zero-second exposures with the CCD shutter closed. But the bias level is not constant over the entire CCD chip.

   Thus, a master bias was obtained by averaging 10–30 bias frames and smoothed first along the image lines and then along the image columns by fitting a cubic spline. After that, the mean value from the overscan, a region at the edge of the CCD frame that is never illuminated, was subtracted from the master bias yielding the so-called slope, that is the structure of the bias on the chip. The bias correction applied to each stellar spectrum thus consisted of two steps: first, the subtraction of the slope, and second, the subtraction of the individual mean value from the overscan.

2. **Aperture tracing:** In order to define the location of the apertures (or spectral orders) on the two-dimensional images, I used the average of all stellar spectra taken in one observing run. The center of each aperture was calculated for every fifth column; each aperture was then traced by fitting a polynomial to these center positions using the IRAF task *apall*.

3. **Flat-field correction:** To correct for pixel-to-pixel variations (both in size and sensitivity), fringing (interference pattern) and dust, flat-field images (so-called flats) are necessary. These are obtained by uniformly illuminating the spectrograph's slit. There are different types of taking flats: either internal flats using a calibration lamp placed in front of the slit or dome flats, where the telescope is pointed to a uniformly illuminated white screen mounted inside the dome. Tests verify that the use of dome flats is better suitable because the light path is the same as for the stellar light.

   A master flat was derived by averaging 10–30 dome flats and subtracting both the slope and the mean value from the overscan. Utilizing the IRAF task *apflatten*, the intensity profile of each order of the master flat was fitted, the pixels inside an order were then divided by the corresponding fitting function. All pixels outside the orders were set to unity. Later, the science frames were divided by this normalized flat.

4. **Stray-light and sky background subtraction:** Stray light (or scattered light) is the diffuse light that is distributed over the complete two-dimensional image caused by scattering and reflections at the optical components of the spectrograph (mostly at the échelle grating). The stray-light distribution was measured from the inter-order pixels and modeled by a sixth-order polynomial along each of the two dimensions and then subtracted from the bias- and flat-corrected science frames.

   The sky background, i.e., the emission from the sky, which enters the spectrograph during the observations, is at least a factor of 30 – mostly even a factor of several 100 (since brigth stars were observed) – smaller than the emission from the star itself, hence can be neglected.

5. **Cosmic-ray removal:** The CCD chip is not only sensitive to light, but also to high-energy particles, so-called cosmics. These particles leave localized impacts/traces on the detector. They were removed by replacing the interfered pixels with the average pixel value of the neighboring, not affected pixels.

6. **Order extraction:** The spectral orders were extracted from the science and calibration frames according to the derived polynomials and using an order width of $\pm 8$ pixels. The pixel values of each column within the defined order width were then summed up for each individual order.

7. **Wavelength calibration:** The wavelength calibration is performed using a hollow cathode lamp containing a mixture of thorium and argon (ThAr lamp), which produces roughly 2000 narrow emission lines in the optical spectrum. At least two consecutive ThAr spectra were taken at the beginning and at the end of every observing night; sometimes also in the middle of the night.

   Using the IRAF task *ecidentify*, several emission lines of an extracted ThAr image were identified and assigned the appropriate wavelength taken from an emission line atlas of a ThAr lamp. A preliminary dispersion solution (two-dimensional function of low order) was computed and used to identify additional lines and to recalculate the dispersion relation. Then, all lines from the catalog were used to locate all features of the ThAr frame and a final dispersion solution was determined by fitting a two-dimensional function of higher order. The most deviant points were removed from the final solution. For each stellar spectrum, a wavelength solution was recalculated using the IRAF task *ecreidentify* and the ThAr frame that was obtained closest in time to the actual stellar spectrum.

8. **Normalization of the continuum:** Following the previous steps, the spectra still contain the blaze function in each order. To normalize the spectra, the blaze function was determined for each order from the extracted and wavelength-calibrated master flat. Subsequently, the science frames were then divided – order by order – by the blaze function and normalized to unity.

## 3.2 The Ap-star survey in the southern hemisphere

### 3.2.1 The HARPS spectrograph

The most precise astronomical spectrometer in the world is the High Accuracy Radial velocity Planetary Searcher (HARPS), operated by the European Southern Observatory (ESO) on its 3.6-meter telescope at La Silla in Chile (Figure 3.4). HARPS is a cross-dispersed échelle spectrograph which is fed by two optical fibers with the light from the telescope and a calibration lamp (ThAr lamp) or the sky background simultaneously. For each fiber, 72 diffraction orders (also called échelle apertures) are formed on the detector, a mosaic of two $2\text{k} \times 4\text{k}$ CCDs with 15 $\mu$m pixels, covering a wavelength range of 3780–5300 Å (Linda: "lower, blue" CCD with orders 161–116) and 5330–6910 Å (Jasmin: "upper, red" CCD with orders 114–89). The fiber diameter corresponds to $1''$ on the sky, resulting in a resolving power of $R = \lambda/\Delta\lambda = 115\,000$.

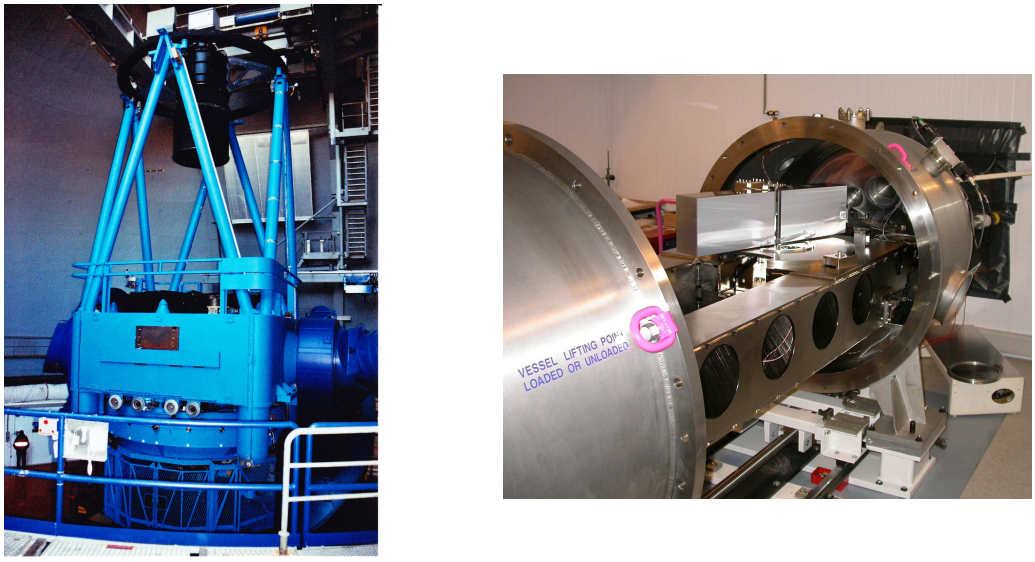


**Figure 3.4:** *Left*: ESO's 3.6-meter telescope at La Silla, Chile (Photo: Michael Hartmann). *Right*: The HARPS spectrograph during laboratory tests. The vacuum tank is open, and the large optical grating is visible on the top of the bench (Credit: ESO).

The spectrograph is placed in a vacuum-sealed tank, where the pressure is always kept below 0.01 mbar (right image in Figure 3.4). The air temperature in the room around the vacuum vessel is accurately controlled to 17 °C by an air-conditioning, providing a long-term stability of the order of 0.01 K. Because of this extraordinary stability, the wavelength solution and instrumental profile are extremely stable. As a consequence, RV drifts measured with a series of ThAr images during several hours remain well below 1 $\mathrm{m\,s^{-1}}$ (details taken from Mayor et al. 2003).

Many extrasolar planets have been discovered with HARPS, as can be seen in more than 40 papers of the series *"The HARPS search for southern extra-solar planets."*

### 3.2.2 Target selection

Chemically peculiar A (Ap) stars are main-sequence stars of spectral type B8–F3 that show large overabundances of some chemical elements (e.g., Si, Sr, Cr, Eu), especially of rare-earth elements. These abundances can be as high as 10 000 times the solar values, or even higher. Furthermore, they do possess strong, global magnetic fields of up to 34 kG. Compared to normal A-type stars, their rotational velocities are markedly lower; rotation periods typically range from several days to tens of years. As a result, spectra of Ap stars contain plenty of relatively narrow absorption lines, thus making these stars ideal targets for precise RV measurements.

Some Ap stars exhibit high-overtone ($n \gg l$), low-degree ($l \leq 3$), non-radial $p$-mode pulsations with periods of 6–24 min and typical peak-to-peak $B$-amplitudes ranging from 0.6 to 16 mmag (see Table 1 in Kurtz et al. 2006). These stars are called rapidly oscillating Ap (roAp) stars. The longest pulsation periods were recently found in the stars HD 177765 (Alentiev et al. 2012, 23.6 min) and HD 225914 (Smalley et al. 2015, 23.4 min). The Ap stars, in which no oscillations were detected so far, are referred to as non-oscillating Ap (noAp) stars in the following.

The first selection criterion was to choose mainly stars from the south side of the sky, i.e., stars with declinations $\delta \lesssim +10°$, to guarantee the visibility of an object for at least eight months per year at the location of the La Silla Observatory (latitude of $\approx -29°$). The second one was to include all accessable roAp stars, of which 35 were known in 2006 and listed in Kurtz et al. (2006). These stars tend to have the longest rotational periods and thus the narrowest spectral lines among Ap stars. I picked all of them except for three stars that did not satisfy the first criterion. Furthermore, one star (HD 99563) was not considered since it was known as a close visual double star with a separation of $1\farcs79$ (Fabricius & Makarov 2000), $1\farcs75$ (Mason et al. 2001) and $1\farcs7$ (Dommanget & Nys 2002), respectively. Additionally, an equal number of noAp stars was selected from the General Catalogue of Ap and Am stars (Renson & Manfroid 2009), for which the spectral classification indicated an overabundance of the elements Si, Sr, Cr or Eu and which had visual magnitudes $V \lesssim 9$.

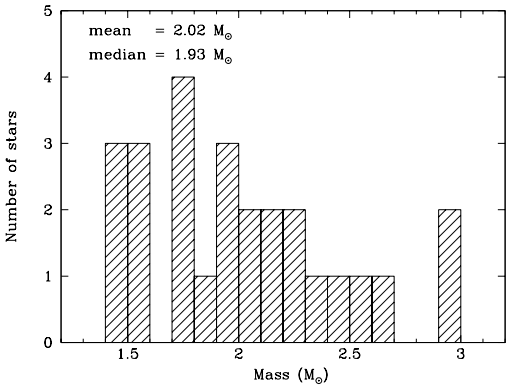


**Figure 3.5:** Histogram of the stellar masses for 26 stars of the Ap-star sample. The masses are taken from Kochukhov & Bagnulo (2006).

The final target list for the HARPS survey contained 62 Ap stars (31 roAp stars and 31 noAp stars). The observed stars are presented in Appendix A together with their fundamental properties (Table A.2). For 26 of the sample stars, Kochukhov & Bagnulo (2006) provided a stellar mass. The histogram of these masses is displayed in Figure 3.5. The distribution has a mean and median value of 2.02 and 1.93 $M_\odot$, respectively. For the eventual calculation of companion masses in Section 6.2, I will thus assume a stellar mass of $2.0 \pm 0.2$ $M_\odot$ for stars not covered by Kochukhov & Bagnulo (2006).

### 3.2.3 Observations

Thirty-eight nights have been allocated to this program distributed over 11 observing campaigns. Almost all observations were performed by myself. For the 62 program stars, a total of 1597 spectra were gathered. The exposure times were chosen in such a way that an average S/N of $\sim 100$ at spectral order 60 ($\approx 6100$ Å) was achieved. For the roAp stars, I adjusted the exposure time to an integer multiple of the pulsation period or – for brighter stars – took multiple observations over one pulsation cycle in order to average out any RV variations caused by pulsations.

The observing strategy was to take preferably several consecutive spectra per star to get an estimation of the error of the RV measurements. Moreover, this practice allowed me to reduce the RV errors by averaging these RVs. However, due to the limited observing time and the medium-sized sample, only one spectrum was acquired for the faintest stars (exposure time $\gtrsim 600$–$900$ s). For the other targets, 2–4 observations in a row were taken depending on the exposure time.

### 3.2.4 Data reduction

In the afternoon before each observing night, standard calibration images were taken, including bias, flat-field and ThAr images. The échelle apertures were identified using the flat-field frames. The wavelength solution for both fibers was determined from the ThAr images.

The complete raw data reduction, consisting of cosmic-ray removal, bias subtraction, flat-field division, order extraction and wavelength calibration, was done by an automatic pipeline, the HARPS Data Reduction Software (DRS).

# 4 Radial-velocity determination

When measuring RVs there appear some problems, which affect adversely the accuracy of the measurements. The stellar image is blurred and wiggles on the spectrograph's slit due to atmospheric turbulence and air mixing in the dome and the tube of the telescope, the so-called *astronomical seeing*. Consequently, this results in a slight displacement of the spectral lines on the detector. Temperature fluctuations inside the spectrograph may also influence the precision of the RV measurements by changing the wavelength dispersion and the instrumental profile (IP). These effects limit the RV precision to a few 100 $\mathrm{m\,s^{-1}}$. But to detect planetary companions, an RV precision of a few $\mathrm{m\,s^{-1}}$ is required.

To achieve such a precision, it is necessary to obtain high-S/N spectra having a large wavelength coverage and a very stable wavelength scale. Two different methods have been established for this purpose: the iodine absorption cell technique and the cross-correlation function (CCF) technique. Both methods will be described in this section.

## 4.1 Iodine-cell technique

During the observations for my F-star survey in Tautenburg, an iodine absorption cell was placed in the optical light path in front of the spectrograph's slit. This cylindrical glass jar is filled with molecular iodine gas ($I_2$) and heated to about 80 °C. The iodine produces a plethora of narrow absorption lines in the optical spectrum (5000–6300 Å) that are superimposed onto the observed stellar spectrum, providing both a very precise wavelength scale and a specification of the spectrograph's instrumental profile (IP) in situ over the spectrum. The calculation of the RV value is a rather complex procedure and computationally very intensive.

The observed spectrum $I_{\mathrm{obs}}(\lambda)$ has to be modeled by means of the transmission function $T_{\mathrm{I_2}}$ of the $I_2$ absorption cell and an intrinsic stellar spectrum $I_{\mathrm{s}}$ without $I_2$ lines (so-called *Template*) (Marcy & Butler 1992):

$$I_{\mathrm{obs}}(\lambda) = k[I_{\mathrm{s}}(\lambda + \Delta\lambda_{\mathrm{s}})T_{\mathrm{I_2}}(\lambda + \Delta\lambda_{\mathrm{I_2}})] \otimes \mathrm{PSF}. \tag{4.1}$$

Here, $\Delta\lambda_{\mathrm{s}}$ and $\Delta\lambda_{\mathrm{I_2}}$ are the shifts of the star spectrum and the $I_2$ transmission function, respectively, while $k$ is a normalization factor. The symbol $\otimes$ represents the convolution. PSF denotes the point-spread function. The resulting Doppler shift $\Delta\lambda$ is simply given by

$$\Delta\lambda = \Delta\lambda_{\mathrm{s}} - \Delta\lambda_{\mathrm{I_2}}. \tag{4.2}$$

The $I_2$ transmission function $T_{\mathrm{I_2}}$ of our absorption cell was taken with the Fourier Transform Spectrometer (FTS) at Kitt Peak National Observatory (Arizona, USA), which gave a resolving power of $R = \lambda/\Delta\lambda = 300\,000$. Compared to normal stellar spectrographs, the PSF of the FTS can be considered as a delta function. The obtained $I_2$ transmission function thus represents indeed $T_{\mathrm{I_2}}$.

Unfortunately, it is not possible to observe also faint stars with the FTS. To obtain the *Template* $I_{\mathrm{s}}$ with the Tautenburg spectrograph, each of the program stars

was observed without the $I_2$ cell in place. But this delivered only $I_{\rm obs} = I_{\rm s} \otimes$ PSF, i.e., the PSF of the spectrograph needs to be determined. This was done by observing a bright, fast-rotating B-type star with $I_2$ cell in a timely manner to the *Template* observation. Since the spectrum of a fast-rotating B star shows only very few and rotationally broadened spectral features, it basically contains the $I_2$ absorption spectrum $T_{\rm obs}$ when passing through the $I_2$ cell. Comparing this spectrum to the FTS $I_2$ transmission function $T_{\rm I_2}$ allowed the calculation of the PSF, hence the generation of the intrinsic stellar spectrum by deconvolution with this PSF:

$$T_{\rm obs} = T_{\rm I_2} \otimes \mathrm{PSF} \Rightarrow \mathrm{PSF} \tag{4.3}$$

$$I_{\rm obs} = I_{\rm s} \otimes \mathrm{PSF} \Rightarrow I_{\rm s}. \tag{4.4}$$

Each *Template* obtained in this way serves now as a reference spectrum for all other spectra of a given star taken with $I_2$ cell, i.e., all RVs are calculated relative to the *Template*. The modeling process is illustrated in Figure 4.1.

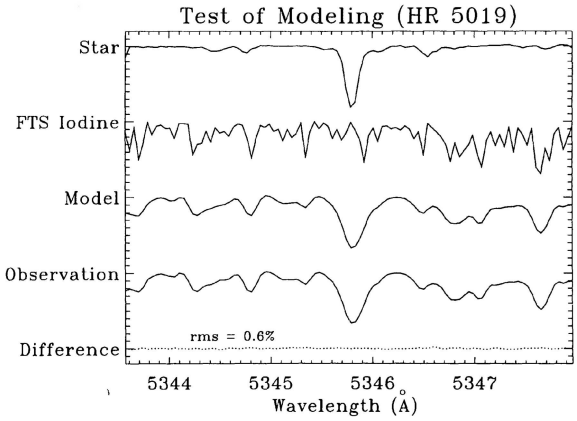


**Figure 4.1:** Principle of the modeling process. Shown are (from top to bottom): the intrinsic stellar spectrum $I_{\rm s}$, the FTS $I_2$ transmission spectrum $T_{\rm I_2}$, the calculated model $(I_{\rm s} \cdot T_{\rm I_2}) \otimes$ PSF, the star spectrum $I_{\rm obs}$ observed through $I_2$ cell and the difference between model and observation (Figure from Marcy & Butler 1992).

For the modeling of the observed spectra, the program RADIAL was utilized, which was mostly developed by W. Cochran over a timeframe of about 10 years and modified by A. Hatzes for the Tautenburg spectrograph. In the following, the modeling procedure for the Tautenburg spectra will be described in more detail.

For the complete modeling process, only the apertures 24–36 (corresponding to the spectral orders 100–112 and the wavelength range of 5050–5740 Å) are used. Initially, each considered order of the spectrum is subdivided into 10 small spectral segments (so-called *chunks*) of $\approx$7–8 Å in length, resulting in a total of 130 *chunks*. Because the PSF is not constant along the entire spectral range, it is necessary to determine the PSF for each *chunk* individually, as ultimately the RV as well. The PSF is fitted by 5 Gaussians: a major Gaussian in the center and two ancillary

Gaussians at each wing. Since every Gaussian has three free parameters (position, width, and height), this would result in determining 15 parameters. To decrease the number of free parameters in the modeling process, the positions of all and the widths of the four ancillary Gaussians were fixed to values that match the PSF properly. In addition, there are two parameters for the wavelength solution (polynomial of degree 2 with one coefficient being fixed), two parameters fitting the continuum (normalization and slope), and the RV itself. Consequently, 11 free parameters per *chunk* have to be determined via a least-squares fitting algorithm.

From each of the 130 *chunks*, an RV value can be extracted and the scatter of these values delivers the internal measurement error. Then, the RV measurements of all *chunks* are combined by a weighted mean and the RV values of former measurements of a star have influence on the determination of the weighting factors. The weigthing factor of a given *chunk* is obtained by the inverse square of the standard deviation of the RV values of that *chunk*. In this case, it is guaranteed that the "good" *chunks* get a high weight, while the "bad" *chunks* (e.g., *chunks* at the edges of an order, where the flux is lower, or *chunks* with less spectral lines) get a low weight. This approach requires at least six spectra for a star to calculate reliable RVs.

Because of the motion of the Earth around the Sun and the Earth's rotation, the RV of a star measured from the Earth would not be constant over time even if the stellar RV would be. It is thus essential to determine accurately both motions of the Earth and to correct the measured RV. Since the observations are taken at different times and positions of the Earth with respect to the Sun, it is necessary to use a reference system that accounts for differences in light travel times – light travel time differences can reach up to 16 minutes corresponding to the time in which light travels twice the distance Sun–Earth. This so-called heliocentric correction is not sufficient for precise RV measurements because the heliocenter is also moving around the barycenter of the solar system. An additional conversion to the barycenter of the solar system needs to be applied (barycentric correction). Therefore, the known masses and orbits of the planets of our solar system – primarily Jupiter and Saturn – have to be taken into account.

To illustrate the required precision, it is worth mentioning that the geographic position of the telescope has to be known to an accuracy of $\approx 20$ m to receive an RV precision of 1 $\mathrm{m\,s^{-1}}$. Attention should be also paid not to exceed an exposure time of about 15 minutes to reach such RV precision because Earth's rotation and orbital motion cause a drift of the spectral lines on the detector over time, resulting in smeared lines on the final spectrum and thus less RV precision.

## 4.2 Cross-correlation technique

The RV measurements obtained with HARPS are normally derived using the cross-correlation function (CCF). In this method, a reduced and wavelength-calibrated stellar spectrum $S(\lambda)$ is cross-correlated with a Doppler-shifted, weighted binary mask $M(\lambda_{v_\mathrm{r}})$, which is different from zero at the theoretical positions and widths of the stellar absorption lines at zero velocity and zero elsewhere. This mask can be expressed by the sum of the weigthed masks $M_i \cdot c_i$ ($M_i = 1$) for the individual stellar absorption lines $i$. The weighting factors, which are equal to the relative depths $c_i$ of the spectral lines against the local continuum, are introduced to account for the correct weight of each line. The weigthed CCF (wCCF) is then obtained by shifting the mask as a function of the Doppler velocity $v_\mathrm{r}$ (see Pepe et al. 2002):

$$\begin{aligned}
\mathrm{wCCF}(v_\mathrm{r}) &= \int S(\lambda) \cdot M(\lambda_{v_\mathrm{r}})\,\mathrm{d}\lambda && (4.5)\\
&= \int S(\lambda) \cdot \sum_i (M_i(\lambda_{v_\mathrm{r}}) \cdot c_i)\,\mathrm{d}\lambda && (4.6)\\
&= \sum_i \int S(\lambda) \cdot M_i(\lambda_{v_\mathrm{r}}) \cdot c_i\,\mathrm{d}\lambda && (4.7)\\
&= \sum_i \mathrm{CCF}_i(v_\mathrm{r}) \cdot c_i, && (4.8)\\
\text{where } \lambda_{v_\mathrm{r}} &= \lambda\sqrt{\frac{1-\frac{v_\mathrm{r}}{c}}{1+\frac{v_\mathrm{r}}{c}}}. && (4.9)
\end{aligned}$$

The resulting wCCF characterizes a kind of "mean" stellar absorption line profile. The RV, defined by the minimum of the wCCF, is calculated by fitting a Gaussian function to its shape. More details on this technique can be found in Queloz (1995) and Pepe et al. (2002). The RV determination, including a barycentric correction, is also implemented in the HARPS DRS.

Binary masks of spectral type G2 V, K0 V and M0 V are provided to the HARPS observer. For the RV measurements of the Ap stars, I used the G2 V mask since it is the earliest spectral type available. Although this method is not optimal for Ap stars, it seems to work quite well in many cases. The minimum of the CCF is clearly visible as a narrow and deep dip for slowly rotating later-type stars (later than spectral type F), and the RV is determined to an accuracy of $\sim 1\ \mathrm{m\,s^{-1}}$ if the RV of the star is known to within 1–2 $\mathrm{km\,s^{-1}}$ and given to the pipeline as a starting value for the line identification. On the other hand, this dip is broader and weaker for Ap stars and the RV was not known to the required accuracy. Therefore, the RV was computed using the pipeline in an iterative process. The CCF was calculated beginning with an unknown RV starting value, the received RV was then used as the new starting value, and so on. Subsequently, the final RV was achieved when the difference between input and output RV was $< 1\ \mathrm{m\,s^{-1}}$.

## 4.3 HARPS-TERRA – A least-squares template-matching method

The CCF method described above is suboptimal in general because it does not exploit the full Doppler information in the stellar spectrum (Pepe et al. 2002) and, in particular, because it is not particularly suitable for early-type stars due to a missing binary mask of that spectral type.

Therefore, I used a new software tool called HARPS-TERRA (Template-Enhanced Radial velocity Re-analysis Application; Anglada-Escudé & Butler 2012), which is based on a least-squares template-matching approach, to recalculate all RVs of my HARPS Ap-star survey. Initially, the highest-S/N observation is used as a preliminary template to obtain the RV for each spectrum. In the next step, a very high-S/N template is generated by co-adding all the spectra taking their individual RV shifts into account to calculate the RVs again. The entire procedure is applied for each échelle aperture individually and the final RV measurement is achieved by a weighted mean of the RVs of all apertures. For an extensive description of the algorithms, I refer the reader to Anglada-Escudé & Butler (2012).

# 5 Analysis of radial-velocity data

## 5.1 Tests for variability and trends

To probe for variability in the RV data, I performed some statistical tests as outlined in Endl et al. (2002). First, I applied the $F$-test comparing the observed RV scatter $\sigma$ with the individual mean internal measurement error $\overline{\sigma_{\mathrm{RV}}}$ for each star:

$$F = \frac{\sigma^2}{\overline{\sigma_{\mathrm{RV}}}^2}. \tag{5.1}$$

With this test, I verified if a star is more variable (or more constant) than its internal RV error would imply. The computed probabilities $P(F)$ indicate how likely the RV scatter can be explained just with the measurement errors. In other words, a low value of $P(F)$ (e.g., $< 0.01$) suggests an excess of RV variability with high probability (99% confidence level).

As a second test, I used the $\chi^2$-test, i.e., I fitted a constant model to the RV measurements (with the zero point as free parameter) and calculated the $\chi^2$ above the weighted RV mean. The probabilities $P(\chi^2_{\mathrm{const}})$ from the $\chi^2$-distribution specify whether the constant model gives a good description of the data. A small value of $P(\chi^2_{\mathrm{const}})$ denotes again that the RV results show a larger scatter than expected from their internal errors, thus providing evidence for variability.

## 5.2 Periodogram analysis

There are several techniques to investigate time series with unequally spaced data to detect periodic signals. One possibility is least-squares fitting of sine waves of various periods to the data (Barning 1963; Lomb 1976). Another approach is periodogram analysis, which is based on the discrete Fourier transform (DFT). The close relationship between these two methods was already mentioned by Lomb (1976). Later, Scargle (1982) established that they are exactly equivalent when a slight modification to the classical definition of the periodogram is applied. Thus, also the statistical behavior retains as simple as in the case of evenly sampled data (exponential distribution), and this method is time-translation invariant.

Nowadays, this commonly used tool is referred to as the Lomb–Scargle periodogram. It is equivalent to a least-squares fitting of sine waves of the form $y = a\cos\omega t + b\sin\omega t$. For a time series $(t_i, y_i)$ with zero mean ($\overline{y} = 0$), it has the following form (normalization from Lomb (1976), see also Zechmeister & Kürster (2009) for details):

$$\begin{aligned}\hat{p}(\omega) &= \frac{1}{\hat{YY}}\left[\frac{\hat{YC}^2_{\hat{\tau}}}{\hat{CC}_{\hat{\tau}}} + \frac{\hat{YS}^2_{\hat{\tau}}}{\hat{SS}_{\hat{\tau}}}\right] \\ &= \frac{1}{\sum_i y_i^2}\left\{\frac{[\sum_i y_i \cos\omega(t_i-\hat{\tau})]^2}{\sum_i \cos^2\omega(t_i-\hat{\tau})} + \frac{[\sum_i y_i \sin\omega(t_i-\hat{\tau})]^2}{\sum_i \sin^2\omega(t_i-\hat{\tau})}\right\},\end{aligned} \tag{5.2}$$

where the parameter $\tau$ is defined as

$$\tan 2\omega\hat{\tau} = \frac{\sum_i \sin 2\omega t_i}{\sum_i \cos 2\omega t_i}. \tag{5.3}$$

This technique, however, has two limitations, *"making it non-robust when the number of observations is small, the sampling is uneven, or for periods comparable to or greater than the duration of the observations"* (Cumming et al. 1999). First, it does not take measurements errors into account, and second, for the analysis the mean of the data has to be subtracted, hence assuming the mean of the data and the zero point of the fitted sine function being the same. These disadvantages can be solved by implementing weighted sums (i.e., using a $\chi^2$-fit) and an offset $c$ into this periodogram, which is then equivalent to a weighted full sine-wave fitting, i.e., $y = a\cos\omega t + b\sin\omega t + c$. This generalization, first introduced by Cumming et al. (1999), who called it "floating-mean periodogram," but did not provide an analytical solution for the computation, was later presented in detail by Zechmeister & Kürster (2009), who called it the generalized Lomb–Scargle periodogram (GLS). This periodogram is equal to the relative $\chi^2$-reduction as a function of frequency $\omega$ and normalized to unity by the $\chi^2$ for the weighted mean, $\chi^2_{const}$. Following the steps in Zechmeister & Kürster (2009) results in

$$p(\omega) = \frac{\chi^2_{\text{const}} - \chi^2_{\sin}(\omega)}{\chi^2_{\text{const}}} \tag{5.4}$$

$$= \frac{1}{YY} \cdot \frac{SS \cdot YC^2 + CC \cdot YS^2 - 2CS \cdot YC \cdot YS}{CC \cdot SS - CS^2} \tag{5.5}$$

with the following abbreviations for the sums (the hats indicate the sums of the classical Lomb–Scargle periodogram):

$$YY = \hat{YY} - Y \cdot Y \qquad \hat{YY} = \sum_i w_i y_i^2 \qquad Y = \sum_i w_i y_i \tag{5.6}$$

$$YC(\omega) = \hat{YC} - Y \cdot C \qquad \hat{YC} = \sum_i w_i y_i \cos\omega t_i \qquad C = \sum_i w_i \cos\omega t_i \tag{5.7}$$

$$YS(\omega) = \hat{YS} - Y \cdot S \qquad \hat{YS} = \sum_i w_i y_i \sin\omega t_i \qquad S = \sum_i w_i \sin\omega t_i \tag{5.8}$$

$$CC(\omega) = \hat{CC} - C \cdot C \qquad \hat{CC} = \sum_i w_i \cos^2\omega t_i \tag{5.9}$$

$$SS(\omega) = \hat{SS} - S \cdot S \qquad \hat{SS} = \sum_i w_i \sin^2\omega t_i \tag{5.10}$$

$$CS(\omega) = \hat{CS} - C \cdot S \qquad \hat{CS} = \sum_i w_i \cos\omega t_i \sin\omega t_i. \tag{5.11}$$

When replacing $t_i$ with $\tau_i = t_i - \tau$ (because of the time-translation invariance it will

not affect the $\chi^2$ of the sine fit) and choosing the parameter $\tau$ as

$$\begin{aligned}\tan 2\omega\tau &= \frac{2\,CS}{CC - SS} \\ &= \frac{\sum_i w_i \sin 2\omega t_i - 2\sum_i w_i \cos\omega t_i \sum_i w_i \sin\omega t_i}{\sum_i w_i \cos 2\omega t_i - [(\sum_i w_i \cos\omega t_i)^2 - (\sum_i w_i \sin\omega t_i)^2]},\end{aligned} \tag{5.12}$$

the interaction term in Equation (5.5) disappears, $CS_\tau = \sum w_i \cos\omega(t_i-\tau)\sin\omega(t_i-\tau) - \sum w_i \cos\omega(t_i-\tau)\sum w_i \sin\omega(t_i-\tau) = 0$ (see appendix in Zechmeister & Kürster 2009). Calculating this parameter $\tau(\omega)$ for each frequency, the periodogram in Equation (5.5) simplifies to

$$p(\omega) = \frac{1}{YY}\left[\frac{YC_\tau^2}{CC_\tau} + \frac{YS_\tau^2}{SS_\tau}\right]. \tag{5.13}$$

The form of this equation is similar to Equation (5.2) of the classical Lomb–Scargle periodogram, but now accounting for measurement errors (weights $w_i$ in all sums) and a floating mean (additional terms in all sums and $\tan 2\omega\tau$). Due to the normalization to unity, the GLS power $p(\omega)$ lies in the range of $0 \leq p \leq 1$, with $p = 0$ ($\chi^2_{\rm sin} = \chi^2_{\rm const}$) showing no improvement of the fit and $p = 1$ ($\chi^2_{\rm sin} = 0$) indicating a "perfect" fit.

Assuming Gaussian noise, the numerator and denominator in Equation (5.4) are $\chi^2$-distributed with $(N-1)-(N-3) = 2$ and $N-1$ degrees of freedom, respectively. The periodogram $p(\omega)$ can be normalized to that estimated noise level $p_{\rm n} = \frac{2}{N-1}$ (Zechmeister & Kürster 2009):

$$P = \frac{p(\omega)}{p_{\rm n}} = \frac{N-1}{2}p(\omega). \tag{5.14}$$

The periodogram power $P$ can be considered as a kind of signal-to-noise ratio and is limited to values between 0 and $\frac{N-1}{2}$. This normalization is typically used for the classical Lomb–Scargle periodogram.

For each star in my samples, I analyzed the RV data by computing a GLS periodogram for periods in the search interval from 1 to 10 000 days. To assess the significance of a peak in the power spectrum, I estimated the false alarm probability (FAP; probability that the detected signal would originate purely from noise) using a bootstrap randomization technique. In this approach, random data sets are generated from an original data set by permuting the RV measurements while keeping the observing times fixed (Kürster et al. 1997). Using this method, the FAP can be determined without any assumptions on the underlying noise distribution (e.g., Gaussian noise). Because these simulations are very time-consuming, I generated only 1000 random data sets per star. I also used nightly-averaged RV data sets, since the validity of the FAP is lower in the case of high temporal concentration at one or several points (i.e., "data clumping" when multiple measurements were taken in one night). For each random data set, the GLS periodogram was calculated and searched for its maximum power. The FAP is then given by the fraction of random data sets having a periodogram power exceeding the one of the original data set.

As a rule, I adopted an FAP threshold of 0.01, which means only signals having an FAP $\leq 0.01$ are considered significant.

## 5.3 Keplerian orbital solutions

So far, I have examined the RV data for significant sinusoidal variations. A companion to a star, however, moves on a Keplerian orbit around the star. The resulting RV variation follows the RV curve in Equation (2.2). To find an orbital solution, it is thus necessary to model an RV curve to the RV measurements. The period derived from the GLS periodogram could serve as a good initial guess for the Keplerian period, but sometimes this may not be the case.

In a first step, I therefore used a program that is based on the Keplerian periodogram of Zechmeister & Kürster (2009). Similar to the GLS periodogram, this program steps through a grid of equidistant frequencies within a given interval, typically corresponding to periods between 1 day and at least the timespan of the whole data set. For each frequency, the best Keplerian orbit is determined by stepping also through the eccentricity $e$ and the time of periastron passage $T_0$ and minimizing the $\chi^2$. Here, it is not necessary to step also through the amplitude $K$, longitude of periastron $\omega$ and RV offset $\gamma$ if the following substitutions are applied (see Zechmeister & Kürster 2009):

$$a = K\cos\omega, \quad b = -K\sin\omega, \quad c = \gamma + Ke\cos\omega. \tag{5.15}$$

Equation (2.2) can now be written as

$$\mathrm{RV}(t) = a\cos\nu(t) + b\sin\nu(t) + c \tag{5.16}$$

and has the same form as the sine model for the GLS periodogram with $\nu$ instead of $\omega t$. The best-fitting Keplerian orbit then corresponds to the solution having the global $\chi^2$-minimum in the 3-dimensional grid $(\omega, e, T_0)$.

In a second approach, these orbital parameters were used as starting values for the nonlinear least-squares fitting program *GaussFit* (Jefferys et al. 1988) to verify the orbital solution. The uncertainties of the orbital parameters were derived from a maximum likelihood estimation.

The Keplerian solutions for the stars with companions (stellar and sub-stellar) will be presented in the following chapter.

# 6 Results and discussion

## 6.1 The F-star survey in the northern hemisphere

### 6.1.1 Spectroscopic binaries with orbit

In this section, I present the orbits of ten single-lined spectroscopic binaries (SB1). First, I will treat three binaries with relatively short orbital periods (less than a year), and second, I will discuss another seven binaries with larger orbital periods (more than 2.5 years). Each of the two parts will be ordered by the star number in the Henry Draper Catalogue (HD number). Six of the orbits are given for the first time, one was shown in a previous Ph.D. thesis, and the other three have been already published in astrophysical journals. Some important stellar parameters will also be provided. In the end, I will summarize the orbits of four more double-lined spectroscopic binaries (SB2) known from the literature, being also part of my star sample.

#### HD 27901

HD 27901 (HIP 20614, HR 1385) has a visual magnitude of $V = 5.965 \pm 0.005$ (Joner et al. 2006) and is listed with a spectral type of F4 V (Cowley & Fraquelli 1974). According to the *Gaia* parallax of $\pi = 21.5337 \pm 0.2115$ mas (Gaia Collaboration 2018), this star is located at a distance of $d = 46.44 \pm 0.46$ pc. Its mass was determined by Holmberg et al. (2007) to be $1.59^{+0.11}_{-0.04}\ M_\odot$. These authors also provide a metallicity of [Fe/H] = 0.08.

The 17 RV data points are spanning 1217 days, and they are given in Figure 6.1 (right panel). The data show huge variations of several tens of $\mathrm{km\,s^{-1}}$. Therefore, the star must be a spectroscopic binary. There appear two higher peaks in the GLS periodogram (Figure 6.1, left panel): the highest one at a period of 403.2 days (GLS

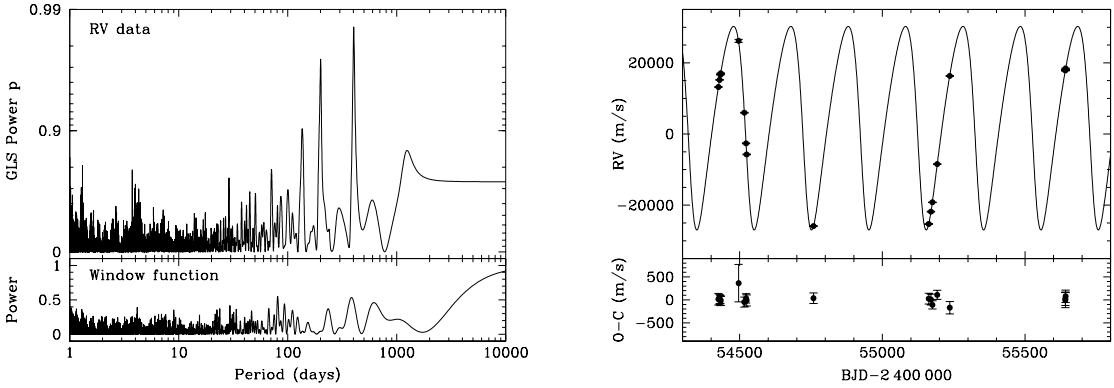


**Figure 6.1:** Results for HD 27901. *Left panel*: GLS periodogram of the RV data and window function of the observations. *Right panel*: RV measurements and best-fit Keplerian orbital solution (solid line). The RV residuals after subtracting the orbital solution are shown below.

**Table 6.1:** Orbital parameters of the stellar companion of HD 27901.

| Parameter | | Value |
|---|---|---|
| $P$ | (days) | $201.028 \pm 0.024$ |
| $K$ | ($\mathrm{m\,s^{-1}}$) | $28\,599 \pm 90$ |
| $e$ | | $0.2466 \pm 0.0020$ |
| $\omega$ | (deg) | $116.20 \pm 0.59$ |
| $T_0$ | ($\mathrm{BJD} - 2\,400\,000$) | $54\,528.08 \pm 0.27$ |
| $RV_0$ | ($\mathrm{m\,s^{-1}}$) | $4739 \pm 44$ |
| $N_{\mathrm{obs}}$ | | 17 |
| $\sigma_{\mathrm{O-C}}$ | ($\mathrm{m\,s^{-1}}$) | 110 |
| $\chi^2_{\mathrm{red}}$ | | 0.54 |
| $a_1 \sin i$ | (AU) | $0.5121 \pm 0.0017$ |
| $f(m_1, m_2, i)$ | ($M_\odot$) | $0.4434 \pm 0.0043$ |
| $m_1$ | ($M_\odot$) | $1.59^{+0.11}_{-0.04}$ |
| $m_2 \sin i$ | ($M_\odot$) | $1.680^{+0.038}_{-0.015}$ |
| $a$ | (AU) | $0.997^{+0.012}_{-0.005}$ |

power $p_{\mathrm{GLS}} = 0.986$) and the next-highest one at 200.5 days ($p_{\mathrm{GLS}} = 0.974$). When using *GaussFit* to model a Keplerian orbit, I was able to find a solution for both periods. The model for the larger period ($\chi^2_{\mathrm{red}} = 12.77$), however, fits the data more poorly compared to the shorter-period model ($\chi^2_{\mathrm{red}} = 0.54$). In addition, the former model would represent a physically unrealistic case because the resulting minimum mass of the companion would then be $\approx 9\ M_\odot$. Consequently, I apply the orbital solution with the 201-day period. The corresponding orbital parameters are listed in Table 6.1. Using a primary mass of 1.59 $M_\odot$ yields a secondary minimum mass of 1.68 $M_\odot$.

### HD 79929

The F6 V star HD 79929 (HIP 45595) has a visual magnitude of $V = 6.748 \pm 0.010$ (Høg et al. 2000). Given the *Gaia* parallax of $\pi = 17.1535 \pm 0.0536$ mas (Gaia Collaboration 2018), the distance to the star amounts to $d = 58.30 \pm 0.18$ pc. Holmberg et al. (2007) determined a stellar mass of $1.29^{+0.05}_{-0.04}\ M_\odot$ and a metallicity of $[\mathrm{Fe/H}] = -0.31$.

Twenty RV measurements were taken over a time span of 1247 days. The periodogram of the RV data shows a strong signal at a period of 13.2573 days (Figure 6.2, left panel). A Keplerian fit yields an accordant value of $13.25754 \pm 0.00011$ days. The RV data phased to this period are displayed in Figure 6.2 (right panel). As can be seen, the points are well distributed over the orbital phase and cover both maximum and minimum of the RV curve, providing very precise orbital elements (Table 6.2). The minimum mass of the companion is $0.1609 \pm 0.0037\ M_\odot$, hence the companion most likely an M star.

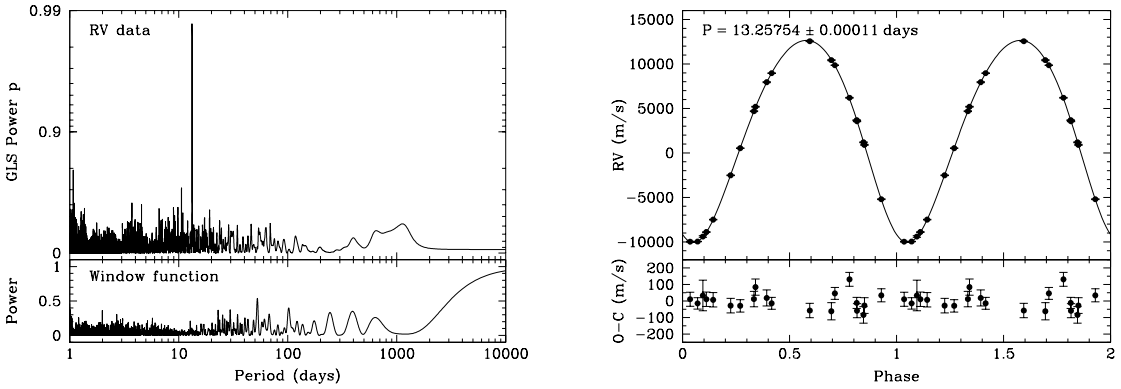


**Figure 6.2:** Results for HD 79929. *Left panel*: GLS periodogram of the RV data and window function of the observations. *Right panel*: RV measurements phased to the orbital period and best-fit Keplerian orbital solution (solid line). Phase zero corresponds to the time of periastron passage. Data points are repeated for the second cycle. The RV residuals after subtracting the orbital solution are shown below.

**Table 6.2:** Orbital parameters of the stellar companion of HD 79929.

| Parameter | | Value |
|---|---|---|
| $P$ | (days) | $13.25754 \pm 0.00011$ |
| $K$ | ($\mathrm{m\,s^{-1}}$) | $28\,363 \pm 22$ |
| $e$ | | $0.1110 \pm 0.0018$ |
| $\omega$ | (deg) | $157.13 \pm 0.87$ |
| $T_0$ | (BJD $-$ 2 400 000) | $55\,223.592 \pm 0.032$ |
| $RV_0$ | ($\mathrm{m\,s^{-1}}$) | $2451 \pm 15$ |
| $N_{\mathrm{obs}}$ | | 20 |
| $\sigma_{\mathrm{O-C}}$ | ($\mathrm{m\,s^{-1}}$) | 51.3 |
| $\chi^2_{\mathrm{red}}$ | | 1.81 |
| $a_1 \sin i$ | (AU) | $0.013761 \pm 0.000026$ |
| $f(m_1, m_2, i)$ | ($M_\odot$) | $0.001978 \pm 0.000012$ |
| $m_1$ | ($M_\odot$) | $1.29 \pm 0.05$ |
| $m_2 \sin i$ | ($M_\odot$) | $0.1609 \pm 0.0037$ |
| $a$ | (AU) | $0.1241 \pm 0.0015$ |

### HD 145228

HD 145228 (HIP 79166) has a visual magnitude of $V = 7.04 \pm 0.01$ (Høg et al. 2000). The *Gaia* parallax of this F0 V star is $\pi = 10.9235 \pm 0.0836$ mas (Gaia Collaboration 2018), thus the distance to the star is $d = 91.55 \pm 0.70$ pc. Its mass and metallicity have values of $1.57^{+0.06}_{-0.07}$ $M_\odot$ and [Fe/H] = −0.19, respectively (Holmberg et al. 2007).

The ten TLS RV measurements cover a timeframe of 1395 days and exhibit huge variations revealing the binary nature of this star. The GLS periodogram in Figure 6.3 (left panel) shows two peaks with similar power at 108.26 days ($p_{\mathrm{GLS}} = 0.9413$) and 41.84 days ($p_{\mathrm{GLS}} = 0.9397$). In contrast, a Keplerian periodogram yields powers of $p_{\mathrm{Kep}} = 0.9954$ and 0.9984, respectively, so the signal with the shorter period has the slightly higher power. A Keplerian solution for the larger period would indeed provide again a physically unrealistic case, resulting in a minimum mass for the companion of $\approx 2.4$ $M_\odot$. Moreover, it was not possible to find a convergent solution for that period with *GaussFit*. Consequently, I consider the smaller period to be the right one, and *GaussFit* gives a period of $41.661 \pm 0.028$ days. The RV data phased to this period are displayed in Figure 6.3 (right panel). The orbital parameters are listed in Table 6.3. The stellar companion has a minimum mass of $0.473 \pm 0.018$ $M_\odot$ and is presumably an M star.

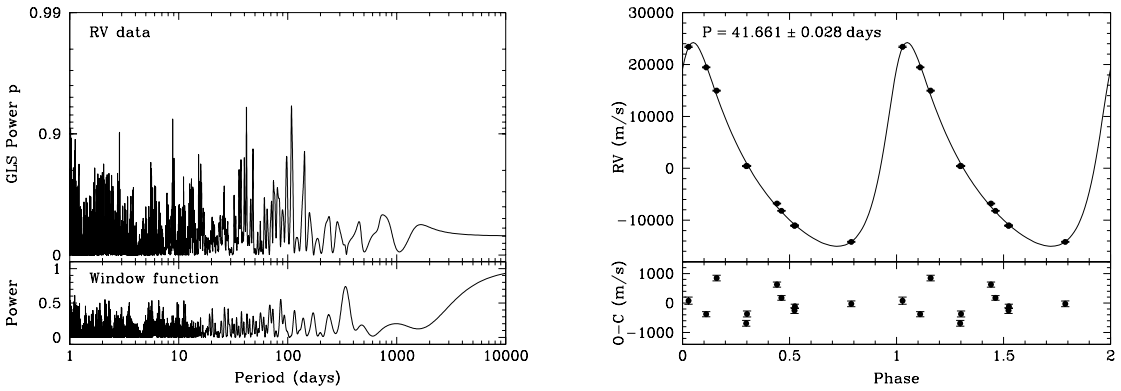


**Figure 6.3:** Results for HD 145228. *Left panel*: GLS periodogram of the RV data and window function of the observations. *Right panel*: RV measurements phased to the orbital period and best-fit Keplerian orbital solution (solid line). Phase zero corresponds to the time of periastron passage. Data points are repeated for the second cycle. The RV residuals after subtracting the orbital solution are shown below.

**Table 6.3:** Orbital parameters of the stellar companion of HD 145228.

| Parameter | | Value |
|---|---|---|
| $P$ | (days) | $41.661 \pm 0.028$ |
| $K$ | ($\mathrm{m\,s^{-1}}$) | $19\,624 \pm 451$ |
| $e$ | | $0.394 \pm 0.038$ |
| $\omega$ | (deg) | $317.9 \pm 3.6$ |
| $T_0$ | (BJD $-$ 2 400 000) | $54\,816.21 \pm 0.53$ |
| $RV_0$ | ($\mathrm{m\,s^{-1}}$) | $-1130 \pm 512$ |
| $N_{\mathrm{obs}}$ | | 10 |
| $\sigma_{\mathrm{O-C}}$ | ($\mathrm{m\,s^{-1}}$) | 468 |
| $\chi^2_{\mathrm{red}}$ | | 56.3 |
| $a_1 \sin i$ | (AU) | $0.0691 \pm 0.0020$ |
| $f(m_1, m_2, i)$ | ($M_\odot$) | $0.0253 \pm 0.0022$ |
| $m_1$ | ($M_\odot$) | $1.57 \pm 0.07$ |
| $m_2 \sin i$ | ($M_\odot$) | $0.473 \pm 0.018$ |
| $a$ | (AU) | $0.2984 \pm 0.0038$ |

## HD 95241

HD 95241 (HIP 53791, HR 4285) is an F9 V star (Gratton et al. 1996) with a visual magnitude of $V = 6.020 \pm 0.010$ (Høg et al. 2000). It is located at a distance of $d = 46.99 \pm 0.33$ pc from the Sun, according to the *Gaia* parallax of $\pi = 21.2801 \pm 0.1508$ mas. The stellar mass provided by Holmberg et al. (2007) is $1.35^{+0.02}_{-0.04}\ M_\odot$. They also obtained a metallicity of [Fe/H] $= -0.23$.

I took 25 RV measurements spanning 2198 days. These cleary show that a long-period stellar companion in a highly eccentric orbit is present (Figure 6.4). The best-fitting Keplerian orbit has a period of $5326 \pm 35$ days and an eccentricity of $0.8190 \pm 0.0015$. Although the data cover less than half an orbit, the obtained precision of the orbital period is rather good. Not least because of the good coverage during the steep RV decline, all other parameters were also determined very precisely (see

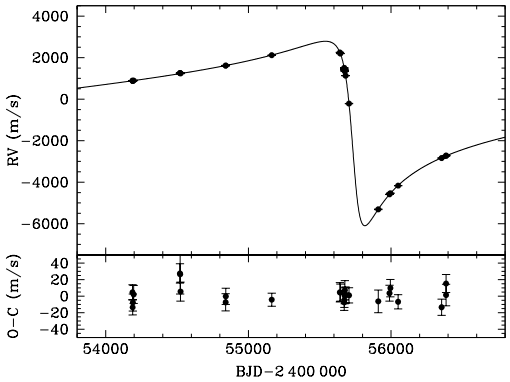


**Figure 6.4:** RV measurements for HD 95241 and best-fit Keplerian orbital solution (solid line). The RV residuals after subtracting the orbital solution are shown below.

**Table 6.4:** Orbital parameters of the stellar companion of HD 95241.

| Parameter | | Value (1) | Value (2) |
|---|---|---|---|
| $P$ | (days) | $5245.2 \pm 1.3$ | $5326 \pm 35$ |
| $K$ | ($\mathrm{m\,s^{-1}}$) | $4454 \pm 30$ | $4443 \pm 13$ |
| $e$ | | $0.8183 \pm 0.0028$ | $0.8190 \pm 0.0015$ |
| $\omega$ | (deg) | $111.73 \pm 0.78$ | $110.71 \pm 0.21$ |
| $T_0$ | (BJD $-$ 2 400 000) | $55\,743.3 \pm 1.2$ | $55\,741.42 \pm 0.27$ |
| $\gamma, RV_0$ | ($\mathrm{m\,s^{-1}}$) | $-8001 \pm 27$ | $-368.1 \pm 3.0$ |
| $N_{\mathrm{obs}}$ | | 177 | 25 |
| $\sigma_{\mathrm{O-C}}$ | ($\mathrm{m\,s^{-1}}$) | 120 | 10.3 |
| $\chi^2_{\mathrm{red}}$ | | ... | 0.95 |
| $a_1 \sin i$ | (AU) | $1.234 \pm 0.012$ | $1.248 \pm 0.010$ |
| $f(m_1, m_2, i)$ | ($M_\odot$) | $0.00912 \pm 0.00026$ | $0.00914 \pm 0.00014$ |
| $m_1$ | ($M_\odot$) | ... | $1.35 \pm 0.04$ |
| $m_2 \sin i$ | ($M_\odot$) | ... | $0.291 \pm 0.005$ |
| $a$ | (AU) | ... | $7.04 \pm 0.07$ |

**References:** (1) Willmarth et al. (2016); (2) This work

Table 6.4). The companion star, with a minimum mass of $0.291 \pm 0.005\ M_\odot$ most likely an M dwarf, orbits its host star at a separation of $7.04 \pm 0.07$ AU.

This star was previously known to be a binary. A first preliminary orbit was determined by Griffin & Suchkov (2003), who published a period of $3949 \pm 22$ days. Their orbital solution was based on six Dominion Astrophysical Observatory (DAO, Canada) measurements from 1919/1920 (Plaskett et al. 1921) and 22 RVs taken from 1993 to 2001 at Observatoire de Haute-Provence (OHP, France) with the CORAVEL spectrometer and at DAO. The authors mentioned that no safe decision was possible between periods of $\sim 3950$ and $\sim 4600$ days due to this large data gap, corresponding to seven and six orbital cycles, respectively, between the 1919/1920 and 1993–2001 data. Later, Griffin (2014) specified a period of $5258 \pm 34$ days using only his Cambridge observations and a period of $5244 \pm 4$ days including two Mount Wilson RVs from 1925 (Adams et al. 1929; Abt 1970).

More recently, Willmarth et al. (2016) found periods of $5267 \pm 50$ days and $5245.2 \pm 1.3$ days (including the two Mount Wilson RVs), which are both in good agreement to that of Griffin (2014). The latter orbit is also given in Table 6.4 and is very similar to my solution with the exception that I find a somewhat larger orbital period (by 81 days or 2.2 $\sigma$).

### HD 111456

HD 111456 (HIP 62512, HR 4867) has a visual magnitude of $V = 5.831 \pm 0.009$ (Høg et al. 2000) and is listed as F6 V star in the Simbad database. Using the Hipparcos parallax of $\pi = 41.59 \pm 2.69$ mas (van Leeuwen 2007), the distance to the star is $d = 24.0 \pm 1.6$ pc. Holmberg et al. (2007) obtained a stellar mass of $1.13^{+0.06}_{-0.07}\ M_\odot$, a metallicity of [Fe/H] $= -0.19$ and $v \sin i = 50\ \mathrm{km\,s^{-1}}$.

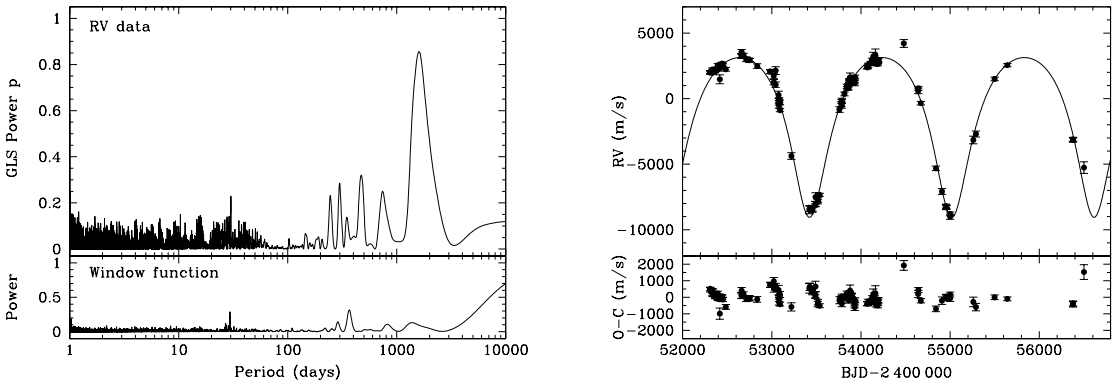


**Figure 6.5:** Results for HD 111456. *Left panel*: GLS periodogram of the RV data and window function of the observations. *Right panel*: RV measurements and best-fit Keplerian orbital solution (solid line). The RV residuals after subtracting the orbital solution are shown below.

**Table 6.5:** Orbital parameters of the stellar companion of HD 111456.

| Parameter | | Value |
|---|---|---|
| $P$ | (days) | $1596.0 \pm 4.2$ |
| $K$ | ($\mathrm{m\,s^{-1}}$) | $6090 \pm 66$ |
| $e$ | | $0.329 \pm 0.010$ |
| $\omega$ | (deg) | $177.4 \pm 1.7$ |
| $T_0$ | (BJD $-$ 2 400 000) | $55\,013.4 \pm 6.7$ |
| $RV_0$ | ($\mathrm{m\,s^{-1}}$) | $-959 \pm 40$ |
| $N_{\mathrm{obs}}$ | | 110 |
| $\sigma_{\mathrm{O-C}}$ | ($\mathrm{m\,s^{-1}}$) | 412 |
| $\chi^2_{\mathrm{red}}$ | | 4.71 |
| $a_1 \sin i$ | (AU) | $0.844 \pm 0.010$ |
| $f(m_1, m_2, i)$ | ($M_\odot$) | $0.0314 \pm 0.0011$ |
| $m_1$ | ($M_\odot$) | $1.13 \pm 0.07$ |
| $m_2 \sin i$ | ($M_\odot$) | $0.423 \pm 0.014$ |
| $a$ | (AU) | $3.095 \pm 0.049$ |

For this star, 110 RV measurements were gathered, distributed over 4193 days. Figure 6.5 shows a peak at 1602.4 days in the periodogram (left panel) and RV variations with an amplitude of several $\mathrm{km\,s^{-1}}$ (right panel). The binary nature was already announced in a previous Ph.D. thesis (Esposito 2009). The Keplerian orbital solution derived in this work is consistant with a stellar companion having a minimum mass of $0.423 \pm 0.014$ $M_\odot$ in an eccentric ($e = 0.329 \pm 0.010$) orbit with a period of $1596.0 \pm 4.2$ days at a separation of $3.095 \pm 0.049$ AU. All orbital parameters are given in Table 6.5.

### HD 153376

The F8 V star HD 153376 (HIP 83083) has a visual magnitude of $V = 6.900 \pm 0.009$ (Oja 1987). The *Gaia* parallax of $\pi = 18.5255 \pm 0.0265$ mas (Gaia Collaboration 2018) yields a distance to the star of $d = 53.98 \pm 0.08$ pc. The stellar mass and metallicity taken from Holmberg et al. (2007) have values of $1.40^{+0.04}_{-0.03}$ $M_\odot$ and [Fe/H] = 0.12, respectively.

I obtained 11 RV measurements during a time frame of 2608 days shown in Figure 6.6. The RV data are consistent with a stellar companion in a long-period, highly eccentric orbit. The period, $P = 4995 \pm 343$ days, could only be determined with less precision because the data do not cover a full orbit. The orbital solution further gives an eccentricity of $e = 0.785 \pm 0.029$. With a minimum mass of $0.268 \pm 0.029$ $M_\odot$, the secondary star is probably an M dwarf orbiting at a separation of $6.78 \pm 0.33$ AU. The entire set of orbital elements is listed in Table 6.6.

It is interesting to mention that the orbital parameters, and thus the behavior of the RV curve, resemble closely the ones for the companion of HD 95241 discussed before.

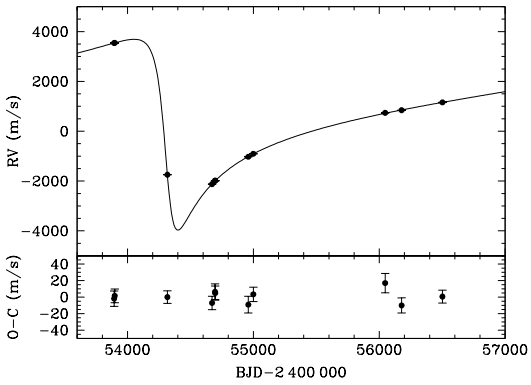


**Figure 6.6:** RV measurements for HD 153376 and best-fit Keplerian orbital solution (solid line). The RV residuals after subtracting the orbital solution are shown below.

### HD 160933

HD 160933 (HIP 86184, HR 6598) has a visual magnitude of $V = 6.42$. While it is listed as F9 V star in Simbad, Gray et al. (2001) gave it a spectral type of F9 IV–V, indicating that the star is starting to evolve off the main sequence. According to the *Gaia* parallax of $\pi = 22.5787 \pm 0.1084$ mas (Gaia Collaboration 2018), the distance to the star is $d = 44.29 \pm 0.21$ pc. The star has a mass of $1.13^{+0.10}_{-0.04}$ $M_\odot$ and its metallicity is [Fe/H] = −0.33 (Holmberg et al. 2007).

Seventeen RV measurements have been collected within a time span of 3775 days. The GLS periodogram shows a strong signal at 2291 days (Figure 6.7, left panel). The corresponding Keplerian orbital solution yields a period of $2226.3 \pm 2.4$ days and an eccentricity of $e = 0.2848 \pm 0.0053$ and is displayed in Figure 6.7 (right

**Table 6.6:** Orbital parameters of the stellar companion of HD 153376.

| Parameter | | Value |
|---|---|---|
| $P$ | (days) | $4995 \pm 343$ |
| $K$ | ($\mathrm{m\,s^{-1}}$) | $3830 \pm 333$ |
| $e$ | | $0.785 \pm 0.029$ |
| $\omega$ | (deg) | $114.2 \pm 1.9$ |
| $T_0$ | (BJD $-$ 2 400 000) | $54\,315.8 \pm 3.8$ |
| $RV_0$ | ($\mathrm{m\,s^{-1}}$) | $1092 \pm 87$ |
| $N_{\mathrm{obs}}$ | | 11 |
| $\sigma_{\mathrm{O-C}}$ | ($\mathrm{m\,s^{-1}}$) | 7.8 |
| $\chi^2_{\mathrm{red}}$ | | 1.18 |
| $a_1 \sin i$ | (AU) | $1.09 \pm 0.14$ |
| $f(m_1, m_2, i)$ | ($M_\odot$) | $0.0069 \pm 0.0023$ |
| $m_1$ | ($M_\odot$) | $1.40 \pm 0.04$ |
| $m_2 \sin i$ | ($M_\odot$) | $0.268 \pm 0.029$ |
| $a$ | (AU) | $6.78 \pm 0.33$ |

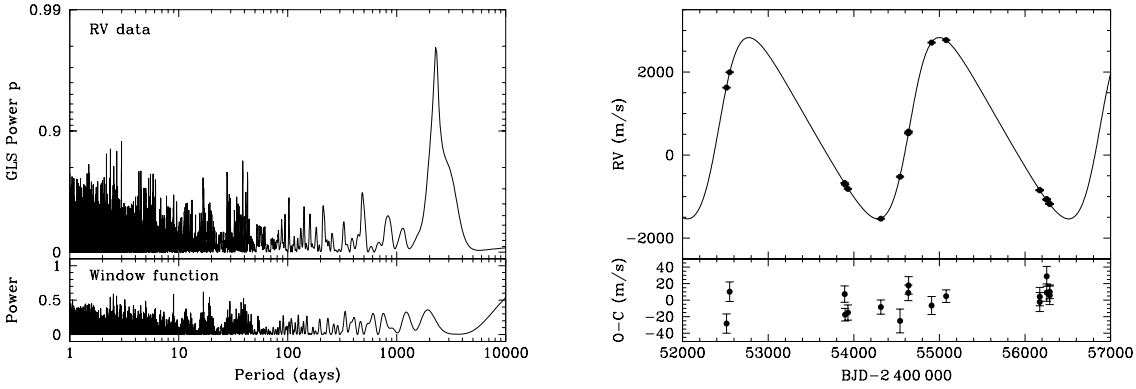


**Figure 6.7:** Results for HD 160933. *Left panel*: GLS periodogram of the RV data and window function of the observations. *Right panel*: RV measurements and best-fit Keplerian orbital solution (solid line). The RV residuals after subtracting the orbital solution are shown below.

**Table 6.7:** Orbital parameters of the stellar companion of HD 160933.

| Parameter | | Value |
|---|---|---|
| $P$ | (days) | $2226.3 \pm 2.3$ |
| $K$ | ($\mathrm{m\,s^{-1}}$) | $2183.2 \pm 7.5$ |
| $e$ | | $0.2848 \pm 0.0052$ |
| $\omega$ | (deg) | $273.2 \pm 1.1$ |
| $T_0$ | ($\mathrm{BJD} - 2\,400\,000$) | $54\,658.6 \pm 4.2$ |
| $RV_0$ | ($\mathrm{m\,s^{-1}}$) | $610.3 \pm 7.7$ |
| $N_{\mathrm{obs}}$ | | 17 |
| $\sigma_{\mathrm{O-C}}$ | ($\mathrm{m\,s^{-1}}$) | 15.3 |
| $\chi^2_{\mathrm{red}}$ | | 2.91 |
| $a_1 \sin i$ | (AU) | $0.4283 \pm 0.0017$ |
| $f(m_1, m_2, i)$ | ($M_\odot$) | $0.002114 \pm 0.000025$ |
| $m_1$ | ($M_\odot$) | $1.13^{+0.10}_{-0.04}$ |
| $m_2 \sin i$ | ($M_\odot$) | $0.1514^{+0.0079}_{-0.0032}$ |
| $a$ | (AU) | $3.624^{+0.095}_{-0.038}$ |

panel). Since the data cover more than 1.5 orbital cycles as well as the maximum and minimum of the RV curve, the orbital parameters are very well constrained (see Table 6.7). From the computed minimum mass of the companion, $0.1514^{+0.0079}_{-0.0032}\ M_\odot$, the secondary star is with high probability an M star and orbits the primary at a separation of $3.624^{+0.095}_{-0.038}$ AU.

### HD 200790

HD 200790 (HIP 104101, HR 8077, 4 Equ) has a visual magnitude of $V = 5.952 \pm 0.010$ (Høg et al. 2000), and its spectral type is F8 V (Gratton et al. 1996). Using the *Gaia* parallax of $\pi = 26.2512 \pm 0.2594$ mas (Gaia Collaboration 2018), the distance to the star is $d = 38.09 \pm 0.38$ pc. Holmberg et al. (2007) determined a stellar mass of $1.33^{+0.05}_{-0.06}\ M_\odot$ and a metallicity of $[\mathrm{Fe/H}] = -0.01$.

For this star, nine RV measurements have been gathered spanning 2104 days. The GLS periodogram shows several peaks, especially for shorter periods (7.06, 3.71, 65.69 days with $p_{\mathrm{GLS}} = 0.9974, 0.9966, 0.9957$, respectively). Nevertheless, the strongest power, $p_{\mathrm{GLS}} = 0.9979$, appears at a period of 1931 days (Figure 6.8, left panel). Due to the low number of RV data points, it was not possible to find a convergent orbital solution with *GaussFit* using a full 6-parameter Keplerian model. Thus, I fixed the eccentricity in steps of 0.001 and let all other parameters vary. For every eccentricity in this grid, I received a solution and a corresponding $\chi^2$-value. The final solution (with $e = 0.366$) was then chosen by the lowest of these $\chi^2$-values. This Keplerian model yields a period of $1973.56 \pm 0.71$ days and supports the long orbital period of the secondary star, whose minimum mass and separation were determined to be $1.091 \pm 0.027\ M_\odot$ and $4.135 \pm 0.041$ AU, respectively. The RV data and the orbit are presented in Figure 6.8 (right panel), and the parameters are given in Table 6.8.

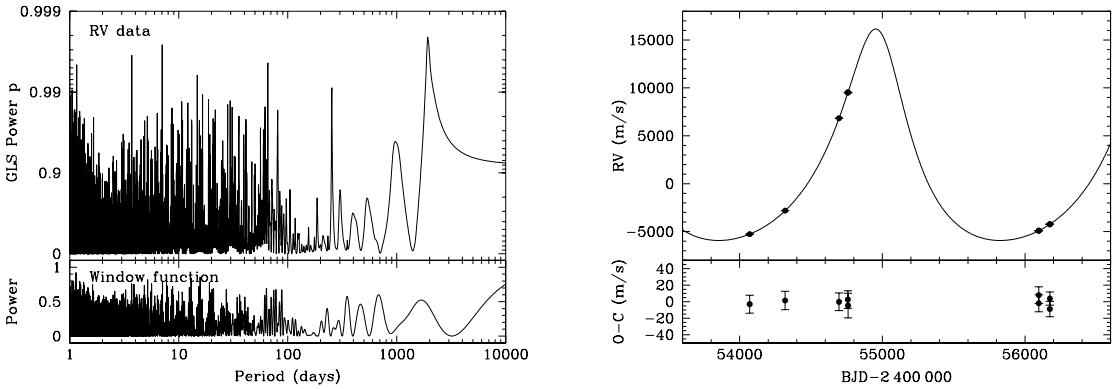


**Figure 6.8:** Results for HD 200790. *Left panel*: GLS periodogram of the RV data and window function of the observations. *Right panel*: RV measurements and best-fit Keplerian orbital solution (solid line). The RV residuals after subtracting the orbital solution are shown below.

**Table 6.8:** Orbital parameters of the stellar companion of HD 200790.

| Parameter | | Value (1) | Value (2) |
|---|---|---|---|
| $P$ | (days) | $1975.76 \pm 0.94$ | $1973.56 \pm 0.71$ |
| $K$ | ($\mathrm{m\,s^{-1}}$) | $10\,585 \pm 61$ | $11\,036 \pm 200$ |
| $e$ | | $0.3937 \pm 0.0047$ | 0.366 (fixed) |
| $\omega$ | (deg) | $14.22 \pm 0.83$ | $13.45 \pm 0.39$ |
| $T_0$ | (BJD $-$ 2 400 000) | $51\,004.2 \pm 4.2$ | $54\,985.6 \pm 7.7$ |
| $\gamma, RV_0$ | ($\mathrm{m\,s^{-1}}$) | $-19\,873 \pm 36$ | $1183 \pm 146$ |
| $N_{\mathrm{obs}}$ | | 65 | 9 |
| $\sigma_{\mathrm{O-C}}$ | ($\mathrm{m\,s^{-1}}$) | 150 | 5.0 |
| $\chi^2_{\mathrm{red}}$ | | ... | 0.51 |
| $a_1 \sin i$ | (AU) | $1.767 \pm 0.011$ | $1.863 \pm 0.034$ |
| $f(m_1, m_2, i)$ | ($M_\odot$) | $0.1886 \pm 0.0035$ | $0.222 \pm 0.012$ |
| $m_1$ | ($M_\odot$) | ... | $1.33 \pm 0.06$ |
| $m_2 \sin i$ | ($M_\odot$) | ... | $1.091 \pm 0.027$ |
| $a$ | (AU) | ... | $4.135 \pm 0.041$ |

**References:** (1) Willmarth et al. (2016); (2) This work

The first conjectures of HD 200790 being a binary came from Anderson & Kraft (1972), who obtained a $\sigma_{\mathrm{RV}} = 1.68\ \mathrm{km\,s^{-1}}$ from six spectra. Further evidence arose from 17 released RVs by Beavers & Eitter (1986) showing a range of more than $20\ \mathrm{km\,s^{-1}}$. The orbit, however, was only reported in a conference abstract (Beavers & Eitter 1988), but has never been published. Later, Nordström et al. (2004) measured a mean RV of $-22.2\ \mathrm{km\,s^{-1}}$ with a standard deviation of the mean of $5.1\ \mathrm{km\,s^{-1}}$. The first orbital elements were then published by Griffin (2011). More recently, Willmarth et al. (2016) analyzed 65 RV measurements obtained at Kitt Peak National Observatory (KPNO) and Fairborn Observatory. Their orbital parameters agree very well with those of Griffin (2011) and my work (see Table 6.8).

It is surprising to note that in the spectra there is no sign of any spectral lines from the secondary even though the determined mass function of about 0.22 $M_{\odot}$ and thus the minimum mass of the companion of about 1.09 $M_{\odot}$ are rather high. Both Griffin (2011) and Willmarth et al. (2016) provide the same findings, and they conclude that the secondary is itself a binary system, probably consisting of a pair of lower-mass dwarfs.

### HD 212754

HD 212754 (HIP 110785, HR 8548, 34 Peg) has a visual magnitude of $V = 5.75$. The stellar spectral type was determined to be F7 V by Houk & Swift (1999), while Gray et al. (2001) obtained F8 IV–V, leading towards the beginning of the evolution off the main sequence. Given the Hipparcos parallax of $\pi = 26.21 \pm 0.93$ mas (van Leeuwen 2007), the distance to the star is $d = 38.2 \pm 1.4$ pc. The stellar mass and metallicity taken from Holmberg et al. (2007) have values of $1.47^{+0.05}_{-0.06}\ M_{\odot}$ and [Fe/H] = 0.10, respectively.

The 19 RV data points taken at TLS cover a time span of 2223 days. The highest peak in the GLS periodogram is visible at a period of 971 days (Figure 6.9, left panel). A Keplerian orbital solution results in a period of $929.83 \pm 0.63$ days and an eccentricity of $e = 0.366 \pm 0.024$ (Figure 6.9, right panel). The parameters of the determined orbit are provided in Table 6.9. With a minimum mass of $0.244 \pm 0.022\ M_{\odot}$, the secondary star is probably an M dwarf orbiting at a separation of $2.231 \pm 0.029$ AU.

HD 212754 has been known to have a stochastic solution in the Hipparcos and Tycho Catalogs (ESA 1997), and a preliminary astrometric orbit was deduced from the Hipparcos data by Goldin & Makarov (2007). Moreover, Griffin & Suchkov (2003) found this star to be a single-lined spectroscopic binary, but their data were insufficient to determine an orbit. A first spectroscopic orbit was then published by Griffin (2010). This author also concluded that the orbital solution of Goldin & Makarov (2007) is rather uncertain except for the period and nearly edge-on orbital inclination.

A newly work by Willmarth et al. (2016) presented an orbit with almost identical elements based on 52 RV measurements taken at Kitt Peak National Observatory (KPNO) and Fairborn Observatory (see Table 6.9). As can be seen, the orbital pa-

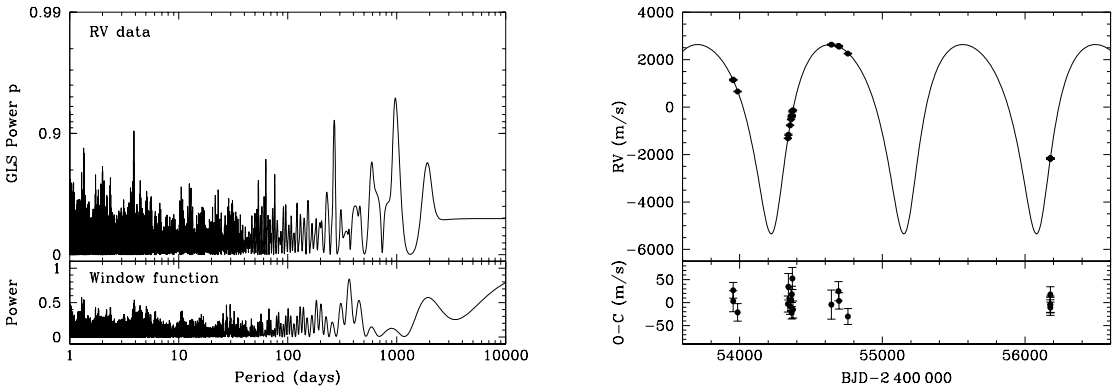


**Figure 6.9:** Results for HD 212754. *Left panel*: GLS periodogram of the RV data and window function of the observations. *Right panel*: RV measurements and best-fit Keplerian orbital solution (solid line). The RV residuals after subtracting the orbital solution are shown below.

**Table 6.9:** Orbital parameters of the stellar companion of HD 212754.

| Parameter | | Value (1) | Value (2) |
|---|---|---|---|
| $P$ | (days) | $929.91 \pm 0.46$ | $929.83 \pm 0.63$ |
| $K$ | ($\mathrm{m\,s^{-1}}$) | $5060 \pm 54$ | $3993 \pm 342$ |
| $e$ | | $0.4358 \pm 0.0062$ | $0.366 \pm 0.024$ |
| $\omega$ | (deg) | $188.5 \pm 1.1$ | $193.0 \pm 3.8$ |
| $T_0$ | ($\mathrm{BJD} - 2\,400\,000$) | $53\,293.9 \pm 3.2$ | $54\,235.7 \pm 10.3$ |
| $\gamma, RV_0$ | ($\mathrm{m\,s^{-1}}$) | $-16\,110 \pm 25$ | $66 \pm 130$ |
| $N_{\mathrm{obs}}$ | | 52 | 19 |
| $\sigma_{\mathrm{O-C}}$ | ($\mathrm{m\,s^{-1}}$) | 160 | 21.2 |
| $\chi^2_{\mathrm{red}}$ | | ... | 1.60 |
| $a_1 \sin i$ | (AU) | $0.3893 \pm 0.0044$ | $0.318 \pm 0.028$ |
| $f(m_1, m_2, i)$ | ($M_\odot$) | $0.00910 \pm 0.00030$ | $0.0049 \pm 0.0013$ |
| $m_1$ | ($M_\odot$) | 1.4 | $1.47 \pm 0.06$ |
| $m_2 \sin i$ | ($M_\odot$) | ... | $0.244 \pm 0.022$ |
| $a$ | (AU) | ... | $2.231 \pm 0.029$ |
| $a_0$ | (mas) | $9.5 \pm 0.3$ | ... |
| $i$ | (deg) | $94.0 \pm 5.0$ | ... |
| $m_2$ | ($M_\odot$) | 0.29 | ... |

**References:** (1) Willmarth et al. (2016); (2) This work

rameters are in very good agreement to the ones obtained in my analysis except for the $K$-amplitude and eccentricity, which differ by more than 2 $\sigma$. This is basically because of the poor coverage near the RV minimum. Nevertheless, using the parameters of Willmarth et al. (2016) would increase the minimum mass of the secondary only to about 0.30 $M_\odot$. Furthermore, Willmarth et al. (2016) could obtain an astrometric solution using the parameters from their spectroscopic orbit. They derived an angular separation, $a_0 = 9.5 \pm 0.3$ mas, and an inclination, $i = 94\overset{\circ}{.}0 \pm 5\overset{\circ}{.}1$. From evolutionary tracks of Girardi et al. (2000), they estimated the stellar mass to be 1.4 $M_\odot$ resulting in a secondary mass of 0.29 $M_\odot$.

### HD 220242

HD 220242 (HIP 115360, HR 8888) is listed as F5 V star in the Simbad database with a visual magnitude of $V = 6.586 \pm 0.010$ (Høg et al. 2000). The star is located at a distance of $d = 71.10 \pm 0.28$ pc according to the *Gaia* parallax of $\pi = 14.0638 \pm 0.0546$ mas (Gaia Collaboration 2018). Its mass and metallicity, as derived by Holmberg et al. (2007), are $1.60^{+0.05}_{-0.04}$ $M_\odot$ and [Fe/H] = −0.06, respectively.

I acquired eigth RV measurements that are spread over 2105 days. Decreasing by more than 7.2 km s$^{-1}$ within this period of time, these RV data clearly show a long-term trend consistent with a binary companion (Figure 6.10, right panel, filled circles). Moreover, the last two measurements also indicate a little bit of curvature. Applying a GLS periodogram to the data, there is a strong signal present at a period of 8447 days (Figure 6.10, left panel). Because of the low number of data points, I searched only for a circular orbit with *GaussFit*. The best solution yields a period of 8450 ± 720 days and is given in Table 6.10. The consequent minimum mass of the companion, which would orbit at a separation of 11.25 ± 0.67 AU, is 1.06 ± 0.10 $M_\odot$.

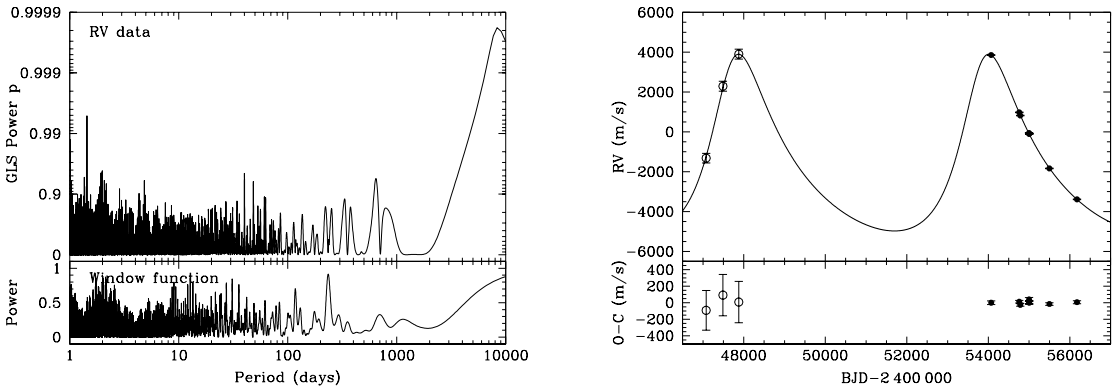


**Figure 6.10:** Results for HD 220242. *Left panel*: GLS periodogram of the RV data and window function of the observations. *Right panel*: RV measurements from TLS (filled circles) and Nordström et al. (1997, open circles). The best-fit Keplerian orbital solution of the combined data is plotted as a solid line. The RV residuals after subtracting the orbital solution are shown below.

**Table 6.10:** Orbital parameters of the stellar companion of HD 220242.

| Parameter | | Value (1) | Value (2) |
|---|---|---|---|
| $P$ | (days) | $8450 \pm 720$ | $6140 \pm 130$ |
| $K$ | ($\mathrm{m\,s^{-1}}$) | $5790 \pm 520$ | $4430 \pm 160$ |
| $e$ | | 0 (fixed) | $0.372 \pm 0.043$ |
| $\omega$ | (deg) | 0 (fixed) | $330.3 \pm 4.4$ |
| $T_0$ | (BJD $- 2\,400\,000$) | $52\,360 \pm 280$ | $53\,789 \pm 55$ |
| $RV_{0_1}$ | ($\mathrm{m\,s^{-1}}$) | $2140 \pm 440$ | $-1970 \pm 350$ |
| $RV_{0_2}$ | ($\mathrm{m\,s^{-1}}$) | ... | $7960 \pm 460$ |
| $N_{\mathrm{obs}}$ | | 8 | 11 |
| $\sigma_{\mathrm{O-C}}$ | ($\mathrm{m\,s^{-1}}$) | 25.0 | 19.9 (TLS RVs)<br>44.6 (all RVs) |
| $\chi^2_{\mathrm{red}}$ | | 3.96 | 2.06 |
| $a_1 \sin i$ | (AU) | $4.50 \pm 0.55$ | $2.32 \pm 0.11$ |
| $f(m_1, m_2, i)$ | ($M_\odot$) | $0.170 \pm 0.048$ | $0.0443 \pm 0.0053$ |
| $m_1$ | ($M_\odot$) | $1.60 \pm 0.05$ | $1.60 \pm 0.05$ |
| $m_2 \sin i$ | ($M_\odot$) | $1.06 \pm 0.10$ | $0.598 \pm 0.026$ |
| $a$ | (AU) | $11.25 \pm 0.67$ | $8.53 \pm 0.15$ |

**References:** (1) TLS RV data; (2) TLS RV data including three RV measurements from Nordström et al. (1997)

Nordström et al. (1997) published three RV measurements for this star that were taken in the late 1980s. These data are also presented in Figure 6.10 (right panel, open circles) and included in the orbit analysis. Although having much poorer precision, these additional RV points helped to improve the orbital solution. The final Keplerian orbit using the combined data has a period of $6140 \pm 130$ days and an eccentricity of $e = 0.372 \pm 0.043$. In this case, the resulting minimum mass of the secondary star decreases to a more realistic value of $0.598 \pm 0.026\ M_\odot$. Thus, the companion is most likely a K dwarf orbiting at a semi-major axis of $8.53 \pm 0.15$ AU.

### HD 33185, HD 74243, HD 101606 and HD 120510

The iodine cell method for determining the RVs, as described in section 4.1, is inapplicable for SB2 systems because the spectral lines of both stellar components are moving against each other, causing problems when modelling the individual observations and comparing them with the template. However, it is known from the literature that the stars HD 33185, HD 74243, HD 101606 and HD 120510, which belong to the investigated sample, are SB2 systems. I therefore provide these orbits in Tables 6.11 and 6.12.

The orbital periods range from 28 to 1469 days. The orbits are eccentric, two of them having even eccentricities of more than 0.85. The minimum masses of the components, $m_{1,2} \sin^3 i$, are about 1 $M_\odot$ for HD 101606 and HD 120510, implying an orbital inclination near 90°. In contrast, HD 33185 must have a very low inclination because the minimum masses of its components are below 0.1 $M_\odot$.

**Table 6.11:** Orbital parameters of the stellar companions of HD 33185 and HD 74243.

| Parameter | | HD 33185 (1) | HD 74243 (2) |
|---|---|---|---|
| $P$ | (days) | $1469.41 \pm 0.58$ | $700.3 \pm 1.0$ |
| $K_1$ | ($\mathrm{km\,s^{-1}}$) | $8.65 \pm 1.21$ | $13.39 \pm 0.14$ |
| $K_2$ | ($\mathrm{km\,s^{-1}}$) | $13.95 \pm 1.65$ | $12.97 \pm 0.25$ |
| $e$ | | $0.9021 \pm 0.0090$ | $0.381 \pm 0.010$ |
| $\omega$ | (deg) | $271.6 \pm 17.1$ | $174.5 \pm 2.1$ |
| $T_0$ | (BJD $-$ 2 400 000) | $49\,346.79 \pm 3.95$ | $52\,388.3 \pm 2.7$ |
| $\gamma$ | ($\mathrm{km\,s^{-1}}$) | $-3.982 \pm 0.214$ | $1.43 \pm 0.11$ |
| $N_1, N_2$ | | 23 | 48, 48 |
| $\sigma_{\mathrm{O-C}}$ | ($\mathrm{km\,s^{-1}}$) | 1.160 | 0.68 |
| $a_1 \sin i$ | ($10^6$ km) | $44.51 \pm 4.01$ | $119.2 \pm 1.3$ |
| $a_2 \sin i$ | ($10^6$ km) | $60.83 \pm 4.96$ | $115.4 \pm 2.3$ |
| $m_1 \sin^3 i$ | ($M_\odot$) | $0.087 \pm 0.036$ | $0.518 \pm 0.024$ |
| $m_2 \sin^3 i$ | ($M_\odot$) | $0.054 \pm 0.023$ | $0.535 \pm 0.017$ |

**References:** (1) Halbwachs et al. (2012); (2) Griffin (2007)

**Table 6.12:** Orbital parameters of the stellar companions of HD 101606 and HD 120510.

| Parameter | | HD 101606 (1) | HD 120510 (2) |
|---|---|---|---|
| $P$ | (days) | $267.5078 \pm 0.0012$ | $28.3974 \pm 0.0007$ |
| $K_1$ | ($\mathrm{km\,s^{-1}}$) | $39.07 \pm 0.11$ | $51.83 \pm 0.12$ |
| $K_2$ | ($\mathrm{km\,s^{-1}}$) | $41.84 \pm 0.16$ | $52.20 \pm 0.16$ |
| $e$ | | $0.8526 \pm 0.0006$ | $0.5454 \pm 0.0015$ |
| $\omega$ | (deg) | $195.65 \pm 0.16$ | $17.45 \pm 0.27$ |
| $T_0$ | (BJD $-$ 2 400 000) | $47\,328.038 \pm 0.018$ | 51 778.212 |
| $\gamma$ | ($\mathrm{km\,s^{-1}}$) | $31.51 \pm 0.07$ | $-19.97 \pm 0.08$ |
| $N_1, N_2$ | | 88, 85 | 28, 27 |
| $\sigma_{\mathrm{O-C}}$ | ($\mathrm{km\,s^{-1}}$) | 0.48 | ... |
| $a_1 \sin i$ | ($10^6$ km) | $75.08 \pm 0.25$ | $16.96 \pm 0.04$ |
| $a_2 \sin i$ | ($10^6$ km) | $80.40 \pm 0.34$ | $17.09 \pm 0.06$ |
| $m_1 \sin^3 i$ | ($M_\odot$) | $1.085 \pm 0.010$ | $0.981 \pm 0.008$ |
| $m_2 \sin^3 i$ | ($M_\odot$) | $1.013 \pm 0.009$ | $0.974 \pm 0.007$ |

**References:** (1) Griffin et al. (1999); (2) Griffin & Suchkov (2003)

### 6.1.2 Spectroscopic binaries without orbit

Here, I will present ten stars of my sample that show long-term RV trends. The data of these stars cover time spans between ∼1550 and ∼2500 days (except for one target with only 344 days), and the peak-to-peak RV variations range from ∼650 to nearly 8000 m s$^{-1}$. Thus, probably all of these objects are spectroscopic binaries, whose orbital periods are exceeding the times the stars were monitored. Most of the RV measurements do not only show a monotonic de- or increasing behavior but also some curvature, in four cases even a turnaround. Nevertheless, the determination of an orbit was not possible for none of the stars. The stars are ordered again according to their HD number.

#### HD 21794

HD 21794 (HIP 16602, HR 1071) is an F7 V star (Appenzeller 1967) with a visual magnitude of $V = 6.380 \pm 0.009$ (Oja 1991). Given the *Gaia* parallax of $\pi = 14.3588 \pm 0.1615$ mas (Gaia Collaboration 2018), the distance to the star is $d = 69.64 \pm 0.78$ pc. Holmberg et al. (2007) provided a metallicity of [Fe/H] = −0.20, but no stellar mass.

The binary nature of this system has been discovered in 1985 in a speckle interferometric survey carried out by Lu et al. (1987) using the CHARA speckle camera system at the KPNO 4 m telescope. After more observation were taken the following years, McAlister et al. (1992) were able to determine a preliminary 13.8-year orbit. They estimated the magnitude difference of the two components to be $\Delta m = 0.2$ mag, which is equivalent to about one spectral subclass for late F-type stars. From the corresponding mass ratio of 1.03, they obtained a mass of 1.21 $M_\odot$ for the primary and 1.17 $M_\odot$ for the secondary star. Furthermore, they provided an RV curve for the years 1990–2010 for both components assuming mass ratios of 1 and 1.2.

Later on, Balega et al. (2002) performed additional interferometric speckle observations with the 6 m telescope of the Special Astrophysical Observatory in Zelenchuk (Russia) and presented improved orbital parameters. They determined $P = 14.47 \pm 0.07$ yr, $T_0 = 1990.15 \pm 0.03$, $e = 0.35 \pm 0.01$, $a = 0\farcs120 \pm 0\farcs001$, $i = 46° \pm 1°$, $\omega = 236° \pm 1°$ and $\Omega = 235° \pm 1°$. They also derived the spectral types of the primary and secondary star to be F0 and F1, respectively, according to the parallax, $V$-magnitude and their $\Delta m$.

I took 17 RV measurements spanning 2246 days. The peak-to-peak RV amplitude is about 650 m s$^{-1}$. An RV minimum is clearly visible at BJD = 2 454 427 (November 2007; see Figure 6.11, left panel). While the time of the predicted RV minimum from McAlister et al. (1992), appearing in the year 2007, agrees very well with the RV minimum in my data, the increase of the RV within the next three years is much less in my data. This would point to a highly inclined orbit in respect to the line of sight, i.e., the orbit is seen nearly pole-on, or the mass of the secondary star should be much less than the mass of the primary.

### HD 89995

HD 89995 (HIP 50870, HR 4079) has a visual magnitude of $V = 6.54$, and Cenarro et al. (2007) obtained a spectral type of F6 V. The distance to the star, as determined from the *Gaia* parallax of $\pi = 17.1102 \pm 0.0850$ mas (Gaia Collaboration 2018), is $d = 58.44 \pm 0.29$ pc. Holmberg et al. (2007) derived a stellar mass of $1.33^{+0.05}_{-0.06}\ M_\odot$ and a metallicity of [Fe/H] $= -0.31$.

The seven RV points cover 1553 days. They show peak-to-peak variations of roughly 3700 m s$^{-1}$ (see Figure 6.11, right panel), indicating the binary nature of this star. Although some kind of curvature is present in the data, the low number of data points and the poor time coverage did not allow the program to calculate a conclusive orbit.

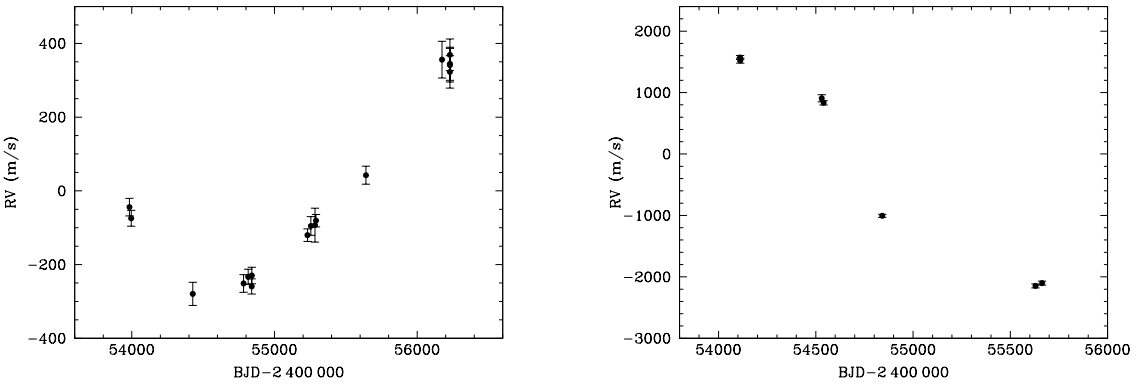


**Figure 6.11:** RV measurements for HD 21794 (*left panel*) and HD 89995 (*right panel*).

### HD 102988

HD 102988 (HIP 57821) has a visual magnitude of $V = 7.055 \pm 0.010$ (Høg et al. 2000). Its spectral type is given by Harlan (1969) to be F6 V. According to the *Gaia* parallax of $\pi = 18.7192 \pm 0.1742$ mas (Gaia Collaboration 2018), the star is located at a distance of $d = 53.42 \pm 0.50$ pc. The following values for the stellar mass and metallicity were determined by Holmberg et al. (2007): $1.16^{+0.08}_{-0.07}\ M_\odot$ and [Fe/H] $= -0.25$, respectively.

The six RV measurements observed at TLS, comprising a time span of 1714 days, yield peak-to-peak variations of nearly 5900 m s$^{-1}$ (see Figure 6.12, left panel). Again, the low number of data points and the poor time sampling did not result in the determination of an orbit.

### HD 122797

The F4 V star HD 122797 (HIP 68707, HR 5275) has a visual magnitude of $V = 6.238 \pm 0.009$ (Høg et al. 2000). The *Gaia* parallax of $\pi = 15.5203 \pm 0.0732$ mas (Gaia Collaboration 2018) results in a distance to the star of $d = 64.43 \pm 0.30$ pc.

Holmberg et al. (2007) obtained a stellar mass of $1.55 \pm 0.06\ M_\odot$ and a metallicity of [Fe/H] = −0.19.

During a timeframe of 1848 days, eight RV measurements have been taken (see Figure 6.12, right panel). The time sampling – the data are clustered around only three areas – is inadequate to calculate an orbit. Nonetheless, the large difference between maximum and minimum RV ($\sim 7900\ \mathrm{m\,s^{-1}}$) clearly points to binarity.

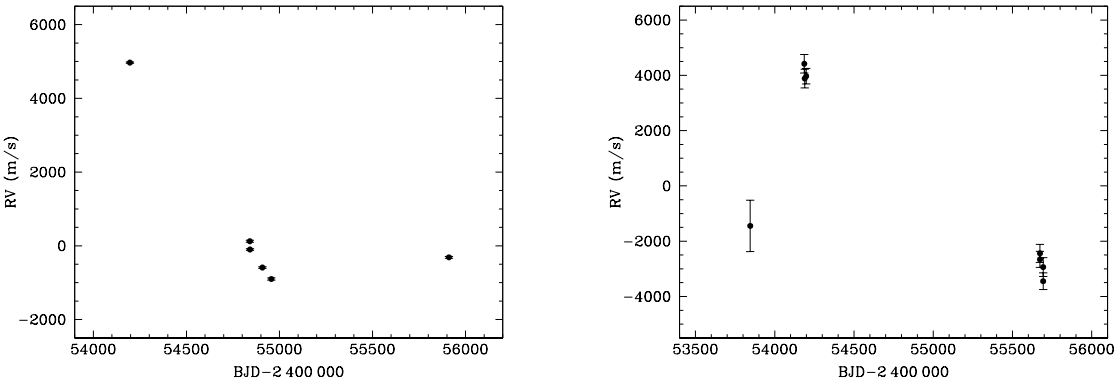


**Figure 6.12:** RV measurements for HD 102988 (*left panel*) and HD 122797 (*right panel*).

### HD 130173

HD 130173 (HIP 72029) is listed as F3 V star in the Simbad database with a visual magnitude of $V = 6.87 \pm 0.01$ (Høg et al. 2000). The distance to the star is $d = 93.62 \pm 0.94$ pc, as calculated from the *Gaia* parallax of $\pi = 10.6813 \pm 0.1069$ mas. The star has a mass of $1.52^{+0.08}_{-0.06}\ M_\odot$ and a metallicity of [Fe/H] = −0.37 (Holmberg et al. 2007).

Even though the star was monitored for only 344 days, the six RV measurements show an increase of almost $5700\ \mathrm{m\,s^{-1}}$ with curvature (see Figure 6.13, left panel), identifying this star to be a binary. This period of time, however, is insufficient to provide any orbital parameters.

### HD 157373

HD 157373 (HIP 84855, HR 6467) has a visual magnitude of $V = 6.43$. While it is listed as F4 V star in Simbad, Barry (1970) classified it as F6 V. The *Gaia* parallax of $\pi = 26.0519 \pm 0.0247$ mas (Gaia Collaboration 2018) yields a distance to the star of $d = 38.385 \pm 0.036$ pc. Holmberg et al. (2007) derived a stellar mass of $1.18^{+0.03}_{-0.10}\ M_\odot$ and a metallicity of [Fe/H] = −0.47.

The 22 RV measurements taken over 2477 days show a linear trend with an increase of about $1700\ \mathrm{m\,s^{-1}}$ (Figure 6.13, right panel). The orbit of the likely stellar companion is thus not yet determinable and must have a very long period, considerably exceeding the observed time span.

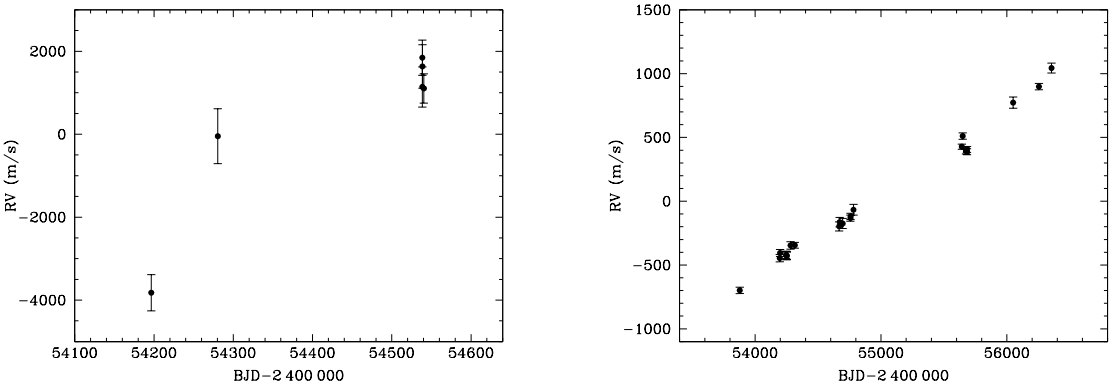


**Figure 6.13:** RV measurements for HD 130173 (*left panel*) and HD 157373 (*right panel*).

### HD 176051

HD 176051 (HIP 93017, HR 7162) has a visual magnitude of $V = 5.25$ (Rakos et al. 1982). This visual binary consists of an F9 V primary and a K1 V secondary (Edwards 1976). Based on the Hipparcos parallax of $\pi = 67.24 \pm 0.37$ mas (van Leeuwen 2007), the distance to the star is $d = 14.87 \pm 0.08$ pc. Mass and metallicity of the star were measured by Holmberg et al. (2007) to be $0.98^{+0.05}_{-0.04}\ M_\odot$ and [Fe/H] $= -0.19$, respectively.

Pannunzio & Delgrosso (1980) determined the provisional orbital elements of this visual binary using two methods. After applying a differential correction to these values, they obtained the corrected orbital elements: $P = 61.39$ yr $\widehat{=}$ 22 423 d, $T_0 = 1972.22 \widehat{=} 2\,441\,398$, $e = 0.25$, $a = 1''.25$, $i = 114^\circ.19$, $\omega = 281^\circ.61$ and $\Omega = 48^\circ.70$.

A very preliminary SB1 orbit was published by Duquennoy & Mayor (1991) using 16 RV measurements from a CORAVEL spectroscopic survey and the aforementioned visual elements $P$, $T_0$, $e$ and $\omega$ as fixed values. They obtained an RV amplitude of $K = 3.51 \pm 0.74$ km s$^{-1}$ and an RV offset of $\gamma = -45.82 \pm 0.69$ km s$^{-1}$. With $i = 115^\circ$ and $M_1 = 1\ M_\odot$, they further derived $M_2 = 0.71\ M_\odot$.

Later, Muterspaugh et al. (2010) announced the detection of a sub-stellar companion candidate around one of the stars in the HD 176051 system. This object was found by means of differential astrometry in the framework of the Palomar High-precision Astrometric Search for Exoplanet Systems (PHASES). The orbital parameters of the stellar and sub-stellar companions were determined in a double Keplerian model, where the eccentricity of the sub-stellar orbit was fixed to zero. This model revealed an orbital period of $P = 1016 \pm 40$ days and a planetary mass of $m_\mathrm{p} = 1.5 \pm 0.3\ M_\mathrm{Jup}$, assuming a distance of 15 pc and a stellar mass of 0.71 $M_\odot$. As stated by Muterspaugh et al. (2010), the planet would have twice the mass if it would revolve around the A component (1.07 $M_\odot$). The Extrasolar Planets Encyclopaedia provides orbital separations of 1.76 and 2.02 AU for these two cases.

I have acquired seven RV measurements within a timeframe of 2007 days. During that time, the RV rises almost linearly by $\sim 850$ m s$^{-1}$ (Figure 6.14, left panel). The determination of the definite binary orbit needs far more long-term monitoring of

this target because the RV data cover less than 10% of the supposed orbital period. Unfortunately, the amount and sampling of the RV data is too poor to find any signatures of the purported planet. Since it cannot be confirmed by RVs and since it is unclear around which component it orbits, I will not consider this planet in my statistical analysis.

### HD 184151

HD 184151 (HIP 96081) has a spectral type of F5 V (Harlan 1969) and a visual magnitude of $V = 6.870 \pm 0.009$ (Høg et al. 2000). The distance to the star is $d = 80.85 \pm 0.27$ pc, as determined from the *Gaia* parallax of $\pi = 12.3681 \pm 0.0409$ mas. The stellar mass is $1.44^{+0.06}_{-0.05}$ $M_\odot$, and the metallicity amounts to [Fe/H] $= -0.36$ (Holmberg et al. 2007).

The 16 RV points are distributed over a time of 2356 days. They exhibit a rather linear increase of about 2300 m s$^{-1}$, only the last measurements deviate slightly from this linear trend (Figure 6.14, right panel). Whether this is a first hint of an upcoming trend reversal needs to be investigated with future observations. Nevertheless, it is beyond question that the companion is of stellar nature.

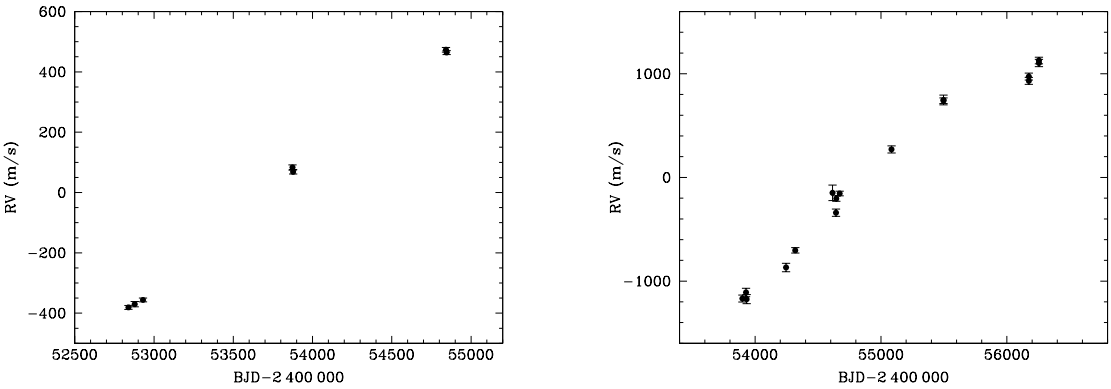


**Figure 6.14:** RV measurements for HD 176051 (*left panel*) and HD 184151 (*right panel*).

### HD 192455

HD 192455 (HIP 99500, HR 7727, 68 Dra) is an F5 V star (Balachandran 1990) and has a visual magnitude of $V = 5.700 \pm 0.009$ (Høg et al. 2000). The *Gaia* parallax is $\pi = 21.0725 \pm 0.0580$ mas (Gaia Collaboration 2018), corresponding to a distance to the star of $d = 47.46 \pm 0.13$ pc. Holmberg et al. (2007) obtained a stellar mass of $1.66^{+0.05}_{-0.04}$ $M_\odot$ and a metallicity of [Fe/H] $= 0.20$.

The star has been monitored for 2445 days, and the 36 RV measurements show the upper turnaround of the RV curve (Figure 6.15, left panel). The difference between the observed maximum and minimum RV is nearly 2600 m s$^{-1}$. Considering the curvature of the RV curve, its minimum is far from being reached, and the orbital period of this probable binary companion must be very long. Note that some of the

points deviate significantly from the curve. To investigate these residuals, however, requires an acceptable orbit, for which a longer time coverage is necessary.

### HD 212395

HD 212395 (HIP 110548, HR 8532, 33 Peg) has a visual magnitude of $V = 6.200 \pm 0.009$ (Oja 1991). Its spectral type was determined to be F7 V by Harlan & Taylor (1970); Abt (1985), on the other hand, classified the star as F7 IV. The *Gaia* parallax of $\pi = 30.0180 \pm 0.0552$ mas (Gaia Collaboration 2018) translates into a distance to the star of $d = 33.31 \pm 0.06$ pc. The mass of the star, $1.09 \pm 0.04\ M_\odot$, and its metallicity, [Fe/H] $= -0.25$, were given by Holmberg et al. (2007).

Sixteen RV data points have been recorded covering a time baseline of 2518 days. As can be seen in Figure 6.15 (right panel), the RV is rising by $\sim 950\ \mathrm{m\,s^{-1}}$ with a declining slope, approximating its maximum. Again, the RV curve is probably caused by a very long-period binary.

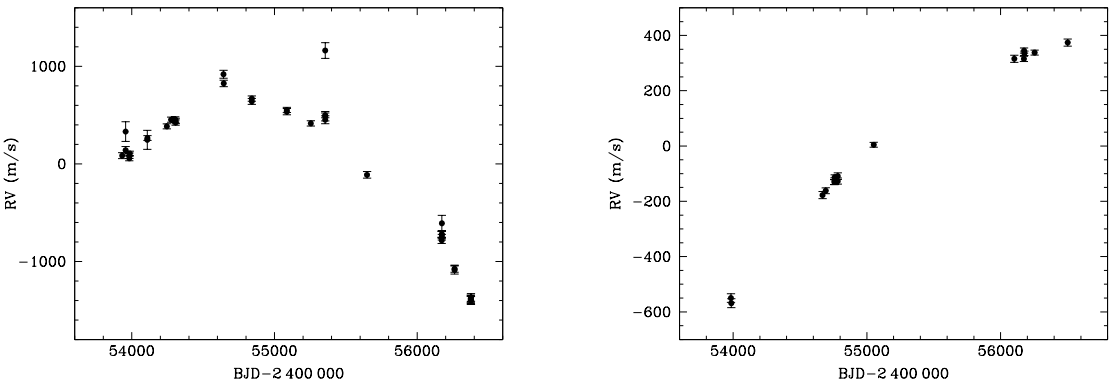


**Figure 6.15:** RV measurements for HD 192455 (*left panel*) and HD 212395 (*right panel*).

### 6.1.3 Sub-stellar companions

In the following section, I will introduce the stars that harbor an extrasolar planet or a brown dwarf. I will start with three objects, around which I discovered a sub-stellar companion, followed by three further stars that host a planet, which were previously published by other planet-hunting groups. Both parts are ordered chronologically by the date of detection. I will provide information on the stellar properties, present the RV measurements with the calculated orbits and compare the orbital elements with values from the literature.

#### HD 16232 (30 Ari B)

The 30 Arietis system (hereafter 30 Ari) is one of the most exotic exoplanetary systems. 30 Ari is a bound visual binary with a separation of $38\farcs2 \pm 0\farcs7$ (Shatsky 2001) consisting of the main components 30 Ari A (HD 16246, HIP 12189, HR 765) and 30 Ari B (HD 16232, HIP 12184, HR 764). Using their *Gaia* parallaxes, the mean distance to the two stars is 44.955 pc, yielding a projected distance between the two stars of 1717 AU. Both components have similar spectral types (F5 V and F6 V) and brightnesses ($V$-magnitudes of 6.48 and 7.09, respectively). The stellar masses, radii and ages were determined using average values for the effective temperatures, $T_{\rm eff}$, and metallicities, [Fe/H], found in the literature and following the method described in da Silva et al. (2006) which is based on evolutionary tracks from Girardi et al. (2000). A summary of the stellar properties is given in Table 6.13.

**Table 6.13:** Stellar properties of the 30 Ari components.

| Parameter | | 30 Ari A | 30 Ari B | Reference |
|---|---|---|---|---|
| Spectral type | | F5V | F6V | (1) |
| $V$ | (mag) | 6.48 | 7.09 | (2) |
| $\pi$ | (mas) | $22.1261 \pm 0.0726$ | $22.3641 \pm 0.0516$ | (3) |
| $d$ | (pc) | $45.1955 \pm 0.1483$ | $44.7145 \pm 0.1031$ | (3) |
| $v \sin i$ | ($\mathrm{km\,s^{-1}}$) | $38.5 \pm 2.6$ | $38.3 \pm 1.8$ | (1) |
| $M_\star$ | ($M_\odot$) | $1.31 \pm 0.04$ | $1.16 \pm 0.04$ | (1) |
| $R_\star$ | ($R_\odot$) | $1.37 \pm 0.03$ | $1.13 \pm 0.03$ | (1) |
| Age | (Gyr) | $0.86 \pm 0.63$ | $0.91 \pm 0.83$ | (1) |

**References:** (1) Guenther et al. (2009); (2) Simbad database; (3) Gaia Collaboration (2018)

30 Ari A is a single-line spectroscopic binary with an orbital period of $1.109526 \pm 0.000010$ days, an eccentricity of $0.062 \pm 0.012$ and an amplitude of $22.41 \pm 0.31$ $\mathrm{km\,s^{-1}}$ (Morbey & Brosterhus 1974). It was detected to be an X-ray source by Rosat with a count rate of $0.472 \pm 0.046$ $\mathrm{cts\,s^{-1}}$ (Zickgraf et al. 2003).

The RV data obtained for 30 Ari B clearly reveal a significant signal at a period of $\sim 348$ days (Figure 6.16, left panel). Originally based on 98 RVs spanning 2213 days, I determined a Keplerian orbital solution with a period of $335.1 \pm 2.5$ days, an eccentricity of $0.289 \pm 0.092$ and an amplitude of $272 \pm 24$ $\mathrm{m\,s^{-1}}$ which is consistent with a

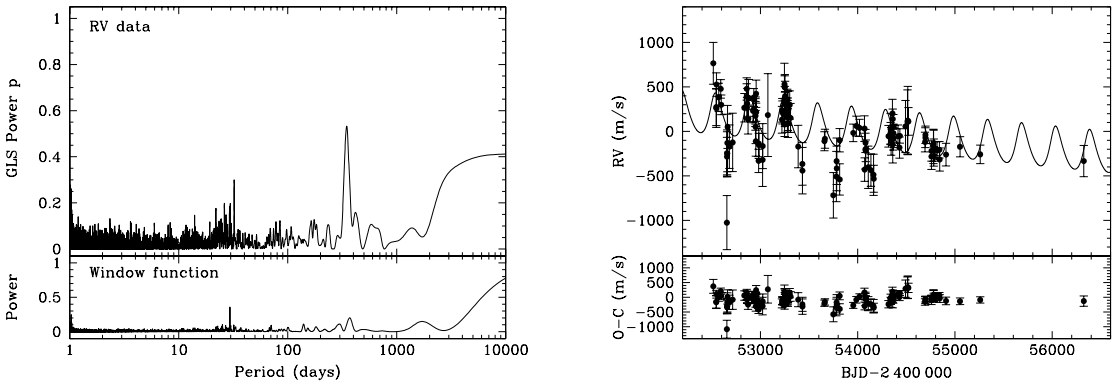


**Figure 6.16:** Results for 30 Ari B. *Left panel*: GLS periodogram of the RV data and window function of the observations. *Right panel*: RV measurements and best-fit Keplerian orbital solution including a linear trend (solid line). The RV residuals after subtracting the orbital solution are shown below.

**Table 6.14:** Orbital parameters of the sub-stellar companion of 30 Ari B.

| Parameter | | Value (1) | Value (2) | Value (3) |
|---|---|---|---|---|
| $P$ | (days) | $335.1 \pm 2.5$ | $345.4 \pm 3.8$ | $349.7 \pm 2.5$ |
| $K$ | ($\mathrm{m\,s^{-1}}$) | $272 \pm 24$ | $177 \pm 26$ | $232 \pm 35$ |
| $e$ | | $0.289 \pm 0.092$ | $0.18 \pm 0.11$ | $0.21 \pm 0.12$ |
| $\omega$ | (deg) | $307 \pm 18$ | $337 \pm 57$ | $334 \pm 35$ |
| $T_0$ | (BJD $-$ 2 400 000) | $54\,538 \pm 20$ | $53\,222.1 \pm 42.4$ | $53\,221 \pm 30$ |
| $RV_0$ | ($\mathrm{m\,s^{-1}}$) | $\cdots$ | $9.8 \pm 17.7$ | $\cdots$ |
| $dv/dt$ | ($\mathrm{m\,s^{-1}\,day^{-1}}$) | 0.0 | $-0.12 \pm 0.03$ | $-0.107 \pm 0.027$ |
| $N_{\mathrm{obs}}$ | | 98 | 110 | 115 |
| $\sigma_{\mathrm{O-C}}$ | ($\mathrm{m\,s^{-1}}$) | 135 | 181.5 | 199.5 |
| $\chi^2_{\mathrm{red}}$ | | 0.75 | 0.82 | 1.27 |
| $a_1 \sin i$ | ($10^{-3}$ AU) | $8.02 \pm 0.74$ | $\cdots$ | $7.3 \pm 1.1$ |
| $f(m_1, m_2, i)$ | ($10^{-7}\,M_\odot$) | $6.1 \pm 1.7$ | $\cdots$ | $4.2 \pm 2.0$ |
| $m_1$ | ($M_\odot$) | $1.16 \pm 0.04$ | $1.16 \pm 0.04$ | $1.16 \pm 0.04$ |
| $m_2 \sin i$ | ($M_{\mathrm{Jup}}$) | $9.88 \pm 0.94$ | $6.6 \pm 0.9$ | $8.7 \pm 1.4$ |
| $a$ | (AU) | $0.995 \pm 0.012$ | $1.01 \pm 0.01$ | $1.023 \pm 0.013$ |

**References:** (1) Guenther et al. (2009); (2) Kane et al. (2015); (3) This work

sub-stellar companion with a minimum mass of $9.88 \pm 0.94\ M_{\mathrm{Jup}}$. This detection was reported in a second-author paper (Guenther et al. 2009). The orbital parameters are given in Table 6.14 (solution 1).

After I collected additional RV measurements and expanded the time baseline by $\sim 300$ days, it was possible to include a linear RV trend ($dv/dt$) as a free parameter into the Keplerian fitting procedure. This updated solution was recently presented in a joint publication (Kane et al. 2015). As can be seen from those new orbital parameters also listed in Table 6.14 (solution 2), there are some changes compared to the solution of Guenther et al. (2009). First, the linear trend is significant at the

$4\,\sigma$ level. Second, the orbital period is marginally higher. Third, the orbit is less eccentric, and last, the RV amplitude is considerably decreased. As a consequence, the minimum mass for the companion is smaller ($6.6 \pm 0.9\ M_{\rm Jup}$), making the planetary nature of the companion more likely.

Including the most recent RV measurements enlarges the data set by another 1273 days to a total of 3809 days. Applying *GaussFit* to model a Keplerian orbit and a linear trend simultaneously results in the third solution presented in Table 6.14. The linear slope of the RV data is still valid at a confidence level of 4 $\sigma$. The orbital period amounts to $349.7 \pm 2.5$ days, the eccentricity to $0.21 \pm 0.12$ and the amplitude to $232 \pm 35\ \mathrm{m\,s^{-1}}$. The minimum mass of the companion is thus $8.7 \pm 1.4\ M_{\rm Jup}$. Both the entire RV data set (115 measurements) and this orbital solution are shown in Figure 6.16 (right panel).

### HD 8673

HD 8673 (HIP 6702, HR 410) is classified as F7 V star (Boesgaard & Friel 1990) and listed with a visual magnitude of $V = 6.31$ in Simbad. Given the *Gaia* parallax of $\pi = 26.3828 \pm 0.0375$ mas (Gaia Collaboration 2018), the distance to the star is $d = 37.90 \pm 0.05$ pc.

Hartmann et al. (2010) have already discovered a sub-stellar companion with a minimum mass of 14.2 $M_{\rm Jup}$ in a long-period ($P = 1634$ days), highly eccentric ($e = 0.723$) orbit based on 135 RV measurements taken over more than one orbital cycle. The stellar mass has been published by several authors: Valenti & Fischer (2005), Holmberg et al. (2007), Takeda et al. (2007), Fuhrmann (2008) and Tsantaki et al. (2014) provide values of $1.36 \pm 0.20\ M_\odot$, $1.28^{+0.05}_{-0.04}\ M_\odot$, $1.312^{+0.024}_{-0.020}\ M_\odot$, $1.39\ M_\odot$, and $1.35 \pm 0.10\ M_\odot$, respectively. All these values are more or less the same. To be consistent and for a direct comparison of the companion mass between Hartmann et al. (2010) and this work, however, I selected the mass from Valenti & Fischer (2005). With [Fe/H] $= -0.01$ (Holmberg et al. 2007), the metallicity of the star is similar to that of the Sun.

Here, I provide 17 additional measurements increasing the data set to a total number of 152 RVs and the time span to 3789 days, i.e., more than two orbital cycles. The highest peak in the GLS periodogram is visible at a period of 1610 days (Figure 6.17, left panel). The Keplerian orbital solution is in very good agreement to the one derived by Hartmann et al. (2010), except that the period is shorter by $\sim 50$ days. Although the rms about the fit is only slightly worse, the reduced $\chi^2$ is now significantly higher (compare solution 1 and 2 in Table 6.15). I then tried a Keplerian model including a linear trend and the resulting fit was considerably improved (Table 6.15, solution 3). The inclusion of the linear trend, significant at a $10\,\sigma$ level, results in a smaller RV amplitude and thus in a smaller minimum companion mass of $12.6 \pm 1.3\ M_{\rm Jup}$. The RV data of HD 8673 and this updated best-fit orbital solution are shown in Figure 6.17 (right panel).

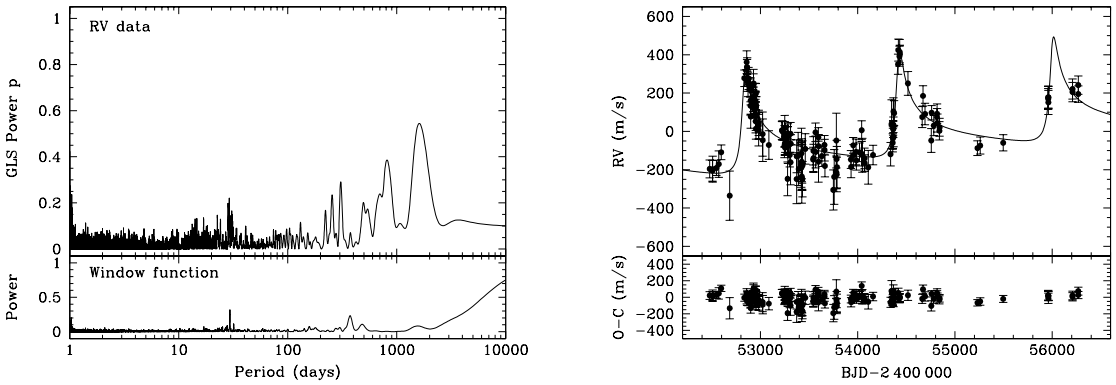


**Figure 6.17:** Results for HD 8673. *Left panel*: GLS periodogram of the RV data and window function of the observations. *Right panel*: RV measurements and best-fit Keplerian orbital solution including a linear trend (solid line). The RV residuals after subtracting the orbital solution are shown below.

**Table 6.15:** Orbital parameters of the sub-stellar companion of HD 8673.

| Parameter | | Value (1) | Value (2) | Value (3) |
|---|---|---|---|---|
| $P$ | (days) | $1634 \pm 17$ | $1583.3 \pm 4.1$ | $1582.2 \pm 4.3$ |
| $K$ | ($\mathrm{m\,s^{-1}}$) | $288 \pm 16$ | $281 \pm 26$ | $263.4 \pm 8.6$ |
| $e$ | | $0.723 \pm 0.016$ | $0.771 \pm 0.028$ | $0.738 \pm 0.014$ |
| $\omega$ | (deg) | $323.4 \pm 3.5$ | $312.4 \pm 4.2$ | $321.0 \pm 3.1$ |
| $T_0$ | (BJD $-$ 2 400 000) | $54\,420.5 \pm 7.9$ | $54\,390.7 \pm 5.3$ | $54\,413.5 \pm 4.9$ |
| $dv/dt$ | ($\mathrm{m\,s^{-1}\,day^{-1}}$) | 0.0 | 0.0 | $0.0536 \pm 0.0052$ |
| $N_{\mathrm{obs}}$ | | 135 | 152 | 152 |
| $\sigma_{\mathrm{O-C}}$ | ($\mathrm{m\,s^{-1}}$) | 71.3 | 76.9 | 61.2 |
| $\chi^2_{\mathrm{red}}$ | | 0.83 | 1.49 | 0.86 |
| $a_1 \sin i$ | ($10^{-3}$ AU) | $29.9 \pm 1.9$ | $26.1 \pm 2.7$ | $25.9 \pm 1.1$ |
| $f(m_1, m_2, i)$ | ($10^{-6}\,M_\odot$) | $1.33 \pm 0.25$ | $0.95 \pm 0.30$ | $0.92 \pm 0.11$ |
| $m_1$ | ($M_\odot$) | $1.36 \pm 0.20$ | $1.36 \pm 0.20$ | $1.36 \pm 0.20$ |
| $m_2 \sin i$ | ($M_{\mathrm{Jup}}$) | $14.2 \pm 1.6$ | $12.7 \pm 1.8$ | $12.6 \pm 1.3$ |
| $a$ | (AU) | $3.02 \pm 0.15$ | $2.95 \pm 0.15$ | $2.95 \pm 0.15$ |

**References:** (1) Hartmann et al. (2010); (2) This work (Keplerian model); (3) This work (Keplerian model with linear trend)

## HD 123845

HD 123845 (HIP 69178) has a visual magnitude of $V = 6.86 \pm 0.01$ (Høg et al. 2000). Its spectral type was given as F7 V by Harlan & Taylor (1970). According to the *Gaia* parallax of $\pi = 16.3130 \pm 0.1236$ mas (Gaia Collaboration 2018), the star is located at a distance of $d = 61.30 \pm 0.46$ pc. Holmberg et al. (2007) determined a stellar mass of $1.29 \pm 0.05\ M_\odot$ and a metallicity of [Fe/H] $= -0.18$.

The data set consists of 30 RV measurements spanning 2263 days (Figure 6.18, right panel). It can be seen that the star shows RV variations in the order of a few

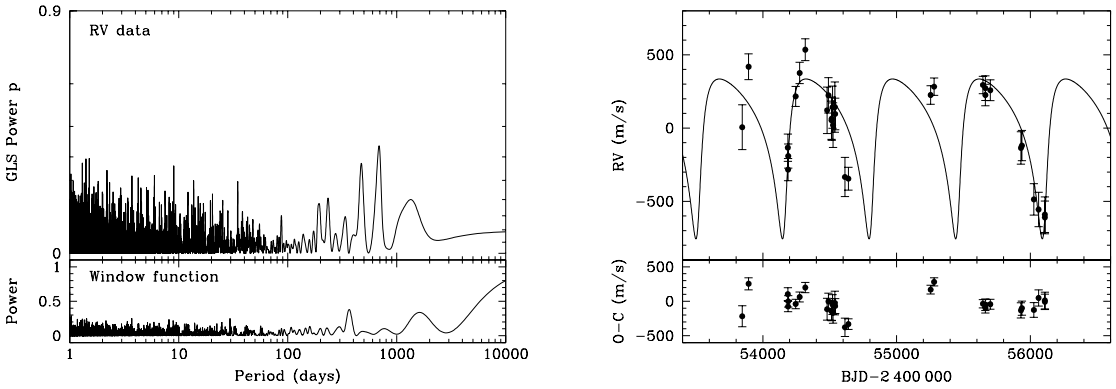


**Figure 6.18:** Results for HD 123845. *Left panel*: GLS periodogram of the RV data and window function of the observations. *Right panel*: RV measurements and best-fit Keplerian orbital solution (solid line). The RV residuals after subtracting the orbital solution are shown below.

**Table 6.16:** Orbital parameters of the sub-stellar companion of HD 123845.

| Parameter | | Value |
|---|---|---|
| $P$ | (days) | $647.4 \pm 7.9$ |
| $K$ | ($\mathrm{m\,s^{-1}}$) | $546 \pm 153$ |
| $e$ | | $0.56 \pm 0.20$ |
| $\omega$ | (deg) | $216 \pm 13$ |
| $T_0$ | (BJD $-$ 2 400 000) | $54\,810 \pm 14$ |
| $RV_0$ | ($\mathrm{m\,s^{-1}}$) | $36 \pm 39$ |
| $N_{\mathrm{obs}}$ | | 30 |
| $\sigma_{\mathrm{O-C}}$ | ($\mathrm{m\,s^{-1}}$) | 147.9 |
| $\chi^2_{\mathrm{red}}$ | | 3.65 |
| $a_1 \sin i$ | ($10^{-3}$ AU) | $26.9 \pm 8.7$ |
| $f(m_1, m_2, i)$ | ($10^{-6}\,M_\odot$) | $6.2 \pm 6.0$ |
| $m_1$ | ($M_\odot$) | $1.29 \pm 0.05$ |
| $m_2 \sin i$ | ($M_{\mathrm{Jup}}$) | $23.1 \pm 7.5$ |
| $a$ | (AU) | $1.603 \pm 0.025$ |

hundred days with an amplitude of several hundred $\mathrm{m\,s^{-1}}$. The highest signal in the periodogram reveals a period of 688.0 days (Figure 6.18, left panel). However, the corresponding power is rather low ($p_{\mathrm{GLS}} = 0.64$).

A Keplerian model is consistent with the presence of a sub-stellar companion with a minimum mass of $23.1 \pm 7.5\ M_{\mathrm{Jup}}$ in an eccentric orbit ($e = 0.56 \pm 0.20$) with a period of $647.4 \pm 7.9$ days and also shown in Figure 6.18 (right panel). The orbital elements are given in Table 6.16. Note that the errors of the $K$-amplitude and the eccentricity are markedly large, which results in a large error of the companion mass. The reduced $\chi^2$ is also quite high because several data points deviate significantly from the orbital fit (see O–C residuals in Figure 6.18, right panel).

A subsequent periodogram analysis of the RV residuals yields a period of

2.61 days, but the signal is statistically not yet significant. More data are needed to prove whether this signal is real and what its origin is (additional companion, stellar rotation, etc.).

### HD 89744

HD 89744 (HIP 50786, HR 4067) is cataloged as F7 V star in the Simbad database. However, according to the classification by Gray et al. (2003, F8 IV), the star is already slightly evolved. Its visual magnitude is $V = 5.720 \pm 0.009$ (Høg et al. 2000), and it is located at a distance of $d = 38.68 \pm 0.11$ pc from the Sun, as determined from the *Gaia* parallax of $\pi = 25.8537 \pm 0.0716$ mas (Gaia Collaboration 2018). Holmberg et al. (2007) derived its mass to be $1.50 \pm 0.04\ M_{\odot}$. With a metallicity of [Fe/H] = 0.18 deduced by the same authors, the star is metal-rich.

The discovery of a massive planet ($m_2 \sin i = 7.2\ M_{\rm Jup}$) in a highly-eccentric ($e = 0.70$) orbit with a period of 256.0 days was announced by Korzennik et al. (2000). Seventy-four RV measurements were taken between 1996 and 1999 using the Advanced Fiber-Optic Échelle (AFOE) spectrograph on the 1.5 m telescope at the Whipple Observatory, and 14 RV measurements were obtained in 1999 November/December with the Hamilton spectrograph at the Lick Observatory coudé auxiliary telescope (CAT) and Shane telescope. The derived orbital elements are summarized in Table 6.17. Note that one RV point was rejected in their orbit fitting due to a $3\,\sigma$ rejection algorithm.

Thirty RV measurements were gathered at TLS for my work over a time span of 4321 days (Figure 6.19, right panel). The strongest peak in the periodogram yields a period of 258.67 days (Figure 6.19, left panel). The orbital parameters of the best Keplerian solution (see Table 6.17) are in good agreement (within the errors) to the results of Korzennik et al. (2000), except for the eccentricity. The fitting program *GaussFit* was not able to reach convergence on a full 6-parameter Keplerian model.

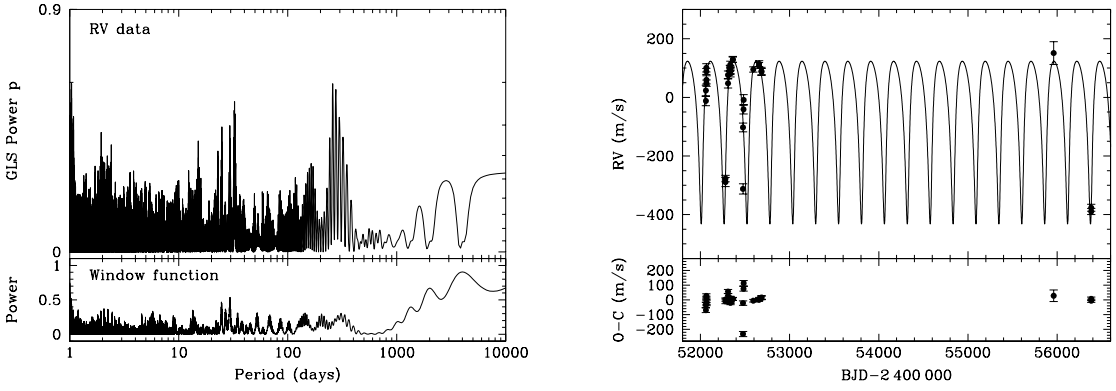


**Figure 6.19:** Results for HD 89744. *Left panel*: GLS periodogram of the RV data and window function of the observations. *Right panel*: RV measurements and best-fit Keplerian orbital solution (solid line). The RV residuals after subtracting the orbital solution are shown below.

**Table 6.17:** Orbital parameters of the sub-stellar companion of HD 89744.

| Parameter | | Value (1) | Value (2) |
|---|---|---|---|
| $P$ | (days) | $256.0 \pm 0.7$ | $256.82 \pm 0.24$ |
| $K$ | ($\mathrm{m\,s^{-1}}$) | $257 \pm 14$ | $278 \pm 38$ |
| $e$ | | $0.70 \pm 0.02$ | 0.47 (fixed) |
| $\omega$ | (deg) | $195 \pm 3$ | $197.2 \pm 8.2$ |
| $T_0$ | (BJD − 2 400 000) | $50\,994 \pm 2$ | $52\,269.3 \pm 5.5$ |
| $RV_0$ | ($\mathrm{m\,s^{-1}}$) | ··· | $-30 \pm 13$ |
| $N_{\mathrm{obs}}$ | | 87 | 30 |
| $\sigma_{\mathrm{O-C}}$ | ($\mathrm{m\,s^{-1}}$) | 20.5 | 54.7 |
| $\chi^2_{\mathrm{red}}$ | | 2.56 | 12.2 |
| $a_1 \sin i$ | ($10^{-3}$ AU) | 4.3 | $5.8 \pm 0.8$ |
| $f(m_1, m_2, i)$ | ($10^{-7}\,M_\odot$) | 1.64 | $3.9 \pm 1.6$ |
| $m_1$ | ($M_\odot$) | 1.4 | $1.50 \pm 0.04$ |
| $m_2 \sin i$ | ($M_{\mathrm{Jup}}$) | 7.2 | $10.1 \pm 1.4$ |
| $a$ | (AU) | 0.88 | $0.907 \pm 0.008$ |

**References:** (1) Korzennik et al. (2000); (2) This work

Thus, I fixed the eccentricity in steps of 0.01 and let all other parameters vary. For every eccentricity in this grid, I received a solution and a corresponding $\chi^2$-value. The final solution (with $e = 0.47$) was then chosen by the lowest of these $\chi^2$-values. Due to the lower eccentricity and the slightly larger $K$-amplitude, the minimum mass of the planet increases to $10.1 \pm 1.4\ M_{\mathrm{Jup}}$.

Korzennik et al. (2000) found a marginally significant linear long-term trend ($\approx 15\ \mathrm{m\,s^{-1}\,yr^{-1}}$) in the residuals to their orbital fit. Although the rms and the reduced $\chi^2$ are rather high after fitting the Keplerian orbit (54.7 $\mathrm{m\,s^{-1}}$ and 12.2, respectively), my data do not support such a linear trend.

### HD 33564

HD 33564 (HIP 25110, HR 1686) has a visual magnitude of $V = 5.084 \pm 0.009$ (Høg et al. 2000). The star is listed with a spectral type of F6 V in the Simbad database, but Gray et al. (2003) classified it as F7 V. The *Gaia* parallax of $\pi = 47.6977 \pm 0.1680$ mas (Gaia Collaboration 2018) results in a distance to the star of $d = 20.97 \pm 0.07$ pc. The stellar mass was determined to be $1.25^{+0.03}_{-0.04}\ M_\odot$, and the metallicity was measured to be [Fe/H] = −0.06 (Holmberg et al. 2007).

An extrasolar planet was already detected around this star (Galland et al. 2005b). From 15 RV measurements taken with the Elodie spectrograph on the 1.93 m telescope at the Observatoire de Haute-Provence in France, they found an object with a minimum mass of 9.1 $M_{\mathrm{Jup}}$ and a period of 388 days. Their orbital parameters are listed in Table 6.18.

I have acquired a total of 23 RV measurements (Figure 6.20, right panel). The corresponding periodogram shows a clear peak at a period of 392.9 days (Figure 6.20, left panel). While the data of Galland et al. (2005b) cover only a time span of

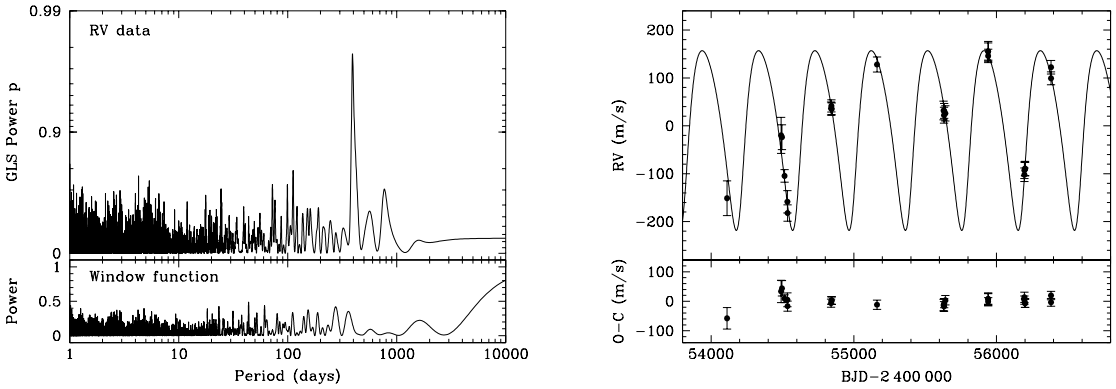


**Figure 6.20:** Results for HD 33564. *Left panel*: GLS periodogram of the RV data and window function of the observations. *Right panel*: RV measurements and best-fit Keplerian orbital solution (solid line). The RV residuals after subtracting the orbital solution are shown below.

**Table 6.18:** Orbital parameters of the sub-stellar companion of HD 33564.

| Parameter | | Value (1) | Value (2) |
|---|---|---|---|
| $P$ | (days) | $388 \pm 3$ | $395.1 \pm 2.1$ |
| $K$ | ($\mathrm{m\,s^{-1}}$) | $232 \pm 5$ | $188 \pm 25$ |
| $e$ | | $0.34 \pm 0.02$ | $0.25 \pm 0.12$ |
| $\omega$ | (deg) | $205 \pm 4$ | $222 \pm 12$ |
| $T_0$ | ($\mathrm{BJD} - 2\,400\,000$) | $52\,603 \pm 8$ | $54\,994.2 \pm 8.5$ |
| $\gamma, RV_0$ | ($\mathrm{m\,s^{-1}}$) | $107 \pm 6$ | $4 \pm 11$ |
| $N_{\mathrm{obs}}$ | | 15 | 23 |
| $\sigma_{\mathrm{O-C}}$ | ($\mathrm{m\,s^{-1}}$) | 6.7 | 19.4 |
| $\chi^2_{\mathrm{red}}$ | | ... | 0.80 |
| $a_1 \sin i$ | ($10^{-3}$ AU) | 7.8 | $6.6 \pm 0.9$ |
| $f(m_1, m_2, i)$ | ($10^{-7}\,M_\odot$) | 4.21 | $2.5 \pm 1.0$ |
| $m_1$ | ($M_\odot$) | 1.25 | $1.25 \pm 0.04$ |
| $m_2 \sin i$ | ($M_{\mathrm{Jup}}$) | 9.1 | $7.6 \pm 1.1$ |
| $a$ | (AU) | 1.1 | $1.137 \pm 0.013$ |

**References:** (1) Galland et al. (2005b); (2) This work

417 days (a little more than one orbital period), my data span 2271 days (more than five orbital periods) and enabled me to determine the orbital period more accurately. The best Keplerian solution (see Table 6.18) yields an orbital period of $395.1 \pm 2.1$ days and is a few days longer than the one derived by Galland et al. (2005b). It is shown in Figure 6.20 (right panel). Another difference is the lower RV amplitude, resulting in a smaller minimum mass of $7.6 \pm 1.1\ M_{\mathrm{Jup}}$ for the planet. Possible explanations might be that the TLS data are missing the exact RV minimum or that the number of RV points per orbit is too small.

### HD 113337

HD 113337 (HIP 63584, HR 4934) has a visual magnitude of $V = 6.008 \pm 0.009$ (Høg et al. 2000) and a spectral type of F6 V (Boesgaard & Tripicco 1986). The *Gaia* parallax of $\pi = 27.6107 \pm 0.0428$ mas (Gaia Collaboration 2018) yields a distance of $d = 36.22 \pm 0.06$ pc from the Sun. The stellar mass and metallicity were determined by Holmberg et al. (2007) to be $1.40^{+0.04}_{-0.03}\ M_\odot$ and [Fe/H] = 0.06, respectively.

The detection of an exoplanet was recently announced by Borgniet et al. (2014). Their analysis was based on 266 RV measurements taken with the Sophie spectrograph on the 1.93 m telescope at Observatoire de Haute-Provence. The planet has a minimum mass of $2.83 \pm 0.24\ M_{\rm Jup}$ (assuming a stellar mass of $1.40 \pm 0.14\ M_\odot$) and revolves around its host star in $324.0^{+1.7}_{-3.3}$ days in an eccentric orbit ($e = 0.46 \pm 0.04$). The orbital parameters are provided in Table 6.19.

The 21 RV measurements taken at TLS, comprising a time span of 1900 days, are given in Figure 6.21 (right panel). The corresponding periodogram does not yield any clear signal (Figure 6.21, left panel); especially in the vicinity of the 324-day period of the reported planet, there is nothing visible.

The RV measurements of Borgniet et al. (2014) also show a long-term change on top of the planetary signal, which they fit with a quadratic law. They stated that this long-term variation is probably not related to an orbiting object, but maybe due to stellar variability. However, they needed 266 RV data points and a dense time sampling to find the planet.

My data set consists of much less measurements with a less denser time sampling, which prevents me from finding the planetary signal. Nevertheless, in the following statistics, I will consider this star to be a planet host.

**Table 6.19:** Orbital parameters of the sub-stellar companion of HD 113337 (Borgniet et al. 2014).

| Parameter | | Value |
|---|---|---|
| $P$ | (days) | $324.0^{+1.7}_{-3.3}$ |
| $K$ | ($\mathrm{m\,s^{-1}}$) | $75.6^{+3.7}_{-3.6}$ |
| $e$ | | $0.46 \pm 0.04$ |
| $\omega$ | (deg) | $219.2^{+3.6}_{-3.7}$ |
| $T_0$ | (BJD $-$ 2 400 000) | $56\,074.5 \pm 2.3$ |
| $N_{\rm obs}$ | | 266 |
| $\sigma_{\rm O-C}$ Sophie | ($\mathrm{m\,s^{-1}}$) | 24.80 |
| $\sigma_{\rm O-C}$ Sophie+ | ($\mathrm{m\,s^{-1}}$) | 18.82 |
| $\chi^2_{\rm red}$ | | 4.55 |
| $a_1 \sin i$ | ($10^{-3}$ AU) | ⋯ |
| $f(m_1, m_2, i)$ | ($10^{-6}\ M_\odot$) | ⋯ |
| $m_1$ | ($M_\odot$) | $1.40 \pm 0.14$ |
| $m_2 \sin i$ | ($M_{\rm Jup}$) | $2.83 \pm 0.24$ |
| $a$ | (AU) | $0.92 \pm 0.09$ |

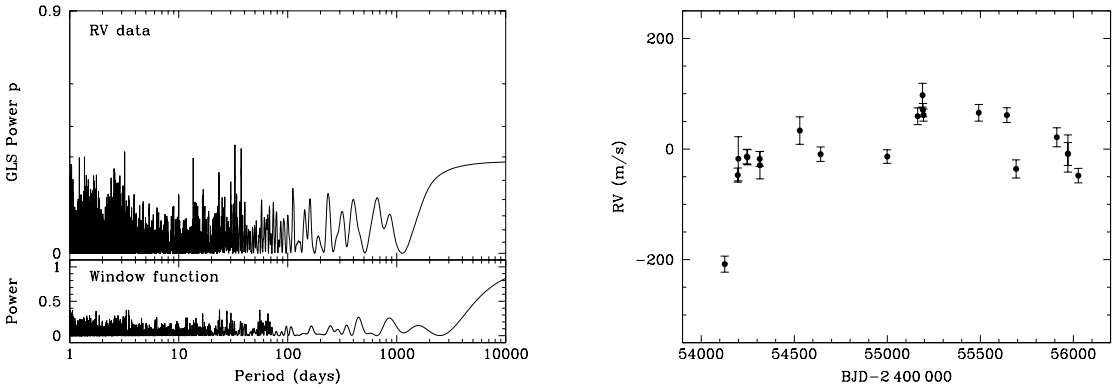


**Figure 6.21:** Results for HD 113337. *Left panel*: GLS periodogram of the RV data and window function of the observations. *Right panel*: RV measurements.

### 6.1.4 Concluding remarks

Investigating the nature of the RV variations is a key issue. Several earmarks have been established that have to be fulfilled in order to attribute an RV signal to Keplerian motion by planetary companions. First of all, the RV variations have to be long-lived and coherent, i.e., the signal should be consistent in period, amplitude and phase over many orbital cycles. Second, the orbital period should be different from the stellar rotation period. This can be estimated using the measured projected stellar rotational velocity, $v \sin i$, and the stellar radius. Due to the unknown inclination of the rotation axis of the star, however, this is only an upper limit of the rotation period.

To further analyze if rotational modulation or stellar pulsations due to surface features play a role, there are auxiliary activity indicators that are important:

(i) **Photometry:** The Hipparcos satellite was in operation from November 1989 until March 1993. The provided data may be useful to look for photometric variations although not contemporaneously taken with the RV measurements.

(ii) **H$\alpha$ line:** Variations in the strength of the H$\alpha$ line can be used to verify if the RV signals are produced by stellar activity. This can be done by measuring the equivalent width of the line.

(iii) **Ca ii lines:** The Ca ii lines are also a good activity indicator (e.g., the Ca ii H line at 3968.5 Å in the UV or the Ca ii line at 8497.613 Å in the IR). In chromospherically active stars, there appears an emission line in the cores of these absorption lines.

(iv) **Bisectors:** Stellar surface stucture results in the deformation of spectral lines. This can be measured by analyzing the so-called bisectors, i.e., the differenes of the mid-points of the lines at different line depths in velocity space. Usually, one can measure the bisector asymmetry via the bisector velocity span (BVS) and the bisector velocity curvature.

**Table 6.20:** Summary of the earmarks that were checked to confirm the planet hypothesis. A checkmark indicates that the corresponding criterion is fulfilled to exclude stellar rotation or activity as cause of the RV variations, supporting their planetary nature; a cross, on the other hand, signifies that this criterion was not investigated.

| Star | Long-lived and coherent RV signal | Max. $P_{\mathrm{rot}}$ | Hipparcos photometry | H$\alpha$ | Ca II | Bisectors |
|---|---|---|---|---|---|---|
| HD 8673 | ✓ | ✓ | ✓ | × | ✓ | ✓ |
| HD 16232 (30 Ari B) | ✓ | ✓ | ✓ | ✓ | × | × |
| HD 33564 | ✓ | ✓ | × | × | ✓ | ✓ |
| HD 89744 | ✓ | ✓ | × | × | × | × |
| HD 113337 | ✓ | ✓ | × | × | × | ✓ |
| HD 123845 | ✓ | ✓ | × | × | × | × |

If any of these indicators shows variability close to the RV period, the planet hypothesis becomes suspicious. The absence of such coincidences, however, represents only a necessary but not a sufficient condition for verifying the planetary nature of the RV variations.

Table 6.20 summarizes which of the aforementioned earmarks have been investigated for the six planet candidates considered in this work. As can be seen, the first criterion is fulfilled for all of the stars. However, this minimum requirement is not always achieved when planets are announced in the literature. Because the maximum stellar rotation period is much smaller than the RV period for the six stars, stellar rotation as cause of the RV variations is less likely. The Hipparcos photometry was analyzed only for HD 8673 (Hartmann et al. 2010) and HD 16232 (Guenther et al. 2009) but no significant variations were found. In the case of HD 16232, Guenther et al. (2009) also showed that the equivalent width of H$\alpha$ is not correlated with the RV. However, examining the H$\alpha$ line is very tricky because photometric observing conditions, which are rare in Germany, are required to measure the equivalent width in a proper way. The Ca II indicator was applied for HD 8673 (Hartmann et al. 2010) and HD 33564 (Galland et al. 2005b). They showed that no emission core was present in the Ca II lines. Since spectroscopic planet surveys usually cover only the optical part, the Ca II lines in the UV or IR are not included in the spectra; thus this method cannot always be used. The bisectors have been analyzed for HD 8673 (Hartmann et al. 2010), HD 33564 (Galland et al. 2005b) and HD 113337 (Borgniet et al. 2014), and no variations with the RV period have been found. But high-quality bisector measurements are difficult to achieve because these require both high-S/N data and spectrographs with resolving power of $R \gtrsim 100\,000$, which is not the case for the three examples from above. Thus, it could well be that the lack of bisector variations is not conclusive.

Sometimes, none of the activity indicators are examined at all. Korzennik et al. (2000), for example, stated in their discovery paper of the planet around HD 89744 that *"there is no known way a stellar signal in a late F-type main-sequence star could mimic a Keplerian orbital signature with such a long period and large amplitude and*

**Table 6.21:** Summary of the main parameters for the F-star planetary systems sorted by increasing orbital period. The values for HD 113337 are taken from Borgniet et al. (2014).

| Star | $P$ (days) | $e$ | $m_2 \sin i$ ($M_{\rm Jup}$) | $m_1$ ($M_\odot$) |
|---|---|---|---|---|
| HD 89744 | $256.82 \pm 0.24$ | 0.47 (fixed) | $10.1 \pm 1.4$ | $1.50 \pm 0.04$ |
| HD 113337 | $324.0\ ^{+\ 1.7}_{-\ 3.3}$ | $0.46 \pm 0.04$ | $2.83 \pm 0.24$ | $1.40 \pm 0.14$ |
| HD 16232 (30 Ari B) | $349.7 \pm 2.5$ | $0.21 \pm 0.12$ | $8.7 \pm 1.4$ | $1.16 \pm 0.04$ |
| HD 33564 | $395.1 \pm 2.1$ | $0.25 \pm 0.12$ | $7.6 \pm 1.1$ | $1.25 \pm 0.04$ |
| HD 123845 | $647.4 \pm 7.9$ | $0.56 \pm 0.20$ | $23.1 \pm 7.5$ | $1.29 \pm 0.05$ |
| HD 8673 | $1582.2 \pm 4.3$ | $0.738 \pm 0.014$ | $12.6 \pm 1.3$ | $1.36 \pm 0.20$ |

*with such a large eccentricity."*

The F-star sample contains six stars that harbor an extrasolar planet. Three of them were newly discovered and two previsously known planets could be confirmed in this work. In addition, there is one more planet in my sample, for which my data are insufficient to detect the corresponding signal. This results in a planet occurrence rate of 4% that is consistent with the planet fraction of solar-like stars and also in agreement with Reffert et al. (2015) for giant stars of $\sim 1.3\ M_\odot$. Nevertheless, this result is inconsistent with other observations of evolved (sub)giant stars. For example, Johnson et al. (2007) and Bowler et al. (2010) deduced planet frequencies of $\sim 9\%$ and $\sim 26\%$, respectivly. On the other hand, my findings do neither support the theoretical predictions of Kennedy & Kenyon (2008) nor Kornet et al. (2006) because the planet fraction for stars between 1.0 and $\approx 1.3\ M_\odot$ seems to be rather flat instead of rising or declining with stellar mass. This outcome is also supported by a recent study of Borgniet et al. (2017), who derived an occurrence rate of 4% for giant planets in the mass interval $1\ M_{\rm Jup} \leq m_{\rm p} \sin i \leq 13\ M_{\rm Jup}$ around stars of 1.1–1.5 $M_\odot$ within a period range of 1–1000 days. Moreover, they find a fraction of 2% for brown dwarfs ($13\ M_{\rm Jup} \leq m_{\rm p} \sin i \leq 80\ M_{\rm Jup}$) considering the same stellar masses and orbital periods. They concluded that there is no significant difference in the occurrence rates compared to solar-like MS stars.

In Table 6.21, the main orbital pararameters of the planetary systems are listed. The stars are ordered according to the orbital periods of the companions. It shows that no short-period planets have been found in this sample, i.e., the fraction of so-called "Hot Jupiter" is $< 1\%$. The shortest period is 257 days and the longest 1582 days. It is conspicuous that three of the six planets have periods within a rather narrow range of 300–400 days. The Extrasolar Planets Encyclopaedia lists 56 F stars with planets (plus HD 113337 for which no entry for the spectral type is given). Among them are four further examples with periods in that range, resulting in a total of seven planets. Eleven of these F-star planets have periods shorter than 10 days, two have periods of 10–20 days, three of 20–100 days, two of 100–200 days and ten of 200–300 days. Taking these numbers into account, there seem to be a lack of planets in the period range of $\sim$ 20–200 days compared to the number of planets with periods of 200–400 days.

Furthermore, all planets have eccentric orbits with eccentricities ranging from moderate values of 0.21 to high values up to 0.74. This seems to be almost consistent with the entries in the Extrasolar Planets Encyclopaedia. When binning the eccentricities in steps of 0.1, most of the planets are in the first bin ($0 \leq e < 0.1$), but these are mainly the short-period planets that have been circularized. Apart from this, most of the other planets have eccentricities of $0.2 \leq e < 0.4$, and the overall median lies between 0.2 and 0.3. Only six planets have $e \geq 0.7$. Although the median eccentricity of the six planets in this study is nearly 0.5, the difference is probably due to low-number statistics.

The reviewed planets are all very massive (minimum masses of 2.8–23.1 $M_{\rm Jup}$). This might be a hint that higher-mass stars tend to have higher-mass planets, as already pointed out by Lovis & Mayor (2007). According to the Extrasolar Planets Encyclopaedia, roughly 50% of the planets around F stars have minimum masses $\gtrsim 2$ $M_{\rm Jup}$. Seven examples in this list have minimum masses above 10 $M_{\rm Jup}$, two of them even above 40 $M_{\rm Jup}$. Finding such massive planets is thus not exceptional. However, the question is why I do not find any planet with minimum mass below 2 $M_{\rm Jup}$. Aside from effects of low-number statistics, there could be also another explanation. Almost all F stars in the Extrasolar Planets Encyclopaedia have spectral types of F8–F9, whereas the mean spectral type of my sample is shifted to somewhat earlier types of F6–F7. Of course, this results in higher rotation rates and thus less precise RV measurements. The RV signals of companions less massive than 2 $M_{\rm Jup}$ are probably too low compared to the intrinsic measurements errors to find these signals.

Interestingly, two of the six stars with planets, HD 8673 and HD 16232, show an additional linear trend in the RV data. This indicates most likely that a wide stellar companion is present in these systems. Moreover, HD 113337 exhibits a quatratic signature in addition to the planetary signal (Borgniet et al. 2014). But instead of attributing this to a gravitationally bound (stellar) companion, these authors suggest that these long-term trend might be related to intrinsic stellar variability (e.g., convection effects), as they see weak long-term variations in their BVS and full width at half maximum (FWHM) data of the CCFs.

Beside the planet detections, many spectroscopic binaries were found as a by-product. The F-star sample contains ten SB1 systems, four SB2 systems and ten stars with long-term RV trends that can be also attributed to stellar companions. Overall, there are 24 binaries corresponding to a fraction of $\sim 16\%$. This is in very good agreement with the binary frequency of evolved K giants of similar stellar masses (Döllinger, private communication).

## 6.2 The Ap-star survey in the southern hemisphere

### 6.2.1 Spectroscopic binaries with orbit

Here, I present ten spectroscopic binaries with orbits. Some of the orbits are provided for the first time, and some have been already known. For a few cases, only the previously published orbit will be given. The most important stellar parameters from the literature will be listed as well.

#### HD 42659

HD 42659 (HIP 29365, UV Lep) is classified as A3 Sr Cr Eu star in the catalog from Renson & Manfroid (2009). Its visual magnitude is given as $V = 6.75 \pm 0.01$ (Høg et al. 2000). Using the *Gaia* parallax of $\pi = 7.6213 \pm 0.0410$ mas (Gaia Collaboration 2018), the star is located at a distance of $d = 131.2 \pm 0.7$ pc. The basic stellar parameters are taken from Kochukhov & Bagnulo (2006), who derived an effective temperature of $\log(T_{\rm eff}/{\rm K}) = 3.900 \pm 0.011$ and a stellar mass of $2.10 \pm 0.10\ M_\odot$.

This star belongs to the subclass of roAp stars. Rapid oscillations were discovered by Martinez & Kurtz (1994a), who carried out photometric observations in 12 nights. They found oscillations with a 9.7-minute period and a peak-to-peak Johnson $B$ amplitude of 0.8 mmag. Since this signal is not seen on some nights, the oscillations must be modulated in amplitude.

A total of 49 spectra were gathered in 16 nights covering a time span of 1535 days. For the analysis with the HARPS-TERRA software, however, one observation was discarded because the S/N was too low to apply this routine. I find significant variability in the RV data of HD 42659. The corresponding GLS periodograms analyzing the HARPS CCF and HARPS-TERRA RV data are displayed in the top panels of Figure 6.22, respectively. Both periodograms show the highest peak at a period of $P_1 = 93.0$ days ($f_1 = 0.01075$ d$^{-1}$), having an FAP of less than $10^{-3}$.

There is a second peak visible in the periodograms at a period of $P_2 = 53.9$ days ($f_2 = 0.01857$ d$^{-1}$; HARPS CCF: FAP = 0.040, HARPS-TERRA: FAP = 0.005). When subtracting the 93.0-day signal from the data, the 53.9-day signal disappears in the periodogram of the residuals, and there is no significant additional signal. The same occurs when first subtracting the 53.9-day signal. Thus, I can conclude that one period is the alias of the other. This is further supported when looking at the window function of the observations. If I subtract both frequencies, i.e., $f_2 - f_1 = 0.00782$ d$^{-1}$ (corresponding to a period of 127.9 days), I derive the period of a maximum in the window function (see peak at 127.6 days in the lower parts of the top panels of Figure 6.22). Therefore, the data sampling does not allow me to distinguish which of the two periods is the true one, but the 93.0-day period is more likely.

The Keplerian orbital solutions for the two data sets yield periods of $93.237 \pm 0.032$ and $93.187 \pm 0.038$ days and are fully consistent with the ones obtained above. The orbit is slightly eccentric ($e = 0.237 \pm 0.037$ and $0.146 \pm 0.027$). Both solutions mostly differ in their amplitudes, resulting in significantly different minimum masses for the companion: $0.701 \pm 0.047$ and $0.468 \pm 0.021\ M_\odot$, respectively. This implies

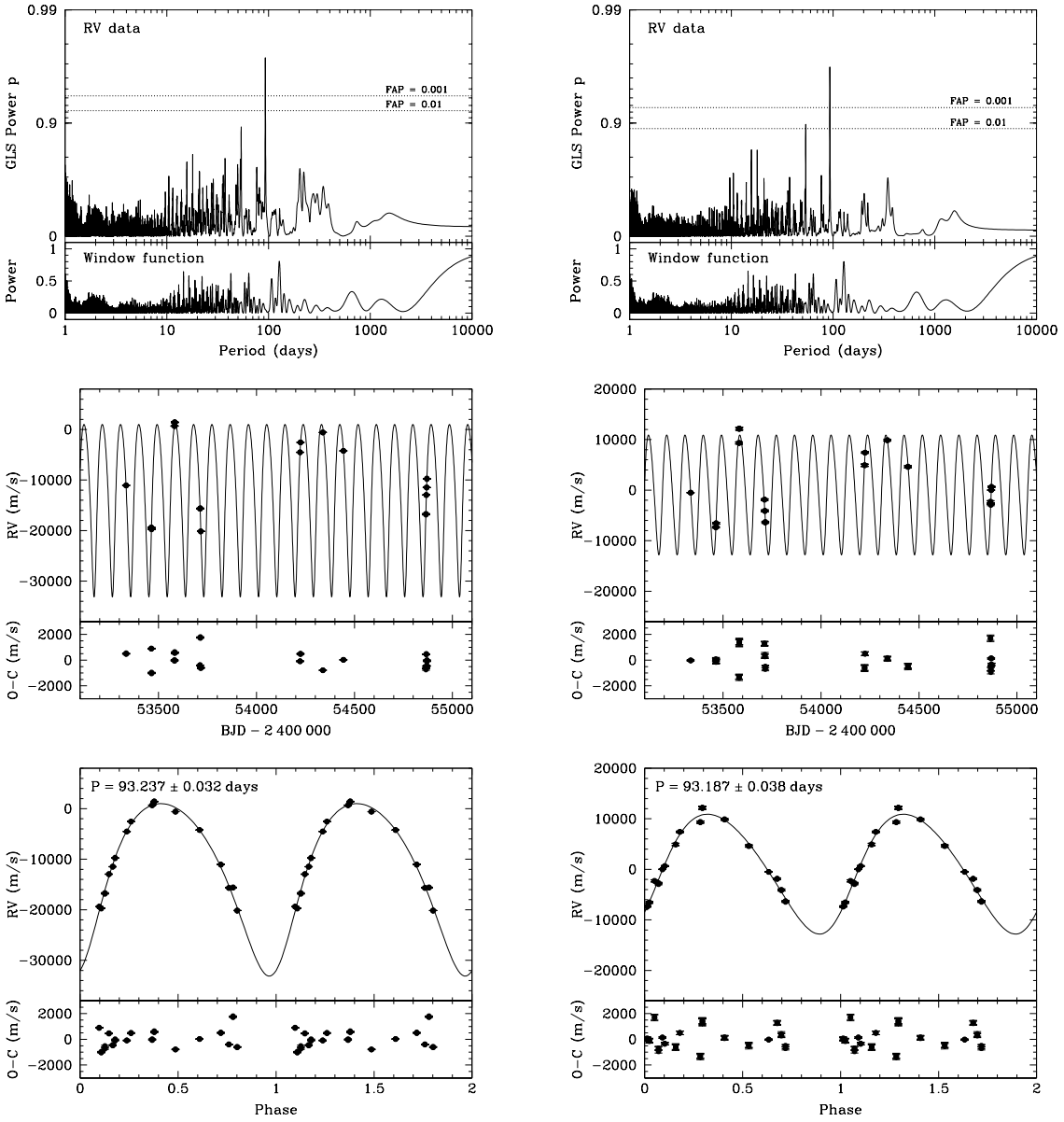


**Figure 6.22:** Results for HD 42659 analyzing the RV data obtained with the HARPS CCF technique (*left panels*) and the HARPS-TERRA software tool (*right panels*), respectively. *Top panels*: GLS periodograms of the RV data. The dotted lines indicate two levels of the FAP. The lower parts display the window function of the observations. *Middle panels*: RV measurements and best-fit Keplerian orbital solution (solid line). The RV residuals after subtracting the orbital solution are shown below. *Bottom panels*: RV measurements phased to the orbital period. Phase zero corresponds to the time of periastron passage. The solid line represents the orbital solution. Data points are repeated for the second cycle. Again, the RV residuals are shown below.

**Table 6.22:** Orbital parameters of the stellar companion of HD 42659.

| Parameter | | HARPS CCF | HARPS-TERRA |
|---|---|---|---|
| $P$ | (days) | $93.237 \pm 0.032$ | $93.187 \pm 0.038$ |
| $K$ | ($\mathrm{km\,s^{-1}}$) | $17.06 \pm 1.06$ | $11.85 \pm 0.43$ |
| $e$ | | $0.237 \pm 0.037$ | $0.146 \pm 0.027$ |
| $\omega$ | (deg) | $200.6 \pm 3.9$ | $230.8 \pm 10.4$ |
| $T_0$ | (BJD $-$ 2 400 000) | $54\,013.8 \pm 0.9$ | $54\,021.4 \pm 2.6$ |
| $\gamma, RV_0$ | ($\mathrm{km\,s^{-1}}$) | $-12.28 \pm 0.38$ | $0.14 \pm 0.19$ |
| $N_{\mathrm{obs}}$ | | 49 | 48 |
| $\sigma_{\mathrm{O-C}}$ | ($\mathrm{m\,s^{-1}}$) | 697 | 796 |
| $a_1 \sin i$ | ($10^{-3}$ AU) | $142.0 \pm 8.9$ | $100.5 \pm 3.7$ |
| $f(m_1, m_2, i)$ | ($10^{-3}\,M_\odot$) | $44.0 \pm 8.3$ | $15.6 \pm 1.7$ |
| $m_1$ | ($M_\odot$) | $2.10 \pm 0.10$ | $2.10 \pm 0.10$ |
| $m_2 \sin i$ | ($M_\odot$) | $0.701 \pm 0.047$ | $0.468 \pm 0.021$ |
| $a$ | (AU) | $0.567 \pm 0.008$ | $0.551 \pm 0.008$ |

the presence of an early M-type or K-type secondary star. The orbits are shown in the RV time series (Figure 6.22, middle panels) as well as phase-folded to the orbital period (Figure 6.22, bottom panels), where the phases were derived using the time of periastron passage as the zero point. The orbital parameters and their errors are given in Table 6.22.

Note that even if the true period was the alias at 53.9 days, the conclusion would still hold that HD 42659 has a short-period binary companion, but with a smaller companion mass.

### HD 50169

HD 50169 (HIP 32965) is listed as A3 Sr Eu Cr star (Renson & Manfroid 2009) and has a visual magnitude of $V = 8.98 \pm 0.02$ (Høg et al. 2000). The *Gaia*-based parallax of $\pi = 1.7384 \pm 0.0612$ mas (Gaia Collaboration 2018) yields a distance of $d = 575 \pm 20$ pc. No rapid oscillations were found in this star.

Twenty-three RV observations have been collected distributed over 1536 days. The long-term RV variations are clearly visible in the RV time series shown in the bottom panels of Figure 6.23 and supported by the highest peaks at long periods in the GLS periodograms (Figure 6.23, top panels).

Applying a Keplerian model for the two data sets gives periods of $1762.7 \pm 5.1$ and $1768.4 \pm 6.3$ days. Both orbital solutions are in very good agreement to each other and displayed in the bottom panels of Figure 6.23. Only the determined eccentricity is slightly different, but consistent within the $3\,\sigma$ errors. Table 6.23 lists the orbital elements with their uncertainties.

For the determination of the mass of the secondary star, I assumed a stellar mass of $2.0 \pm 0.2\ M_\odot$, resulting in a minimum companion mass of $0.147 \pm 0.009$ and $0.146 \pm 0.009\ M_\odot$, respectively. Thus, the companion to HD 50169 is most likely an M dwarf.

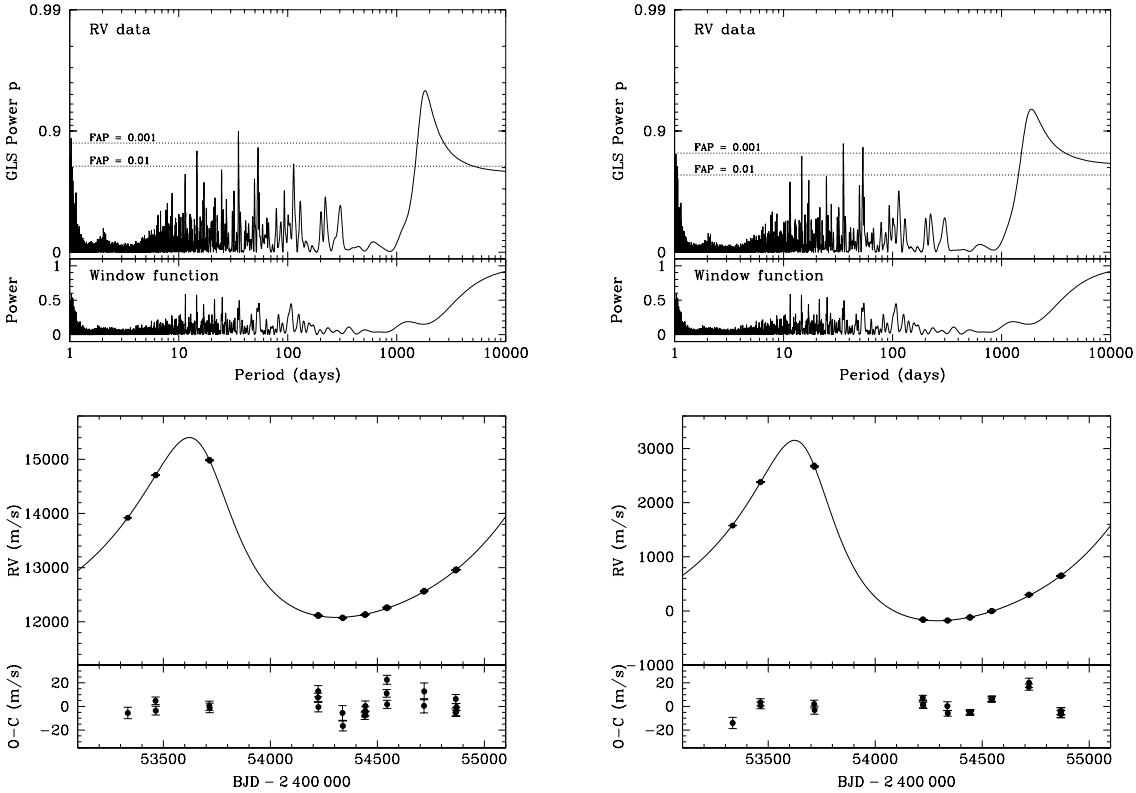


**Figure 6.23:** Results for HD 50169 analyzing the RV data obtained with the HARPS CCF technique (*left panels*) and the HARPS-TERRA software tool (*right panels*), respectively. *Top panels*: GLS periodograms of the RV data. The dotted lines indicate two levels of the FAP. The lower parts display the window function of the observations. *Bottom panels*: RV measurements and best-fit Keplerian orbital solution (solid line). The RV residuals after subtracting the orbital solution are shown below.

**Table 6.23:** Orbital parameters of the stellar companion of HD 50169.

| Parameter | | HARPS CCF | HARPS-TERRA |
|---|---|---|---|
| $P$ | (days) | $1762.7 \pm 5.1$ | $1768.4 \pm 6.3$ |
| $K$ | ($\mathrm{m\,s^{-1}}$) | $1661 \pm 11$ | $1666 \pm 15$ |
| $e$ | | $0.3473 \pm 0.0061$ | $0.3805 \pm 0.0067$ |
| $\omega$ | (deg) | $28.4 \pm 0.9$ | $28.6 \pm 0.9$ |
| $T_0$ | (BJD $-$ 2 400 000) | $53\,686.3 \pm 3.4$ | $53\,682.9 \pm 3.6$ |
| $\gamma, RV_0$ | ($\mathrm{m\,s^{-1}}$) | $13\,233.8 \pm 4.4$ | $928.5 \pm 4.2$ |
| $N_{\mathrm{obs}}$ | | 23 | 23 |
| $\sigma_{\mathrm{O-C}}$ | ($\mathrm{m\,s^{-1}}$) | 8.5 | 7.7 |
| $a_1 \sin i$ | ($10^{-3}$ AU) | $252.4 \pm 2.0$ | $250.4 \pm 2.5$ |
| $f(m_1, m_2, i)$ | ($10^{-3}\,M_\odot$) | $0.690 \pm 0.015$ | $0.670 \pm 0.019$ |
| $m_1$ | ($M_\odot$) | $2.0 \pm 0.2$ | $2.0 \pm 0.2$ |
| $m_2 \sin i$ | ($M_\odot$) | $0.147 \pm 0.009$ | $0.146 \pm 0.009$ |
| $a$ | (AU) | $3.68 \pm 0.12$ | $3.69 \pm 0.12$ |

**Table 6.24:** Orbital parameters of the stellar companion of HR 5049.

| Parameter | | Value (1) | HARPS CCF (2) | HARPS-TERRA (2) |
|---|---|---|---|---|
| $P$ | (days) | $126.18 \pm 0.06$ | $126.2417 \pm 0.0026$ | $126.2514 \pm 0.0086$ |
| $K$ | ($\mathrm{km\,s^{-1}}$) | $14.4 \pm 0.4$ | $20.6 \pm 4.7$ | $21.9 \pm 1.3$ |
| $e$ | | $0.15 \pm 0.03$ | $0.261 \pm 0.080$ | $0.261 \pm 0.000$ (fixed) |
| $\omega$ | (deg) | $68 \pm 24$ | $28.2 \pm 8.4$ | $18.2 \pm 6.1$ |
| $T_0$ | (BJD $-$ 2 400 000) | $41\,421 \pm 9$ | $54\,155.7 \pm 3.4$ | $54\,151.2 \pm 3.5$ |
| $\gamma, RV_0$ | ($\mathrm{km\,s^{-1}}$) | $2.5 \pm 0.5$ | $5.2 \pm 1.7$ | $13.1 \pm 1.1$ |
| $N_{\mathrm{obs}}$ | | 25 | 18 | 18 |
| $\sigma_{\mathrm{O-C}}$ | ($\mathrm{m\,s^{-1}}$) | 1700 | 4.1 | 134.3 |
| $a_1 \sin i$ | (AU) | $0.166 \pm 0.006$ | $0.231 \pm 0.053$ | $0.246 \pm 0.015$ |
| $f(m_1, m_2, i)$ | ($M_\odot$) | $0.038 \pm 0.004$ | $0.104 \pm 0.071$ | $0.124 \pm 0.022$ |
| $m_1$ | ($M_\odot$) | ... | $2.93 \pm 0.10$ | $2.93 \pm 0.10$ |
| $m_2 \sin i$ | ($M_\odot$) | ... | $1.21 \pm 0.28$ | $1.31 \pm 0.08$ |
| $a$ | (AU) | ... | $0.791 \pm 0.022$ | $0.797 \pm 0.009$ |

**References:** (1) Dworetsky (1982); (2) This work

### HR 5049

HR 5049 (HD 116458, HIP 65522, 67 Mus) is an A0 Eu Cr star (Renson & Manfroid 2009) with a visual magnitude of $V = 5.651 \pm 0.009$ (Høg et al. 2000). Given the *Gaia* parallax of $\pi = 7.7592 \pm 0.1811$ mas (Gaia Collaboration 2018), the distance from the Sun is $d = 128.9 \pm 3.0$ pc. The star has an effective temperature of $\log(T_{\mathrm{eff}}/\mathrm{K}) = 4.012 \pm 0.013$ and a stellar mass of $2.93 \pm 0.10\ M_\odot$ (Kochukhov & Bagnulo 2006). Moreover, it is a non-oscillationg Ap star.

HR 5049 was already known to be a single-lined spectroscopic binary. Dworetsky (1982) determined an orbital period of $126.18 \pm 0.06$ days using 25 RV measurements from coudé spectrograms taken between 1964 and 1980.

Analyzing the 18 HARPS CCF and HARPS-TERRA RV measurements taken over a timeframe of 1082 days, I find the same period, which is demonstrated by the highest peak in the respective GLS periodogram at 126.3 days (Figure 6.24, top panels). In both cases, the FAP of the signal is below $10^{-3}$. A calculated Keplerian orbital solution using *GaussFit* for the HARPS CCF data provided a period of $126.2417 \pm 0.0026$ days and an eccentricity of $e = 0.261 \pm 0.080$. For the HARPS-TERRA RVs, on the other hand, it was not possible to find a convergent solution for a full 6-parameter Keplerian model. Therefore, I fixed the eccentricity to the aforementioned value of the HARPS CCF orbit and let only the other five parameters vary, which resulted in similar orbital elements. These are recorded in Table 6.24. The RV measurements with the corresponding orbits are shown in Figure 6.24 as a time series (middle panels) and phased to the orbital period (bottom panels).

Although this period resembles closely the one derived by Dworetsky (1982), the $K$-amplitude and eccentricity are markedly larger. As can be seen in the bottom panels of Figure 6.24, the phase coverage of the RV measurements is rather poor

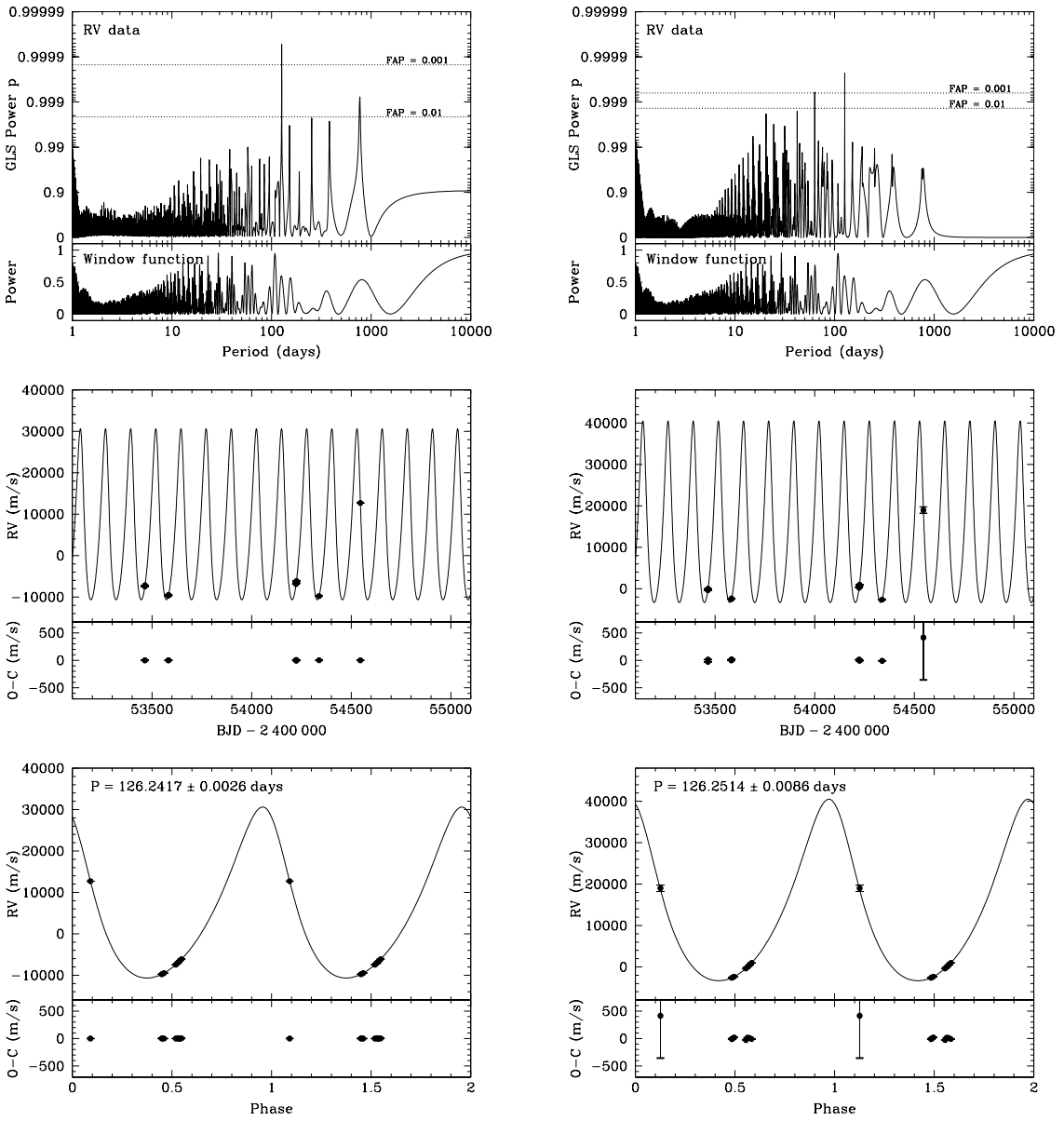


**Figure 6.24:** Results for HR 5049 analyzing the RV data obtained with the HARPS CCF technique (*left panels*) and the HARPS-TERRA software tool (*right panels*), respectively. *Top panels*: GLS periodograms of the RV data. The dotted lines indicate two levels of the FAP. The lower parts display the window function of the observations. *Middle panels*: RV measurements and best-fit Keplerian orbital solution (solid line). The RV residuals after subtracting the orbital solution are shown below. *Bottom panels*: RV measurements phased to the orbital period. Phase zero corresponds to the time of periastron passage. The solid line represents the orbital solution. Data points are repeated for the second cycle. Again, the RV residuals are shown below.

with no points on the top part of the RV curve, resulting in a worse precision of the $K$-amplitude and eccentricity compared to the values of Dworetsky (1982). On that account, it might be possible that I have overestimated the $K$-amplitude and thus the minimum companion mass. Nevertheless, as deduced from the solution of the HARPS CCF and HARPS-TERRA data, the minimum mass of the secondary star is $1.21 \pm 0.28$ and $1.31 \pm 0.08$ $M_{\odot}$, respectively.

### HD 125248

HD 125248 (HIP 69929, HR 5355, CS Vir) is recorded as A1 Eu Cr star (Renson & Manfroid 2009) with a visual magnitude of $V = 5.90$ (Ducati 2002). It is located at a distance of $d = 78.5 \pm 1.7$ pc from the Sun, according to the *Gaia* parallax of $\pi = 12.7439 \pm 0.2802$ mas (Gaia Collaboration et al. 2016). The stellar mass, $2.27 \pm 0.07$ $M_{\odot}$, and the effective temperature, $\log(T_{\rm eff}/{\rm K}) = 3.992 \pm 0.013$, were determined by Kochukhov & Bagnulo (2006). Again, this star belongs to the non-oscillationg Ap stars.

During 19 nights, 43 RV observations have been carried out spanning 1407 days. The RV data exhibit long-term variations (Figure 6.25, bottom panels). This is also demonstrated by the highest peaks at 1550 and 1507 days in the GLS periodograms (Figure 6.25, top panels).

The corresponding Keplerian models yield periods of $1666 \pm 22$ and $1550 \pm 21$ days and modest eccentricities of $0.175 \pm 0.022$ and $0.119 \pm 0.029$, respectively. Figure 6.25 (bottom panels) illustrates the orbital solutions. It can be seen by eye that both solutions have slightly different shapes, which is confirmed by some differences in the orbital elements provided in Table 6.25. The period of the HARPS CCF orbit is 116 days longer than the period of the HARPS-TERRA orbit, a difference of 2.7 $\sigma$. Moreover, eccentricity, longitude of periastron and $K$-amplitude differ by 1.1–1.6 $\sigma$. Possible reasons for this behavior could be the lack of RV points around the RV maximum and that the orbital period exceeds the time baseline of the RV measurements. The minimum companion mass derived from the parameters of Table 6.25 is $0.645 \pm 0.024$ and $0.758 \pm 0.047$ $M_{\odot}$ for the HARPS CCF and HARPS-TERRA solution, respectively.

Babcock (1958) already claimed that this star might be a spectroscopic binary because of a secular variation seen in the mean velocity. Three independent sets of orbital parameters are available in the literature. These were summarized in Abt & Snowden (1973) containing a solution from Deutsch, who analyzed 55 coudé measures (many of them unpublished), a solution from Hockey (1969) and their own solution. The latter yields a period of 1643.6 days and an eccentricity of $0.22 \pm 0.06$, which is consistent with the HARPS CCF orbit, making it preferable compared to the HARPS-TERRA orbit.

### HD 142070

HD 142070 (HIP 77752, V373 Ser) is an A0 Sr Cr Eu star (Renson & Manfroid 2009) and has a visual magnitude of $V = 7.97 \pm 0.01$ (Høg et al. 2000). As derived from the

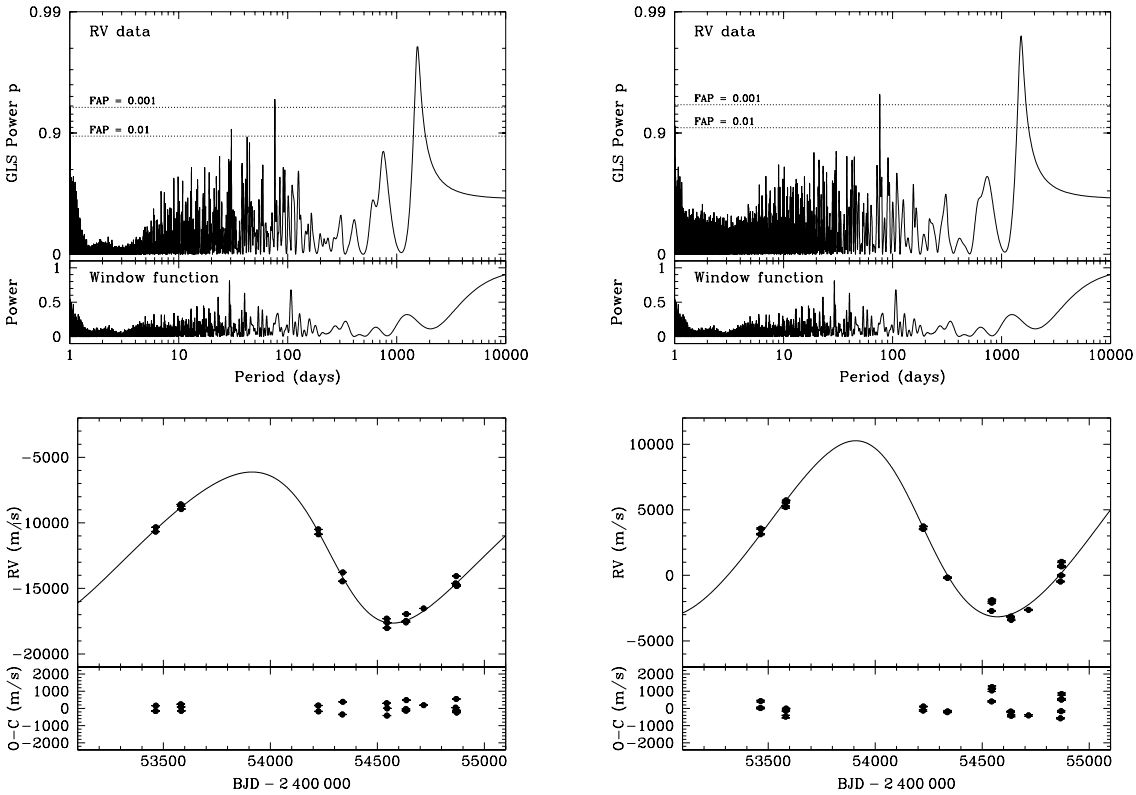


**Figure 6.25:** Results for HD 125248 analyzing the RV data obtained with the HARPS CCF technique (*left panels*) and the HARPS-TERRA software tool (*right panels*), respectively. *Top panels*: GLS periodograms of the RV data. The dotted lines indicate two levels of the FAP. The lower parts display the window function of the observations. *Bottom panels*: RV measurements and best-fit Keplerian orbital solution (solid line). The RV residuals after subtracting the orbital solution are shown below.

**Table 6.25:** Orbital parameters of the stellar companion of HD 125248.

| Parameter | | HARPS CCF | HARPS-TERRA |
|---|---|---|---|
| $P$ | (days) | $1666 \pm 22$ | $1550 \pm 21$ |
| $K$ | ($\mathrm{km\,s^{-1}}$) | $5.76 \pm 0.19$ | $6.71 \pm 0.40$ |
| $e$ | | $0.175 \pm 0.022$ | $0.119 \pm 0.029$ |
| $\omega$ | (deg) | $107 \pm 8$ | $74 \pm 15$ |
| $T_0$ | (BJD $-$ 2 400 000) | $54\,319 \pm 33$ | $54\,174 \pm 63$ |
| $\gamma, RV_0$ | ($\mathrm{km\,s^{-1}}$) | $-11.58 \pm 0.09$ | $3.34 \pm 0.21$ |
| $N_{\mathrm{obs}}$ | | 43 | 43 |
| $\sigma_{\mathrm{O-C}}$ | ($\mathrm{m\,s^{-1}}$) | 260 | 496 |
| $a_1 \sin i$ | ($10^{-3}$ AU) | $869 \pm 30$ | $949 \pm 58$ |
| $f(m_1, m_2, i)$ | ($10^{-3}\,M_\odot$) | $31.5 \pm 3.1$ | $47.5 \pm 8.6$ |
| $m_1$ | ($M_\odot$) | $2.27 \pm 0.07$ | $2.27 \pm 0.07$ |
| $m_2 \sin i$ | ($M_\odot$) | $0.645 \pm 0.024$ | $0.758 \pm 0.047$ |
| $a$ | (AU) | $3.93 \pm 0.05$ | $3.79 \pm 0.05$ |

*Gaia* parallax of $\pi = 5.5393 \pm 0.0666$ mas (Gaia Collaboration 2018), the distance to the star is $d = 180.5 \pm 2.2$ pc. It also belongs to the non-oscillationg Ap stars.

For this star, 38 spectra have been acquired during 15 nights, covering a time span of 1406 days. The RVs vary by a few $\mathrm{km\,s^{-1}}$ (see Figure 6.26, middle panels). Both the HARPS CCF and HARPS-TERRA RVs give similar results. There appear two closely located peaks with an FAP of less than 0.1% in each of the GLS periodograms at the same positions (Figure 6.26, top panels): the slightly higher one at 120.4 days, the other one at 115.1 days. Additionally, a few more peaks are present exceeding the 1% FAP level at smaller periods and at $\sim$1600 days.

The data are not sufficient to determine a Keplerian orbit yet, and I cannot definitely specify which of the periods is the true one, but I will provide preliminary circular orbital solutions for the period with the highest power (Table 6.26). These are shown in Figure 6.26 as a time series (middle panels) and phased to the orbital period (bottom panels). For the sake of completeness, I also calculated circular orbits for the long period, which resulted in $1617 \pm 38$ and $1564 \pm 44$ days.

For the 120-day period, the minimum masses of the companion for the HARPS CCF and HARPS-TERRA orbits are $0.0670 \pm 0.0045$ and $0.0678 \pm 0.0048$ $M_\odot$ or $70.2 \pm 4.8$ and $71.1 \pm 5.1$ $M_\mathrm{Jup}$, respectively. The long-period orbit, on the other hand, would lead to minimum masses of $0.172 \pm 0.012$ and $0.169 \pm 0.013$ $M_\odot$ for the two data sets. It is interesting to note that if the short period is the true one and the orbit is seen (almost) equator-on, the companion mass would lie close to the edge of the transition between brown dwarfs and stars. However, since the long period cannot be excluded so far and since it is unlikely to see the orbit exactly equator-on, I consider this companion as a stellar companion in this work.

**Table 6.26:** Orbital parameters of the stellar companion of HD 142070.

| Parameter | | HARPS CCF | HARPS-TERRA |
|---|---|---|---|
| $P$ | (days) | $120.37 \pm 0.09$ | $120.44 \pm 0.10$ |
| $K$ | ($\mathrm{m\,s^{-1}}$) | $1781 \pm 38$ | $1802 \pm 53$ |
| $e$ | | $0.0 \pm 0.0$ (fixed) | $0.0 \pm 0.0$ (fixed) |
| $\omega$ | (deg) | $0.0 \pm 0.0$ (fixed) | $0.0 \pm 0.0$ (fixed) |
| $T_0$ | (BJD $-$ 2 400 000) | $54\,278.71 \pm 0.38$ | $54\,278.63 \pm 0.54$ |
| $\gamma, RV_0$ | ($\mathrm{m\,s^{-1}}$) | $-9313 \pm 28$ | $-256 \pm 40$ |
| $N_\mathrm{obs}$ | | 38 | 37 |
| $\sigma_\mathrm{O-C}$ | ($\mathrm{m\,s^{-1}}$) | 310 | 232 |
| $a_1 \sin i$ | ($10^{-3}$ AU) | $19.70 \pm 0.42$ | $19.95 \pm 0.59$ |
| $f(m_1, m_2, i)$ | ($10^{-3}$ $M_\odot$) | $0.0704 \pm 0.0045$ | $0.0730 \pm 0.0065$ |
| $m_1$ | ($M_\odot$) | $2.0 \pm 0.2$ | $2.0 \pm 0.2$ |
| $m_2 \sin i$ | ($M_\odot$) | $0.0670 \pm 0.0045$ | $0.0678 \pm 0.0048$ |
| | ($M_\mathrm{Jup}$) | $70.2 \pm 4.8$ | $71.1 \pm 5.1$ |
| $a$ | (AU) | $0.608 \pm 0.020$ | $0.608 \pm 0.020$ |

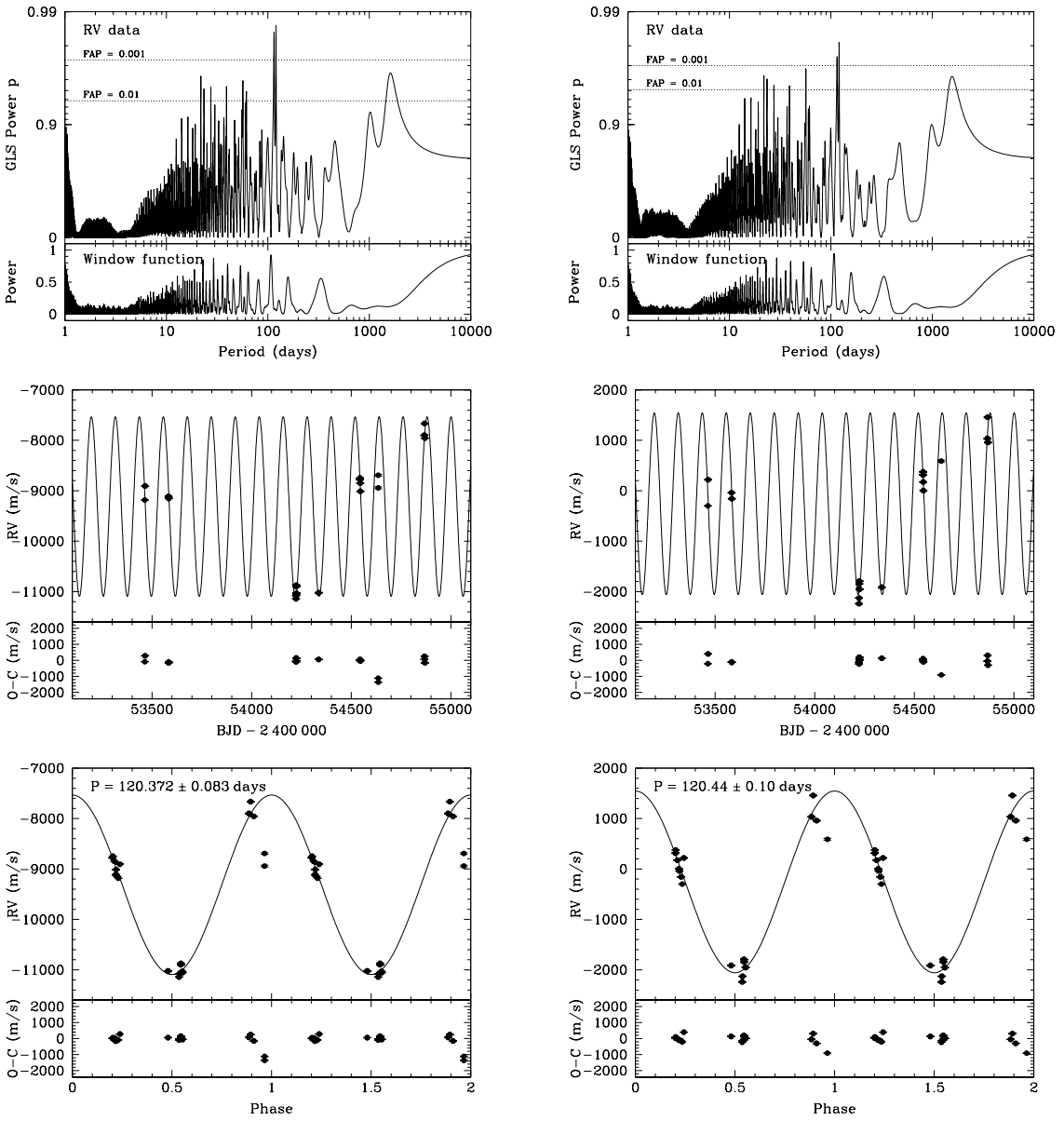


**Figure 6.26:** Results for HD 142070 analyzing the RV data obtained with the HARPS CCF technique (*left panels*) and the HARPS-TERRA software tool (*right panels*), respectively. *Top panels*: GLS periodograms of the RV data. The dotted lines indicate two levels of the FAP. The lower parts display the window function of the observations. *Middle panels*: RV measurements and best-fit Keplerian orbital solution (solid line). The RV residuals after subtracting the orbital solution are shown below. *Bottom panels*: RV measurements phased to the orbital period. Phase zero corresponds to the time of periastron passage. The solid line represents the orbital solution. Data points are repeated for the second cycle. Again, the RV residuals are shown below.

### HD 144059

HD 144059 (HIP 79076) has a visual magnitude of $V = 9.02 \pm 0.01$ (Høg et al. 2000). The spectral type is given by Renson & Manfroid (2009) to be A0 Si. The *Gaia* parallax of $\pi = 1.2117 \pm 0.0576$ mas (Gaia Collaboration 2018) translates into a distance to the star of $d = 825 \pm 39$ pc. This star is also a member of the subsample of non-oscillationg Ap stars.

I obtained 12 RV data points spanning 1405 days. The HARPS CCF RVs reveal variations of a few tens of $\mathrm{km\,s^{-1}}$. The HARPS-TERRA RVs, on the other hand, seem to be implausible again. Thus, this star is probably an SB2, although no indications of secondary spectral lines are seen. There is one peak visible above the 0.1% FAP level in the GLS periodogram (Figure 6.27, left panel). The corresponding period is 122.85 days. A Keplerian model yields a period of $122.876 \pm 0.038$ days and a slight eccentricity ($e = 0.1268 \pm 0.0043$). The orbital elements are provided in Table 6.27, the phase-folded orbit is shown in the right panel of Figure 6.27. For an adopted stellar mass of $m_1 = 2.0 \pm 0.2\ M_\odot$, the minimum mass of the companion would be $1.14 \pm 0.05\ M_\odot$.

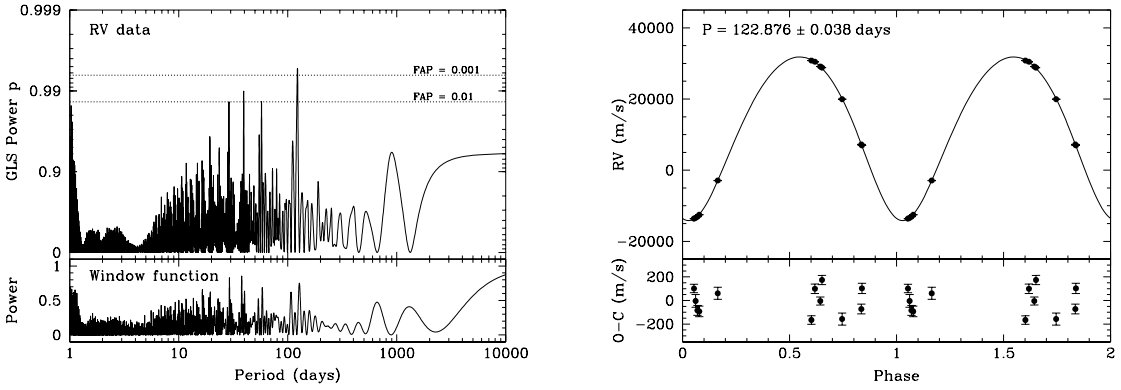


**Figure 6.27:** Results for HD 144059 analyzing the RV data obtained with the HARPS CCF technique. *Left panel*: GLS periodogram of the RV data and window function of the observations. The dotted lines indicate two levels of the FAP. *Right panel*: RV measurements phased to the given orbital period and best-fit Keplerian orbital solution (solid line). Phase zero corresponds to the time of periastron passage. Data points are repeated for the second cycle. The RV residuals after subtracting the orbital solution are shown below.

### HR 2727

HR 2727 (HD 55719, HIP 34802, E Pup) is listed with a visual magnitude of $V = 5.31$ in the Simbad database. Renson & Manfroid (2009) assign it a spectral type of A3 Sr Cr Eu. The Hipparcos parallax of $\pi = 7.93 \pm 0.38$ mas (van Leeuwen 2007) results in a distance to the star of $d = 126 \pm 6$ pc. Kochukhov & Bagnulo (2006) obtained the following values for the stellar mass and the effective temperature:

**Table 6.27:** Orbital parameters of the stellar companion of HD 144059.

| Parameter | | HARPS CCF |
|---|---|---|
| $P$ | (days) | $122.876 \pm 0.038$ |
| $K$ | ($\mathrm{km\,s^{-1}}$) | $23.00 \pm 0.10$ |
| $e$ | | $0.1268 \pm 0.0043$ |
| $\omega$ | (deg) | $166.7 \pm 4.8$ |
| $T_0$ | (BJD $-$ 2 400 000) | $54\,367.8 \pm 1.5$ |
| $\gamma$ | ($\mathrm{km\,s^{-1}}$) | $11.66 \pm 0.17$ |
| $N_{\mathrm{obs}}$ | | 12 |
| $\sigma_{\mathrm{O-C}}$ | ($\mathrm{m\,s^{-1}}$) | 112 |
| $a_1 \sin i$ | ($10^{-3}$ AU) | $257.6 \pm 1.1$ |
| $f(m_1, m_2, i)$ | ($10^{-3}\,M_\odot$) | $151.1 \pm 2.0$ |
| $m_1$ | ($M_\odot$) | $2.0 \pm 0.2$ |
| $m_2 \sin i$ | ($M_\odot$) | $1.14 \pm 0.05$ |
| $a$ | (AU) | $0.709 \pm 0.016$ |

**Table 6.28:** Orbital parameters of the stellar companion of HR 2727.

| Parameter | | Value (1) | Value (2) |
|---|---|---|---|
| $P$ | (days) | $46.314 \pm 0.003$ | $46.3387 \pm 0.0021$ |
| $K$ | ($\mathrm{km\,s^{-1}}$) | $48.53 \pm 0.22$ | $48.00 \pm 0.48$ |
| $e$ | | $0.1264 \pm 0.0035$ | $0.1223 \pm 0.0046$ |
| $\omega$ | (deg) | $209.7 \pm 2.0$ | $213.6 \pm 4.4$ |
| $T_0$ | (BJD $-$ 2 400 000) | $41\,674.94 \pm 0.25$ | $53\,718.17 \pm 0.50$ |
| $\gamma, \gamma_1$ | ($\mathrm{km\,s^{-1}}$) | $-4.43 \pm 0.16$ | $-5.47 \pm 7.04$ |
| $\gamma_2$ | ($\mathrm{km\,s^{-1}}$) | ... | $-8.14 \pm 0.34$ |
| $N_{\mathrm{obs}}$ | | 24 | 43 |
| $\sigma_{\mathrm{O-C}}$ | ($\mathrm{m\,s^{-1}}$) | 600 | 400 (only HARPS RVs) |
| $a_1 \sin i$ | (AU) | $0.2049 \pm 0.0009$ | $0.2029 \pm 0.0020$ |
| $f(m_1, m_2, i)$ | ($M_\odot$) | 0.5375 | $0.519 \pm 0.016$ |
| $m_1$ | ($M_\odot$) | ... | $2.49 \pm 0.07$ |
| $m_2 \sin i$ | ($M_\odot$) | ... | $2.28 \pm 0.03$ |
| $a$ | (AU) | ... | $0.4249 \pm 0.0025$ |

**References:** (1) Bonsack (1976); (2) Combined solution using RVs from this work and from Bonsack (1976)

$2.49 \pm 0.07\ M_\odot$ and $\log(T_{\mathrm{eff}}/\mathrm{K}) = 3.960 \pm 0.014$, respectively. This star is a non-oscillationg Ap star.

Nineteen observations have been taken during a time span of 1531 days. The RV measurements extracted with the HARPS pipeline show huge variations of several tens of $\mathrm{km\,s^{-1}}$. From these changes it is clear that the star has to be a spectroscopic binary. In contrast, the HARPS-TERRA RVs exhibit variations that are much smaller and inconsistent with the HARPS CCF RVs. The former data are thus useless and indicate that HR 2727 is an SB2 system, for which the HARPS-

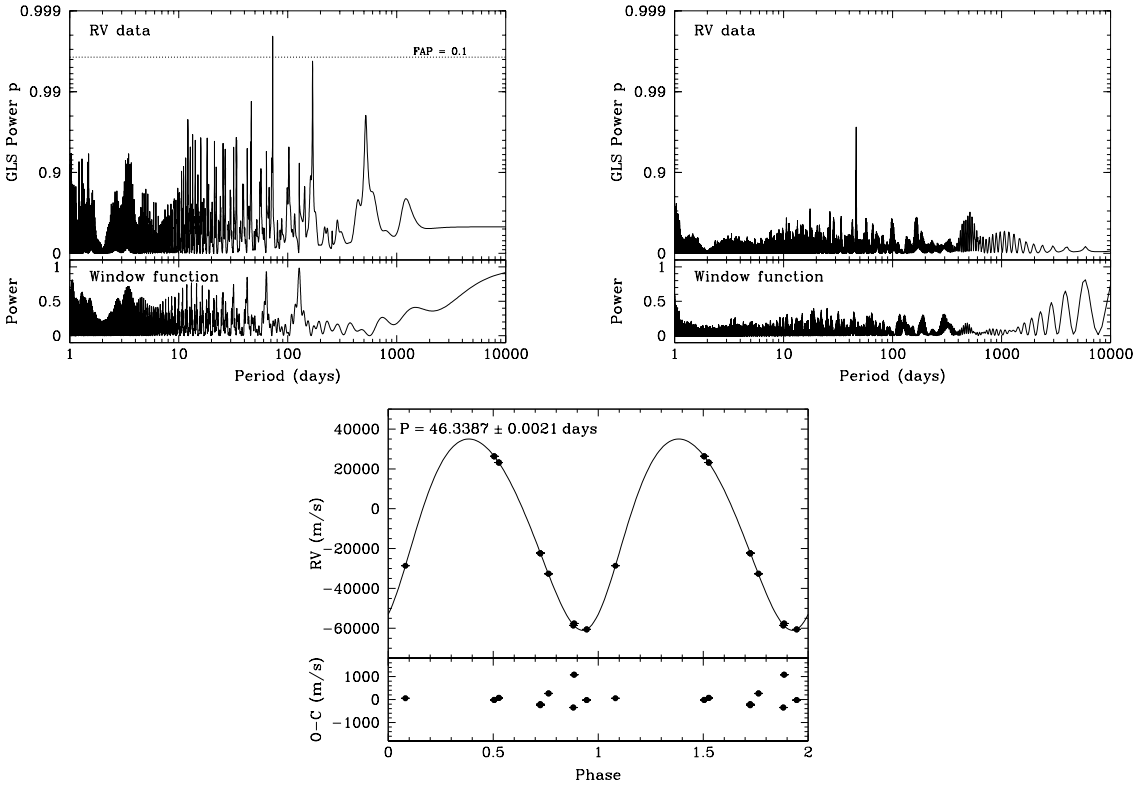


**Figure 6.28:** Results for HR 2727 analyzing the RV data obtained with the HARPS CCF technique. *Top panels*: GLS periodograms of the HARPS RV data (*left*) and in combination with the RV data of Bonsack (1976, *right)*. The dotted lines indicate the FAP. The lower parts display the window function of the observations. *Bottom panel*: RV measurements phased to the given orbital period and best-fit Keplerian orbital solution (solid line). Phase zero corresponds to the time of periastron passage. Data points are repeated for the second cycle. The RV residuals after subtracting the orbital solution are shown below.

TERRA tool cannot produce reliable results. As a consequence, I will analyze only the HARPS CCF RVs. The GLS periodogram is given in Figure 6.28 (top left panel). There is only one peak with an FAP of less than 10% visible at a period of 72.8 days. The second- and third-highest signals are present at periods of 169.2 and 46.4 days, respectively, but with FAPs of more than 10%.

HR 2727 was already known to be an SB2. Bonsack (1976) published 24 RVs collected with the coudé spectrograph of the 2.2 m telescope at the Mauna Kea Observatory between January 1973 and September 1975. He found the orbit given in Table 6.28, including the orbital period of $46.314 \pm 0.003$ days. Thus, I know that the third-highest peak in Figure 6.28 (top left panel) represents the true period. To verify this period, I also calculated a periodogram of the combined RV data sets (Figure 6.28, top right panel), where only one significant signal is seen at the correct period of 46.3 days.

A Keplerian orbital solution using the combined data yields a period of 46.3387± 0.0021 days. It is about 0.025 days longer than the period found by Bonsack (1976), which is significant at a confidence level of almost 5 $\sigma$. The other orbital elements are identical within their errors and listed in Table 6.28. In Figure 6.28 (bottom panel), the HARPS CCF RV data and this orbit are displayed phased to the given period. The minimum mass of the secondary star was calculated to be $2.28 \pm 0.03\ M_\odot$. This is consistent with a binary system consisting of two A-type stars. Bonsack (1976) stated that the companion star is an almost normal A-type star of spectral type A1 or A2 with a slight excess of calcium. He derived a mass ratio of the two stars of $m_1/m_2 = 0.75 \pm 0.03$ and minimum masses of the components of $m_1 \sin^3 i = 1.23\ M_\odot$ and $m_2 \sin^3 i = 1.65\ M_\odot$. Adopting the stellar mass from Kochukhov & Bagnulo (2006), $m_1 = 2.49\ M_\odot$, leads to an inclination of $i = 52\overset{\circ}{.}2$ and a stellar mass of $m_2 = 3.34\ M_\odot$ for the secondary.

### HD 59435

HD 59435 (HIP 36419, V827 Mon) is an A4 Sr Cr Eu star (Renson & Manfroid 2009) with a visual magnitude of $V = 7.94 \pm 0.01$ (Høg et al. 2000). The distance to the star is $d = 521 \pm 11$ pc, as computed from the *Gaia* parallax of $\pi = 1.9193 \pm 0.0417$ mas (Gaia Collaboration 2018). This star is a non-oscillationg Ap star.

I have acquired five RV measurements distributed over a time of 889 days. They differ by a few $\mathrm{km\,s^{-1}}$ and indicate the binary nature of this star. However, five RV points are insufficient to determine any orbital parameters.

Nevertheless, the detection of this SB2 system and the presentation of the orbit has been announced quite some time ago. Wade et al. (1996) realized observations with CORAVEL on the 1 m Swiss telescope at the Observatoire de Haute-Provence and gathered 50 RVs. Additional 19 RVs have been taken at ESO's 1.4 m Coudé Auxiliary Telescope and the Coudé Échelle Spectrograph. They derived the orbits of both components; the parameters are listed in Table 6.29. The orbital period was determined to be $1387.3 \pm 1.9$ days. According to these authors, this system consists of an evolved G8 or K0 giant (primary) and a magnetic Ap star (secondary), both

**Table 6.29:** Orbital parameters of the stellar companion of HD 59435 (Wade et al. 1996).

| Parameter | | Primary | Secondary |
|---|---|---|---|
| $P$ | (days) | $1387.3 \pm 1.9$ | |
| $K_{1,2}$ | ($\mathrm{km\,s^{-1}}$) | $16.92 \pm 0.14$ | $18.20 \pm 0.14$ |
| $e$ | | $0.284 \pm 0.005$ | |
| $\omega_{1,2}$ | (deg) | $87.3 \pm 1.5$ | $267.3 \pm 1.5$ |
| $T_0$ | (BJD − 2 400 000) | $46\,265.2 \pm 7.1$ | |
| $\gamma$ | ($\mathrm{m\,s^{-1}}$) | $40.34 \pm 0.06$ | |
| $N_{\mathrm{obs}}$ | | 69 | 69 |
| $\sigma_{\mathrm{O-C}}$ | ($\mathrm{km\,s^{-1}}$) | 0.74 | |
| $a_{1,2} \sin i$ | ($10^6\ \mathrm{km\,s^{-1}}$) | $309.45 \pm 2.60$ | $332.88 \pm 2.71$ |
| $m_{1,2} \sin^3 i$ | ($M_\odot$) | $2.850 \pm 0.053$ | $2.650 \pm 0.050$ |

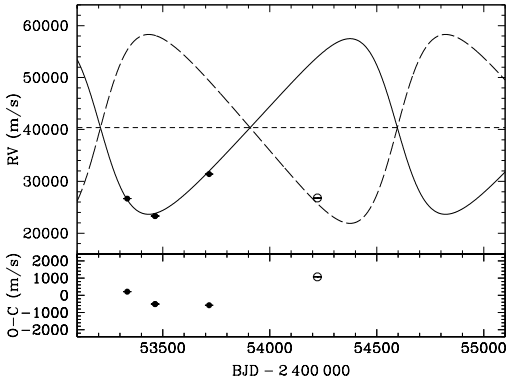


**Figure 6.29:** RV measurements for HD 59435: filled circles for the primary (evolved G8/K0 giant), open circles for the secondary (magnetic Ap star). The orbital solutions from Wade et al. (1996) are given for the primary (solid line) and the secondary (long-dashed line). The short-dashed line represents the $\gamma$-velocity. The RV residuals after subtracting the orbital solutions are shown below.

of which are slowly rotating and have similar luminosities. They further deduced an upper limit of 3.0 $M_\odot$ for the mass of the secondary star, which leads to $\sin^3 \geq 2.65/3.0$ and results in an inclination of $74° \leq i \leq 90°$. Therefore, the mass of the primary star lies between 2.85 and 3.23 $M_\odot$.

In Figure 6.29, my RV data are shown together with the RV curves of Wade et al. (1996). As can be seen, the HARPS RV points are fairly compatible with these orbits, but they provide – except for the last RV value – indeed measurements of the primary giant star instead of the Ap star. It turned out that the wrong dip of the CCF was measured by mistake because the lines of both components are narrow and have similar strengths.

### HD 81009

HD 81009 (HIP 45999, HR 3724, KU Hya) is listed as A3 Cr Sr Si star in the catalog of Renson & Manfroid (2009) and has a visual magnitude of $V = 6.53$ (Ducati 2002). The Hipparcos parallax of $\pi = 6.92 \pm 0.61$ mas (van Leeuwen 2007) yields a distance to the star of $d = 145 \pm 13$ pc. Kochukhov & Bagnulo (2006) derived a stellar mass of $2.04 \pm 0.09$ $M_\odot$ and an effective temperature of $\log(T_{\rm eff}/{\rm K}) = 3.900 \pm 0.011$. This star belongs to the subsample of the non-oscillationg Ap stars.

In 13 nights, 43 RV points have been recorded. The time series spans 1407 days and shows an almost linear increase of more than 1000 m s$^{-1}$ (see Figure 6.30, upper panels).

The binary nature of HD 81009 is known since several decades, and a few astrometric orbital solutions have already been published (Finsen 1968; van Dessel 1972; Starikova 1981). Combining astrometric and RV observations, Wade et al. (2000) performed a detailed study of this system. Their modelling revealed a highly eccentric ($e = 0.718 \pm 0.006$), very long-period ($P = 29.30 \pm 0.27$ years) binary orbit

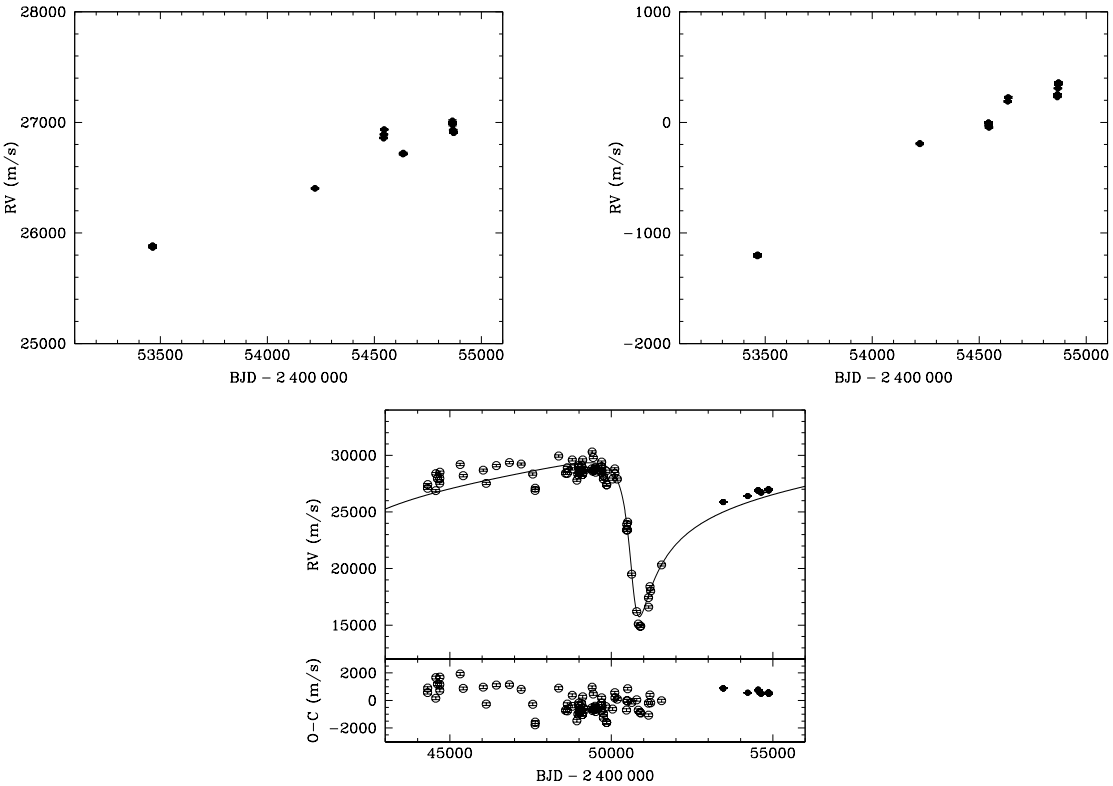


**Figure 6.30:** *Top panels*: RV measurements for HD 81009 obtained with the HARPS CCF technique (*left panel*) and the HARPS-TERRA software tool (*right panel*). *Bottom panel*: RV measurements for HD 81009 taken from Wade et al. (2000, open circles) together with the HARPS CCF RVs (filled circles). The orbital solution from Wade et al. (2000) is given as a solid line. The RV residuals after subtracting the orbital solution are shown below.

**Table 6.30:** Orbital parameters of the stellar companion of HD 81009 (Wade et al. 2000).

| Parameter | | Value |
|---|---|---|
| $P$ | (years) | $29.30 \pm 0.27$ |
| | (days) | $10673 \pm 99$ |
| $K$ | ($\mathrm{km\,s^{-1}}$) | $6.80 \pm 0.09$ |
| $e$ | | $0.718 \pm 0.006$ |
| $\omega$ | (deg) | $134.24 \pm 0.77$ |
| $T_0$ | (BJD $-$ 2 400 000) | $50\,695 \pm 8$ |
| $\gamma$ | ($\mathrm{km\,s^{-1}}$) | $25.95 \pm 0.10$ |
| $N_{\mathrm{obs}}$ | | 72 |
| $i$ | (deg) | $138.6 \pm 1.8$ |
| $m_1$ | ($M_\odot$) | $2.6 \pm 1.5$ |
| $m_2$ | ($M_\odot$) | $1.6 \pm 0.5$ |
| $a_1 \sin i$ | (AU) | 4.647 |
| $a_2 \sin i$ | (AU) | 7.346 |

(Figure 6.30, bottom panel). The orbital parameters are summarized in Table 6.30. Both components are main-sequence A-type stars with masses of $m_1 = 2.6 \pm 1.5\ M_\odot$ and $m_2 = 1.6 \pm 0.5\ M_\odot$, where the primary is a slowly rotating Ap star.

### HD 92106

HD 92106 (HIP 51632, DQ Cha) has a spectral type of A0 Sr Eu Cr star (Renson & Manfroid 2009) and a visual magnitude of $V = 7.77 \pm 0.01$ (Høg et al. 2000). According to the *Gaia* parallax of $\pi = 4.3276 \pm 0.0352$ mas (Gaia Collaboration 2018), the star is located at a distance of $d = 231.1 \pm 1.9$ pc. This star is a non-oscillationg Ap star.

For this star, 13 RV measurements were collected covering 1211 days. While the HARPS CCF RVs exhibit huge variations of several tens of $\mathrm{km\,s^{-1}}$, the HARPS-TERRA RVs are again producing non-reliable values, pointing to the SB2 nature of this star. The GLS periodogram in Figure 6.31 (left panel) shows two peaks with similar power at 1.1495 days ($p_{\mathrm{GLS}} = 0.9976$) and 4.811 days ($p_{\mathrm{GLS}} = 0.9966$). Both signals have an FAP of more than 10%. However, the estimated FAP – based on nightly averaged RVs – might be too conservative because a significant RV change is already visible in two consecutive observations per night. Thus, taking each RV value as an independent measurement would have been a better approach for calculating the FAP in this case. Despite that, there is no question that the RV variations are due to a short-period binary, even though the definite period cannot be ascertained.

For now, I provide a preliminary sinusoidal orbital solution for the 1.1495-day period, since it is the highest and hence the most likely signal. The corresponding parameters are listed in Table 6.31, and the phased orbit is displayed in Figure 6.31 (right panel). Assuming a mass of $2.0 \pm 0.2\ M_\odot$ for the primary, the minimum mass

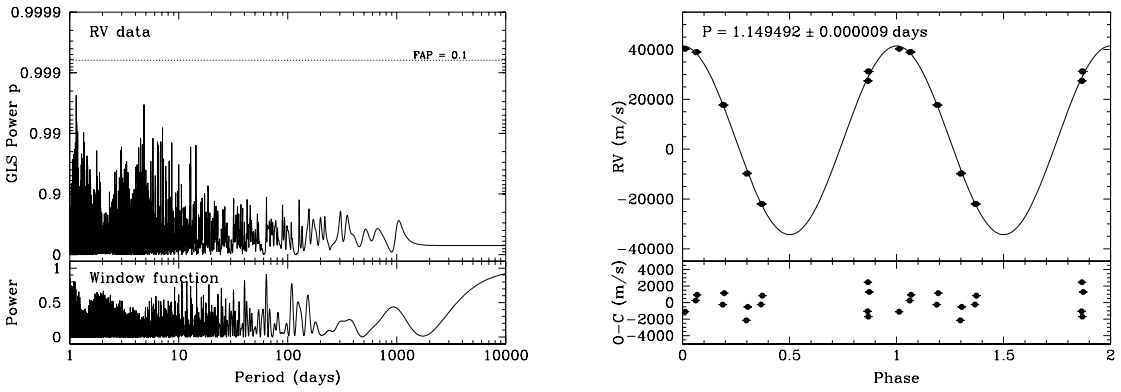


**Figure 6.31:** Results for HD 92106 analyzing the RV data obtained with the HARPS CCF technique. *Left panel*: GLS periodogram of the RV data and window function of the observations. The dotted line indicates the FAP. *Right panel*: RV measurements phased to the given orbital period and best-fit sinusoidal orbital solution (solid line). Phase zero corresponds to the time of periastron passage. Data points are repeated for the second cycle. The RV residuals after subtracting the orbital solution are shown below.

**Table 6.31:** Orbital parameters of the stellar companion of HD 92106.

| Parameter | | HARPS CCF |
|---|---|---|
| $P$ | (days) | $1.149492 \pm 0.000009$ |
| $K$ | ($\mathrm{km\,s^{-1}}$) | $37.89 \pm 0.96$ |
| $e$ | | $0.0 \pm 0.0$ (fixed) |
| $\omega$ | (deg) | $0.0 \pm 0.0$ (fixed) |
| $T_0$ | (BJD $-$ 2 400 000) | $54\,091.2771 \pm 0.0035$ |
| $\gamma$ | ($\mathrm{km\,s^{-1}}$) | $3.56 \pm 0.55$ |
| $N_{\mathrm{obs}}$ | | 13 |
| $\sigma_{\mathrm{O-C}}$ | ($\mathrm{m\,s^{-1}}$) | 1319 |
| $a_1 \sin i$ | ($10^{-3}$ AU) | $4.00 \pm 0.10$ |
| $f(m_1, m_2, i)$ | ($10^{-3}\,M_\odot$) | $6.48 \pm 0.49$ |
| $m_1$ | ($M_\odot$) | $2.0 \pm 0.2$ |
| $m_2 \sin i$ | ($M_\odot$) | $0.327 \pm 0.021$ |
| $a$ | (AU) | $0.0285 \pm 0.0008$ |

of the secondary is $0.327 \pm 0.021\ M_\odot$.

### 6.2.2 Spectroscopic binaries without orbit

Seven stars of my sample show long-term RV trends which will be discussed in this section. The data of these stars cover time spans between $\sim$1250 and $\sim$1530 days (except for one target with only 642 days), and the minimum-to-maximum RV changes range from $\sim$700 up to more than 17 000 $\mathrm{m\,s^{-1}}$. Thus, probably all of these objects are spectroscopic binaries, whose orbital periods are exceeding the times the stars were monitored. Sometimes, the RV measurements do not only show a linear trend, but also some curvature. The calculation of an orbit, however, was not possible for none of the stars. The presented stars are ordered by their right ascension.

#### HD 53116

HD 53116 (HIP 34049, V646 Mon) is an A0 Sr Eu star (Renson & Manfroid 2009) with a visual magnitude of $V = 8.90 \pm 0.02$ (Høg et al. 2000). Given the *Gaia* parallax of $\pi = 1.4379 \pm 0.1107$ mas (Gaia Collaboration 2018), the distance to the star is $d = 695 \pm 54$ pc. This star is a non-oscillationg Ap star.

The 23 RV measurements were taken in 18 nights. Both the HARPS CCF and HARPS-TERRA data show a linearly rising trend with an increase of about 4000 $\mathrm{m\,s^{-1}}$ over the 1535-day time baseline (see Figure 6.32). These variations are with high probability due to a stellar companion with very long period.

#### HD 116114

HD 116114 (HIP 65203) is an F0 Sr Cr Eu star (Renson & Manfroid 2009) with a visual magnitude of $V = 7.02 \pm 0.01$ (Høg et al. 2000). The distance to the star, as

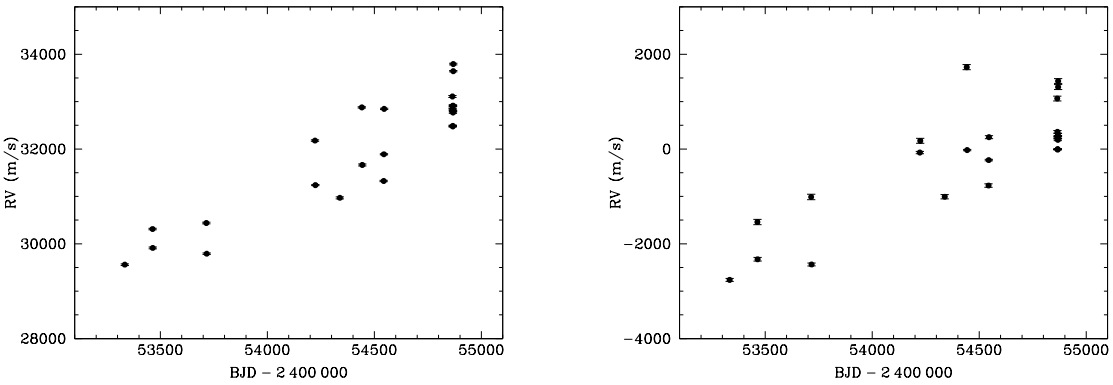


**Figure 6.32:** RV measurements for HD 53116 obtained with the HARPS CCF technique (*left panel*) and the HARPS-TERRA software tool (*right panel*).

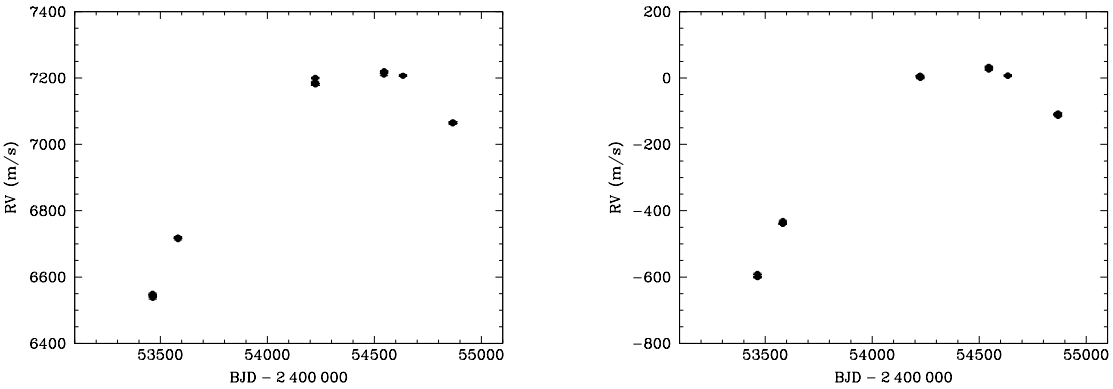


**Figure 6.33:** RV measurements for HD 116114 obtained with the HARPS CCF technique (*left panel*) and the HARPS-TERRA software tool (*right panel*).

determined from the *Gaia* parallax, $\pi = 7.3972 \pm 0.0665$ mas (Gaia Collaboration 2018), is $d = 135.2 \pm 1.2$ pc. Stellar mass and effective temperature were measured by Kochukhov & Bagnulo (2006) to be $1.92 \pm 0.10\ M_\odot$ and $\log(T_{\rm eff}/{\rm K}) = 3.870 \pm 0.012$, respectively.

This star was assumed to be a non-oscillationg Ap star because no variability has been detected in previous photometric surveys (Nelson & Kreidl 1993; Martinez & Kurtz 1994b). But later, based on 111 spectroscopic observations carried out in a 2-hour observing period with the high-resolution Ultraviolet and Visual Échelle Spectrograph (UVES) on UT2 of the Very Large Telescope (VLT) at ESO, Elkin et al. (2005) found rapid oscillations with a period of 21 min. These authors also stated that *"the long time series of observations obtained to study the mean magnetic field modulus of HD 116114 also revealed that it is a spectroscopic binary with widely separated components."* They specified that *"the orbital period must be longer than 6.5 years."*

During a timeframe of 1405 days, I acquired two consecutive spectra in 12 nights, resulting in 24 RV points. The difference between minimum and maximum RV is

almost 700 m s$^{-1}$. Moreover, the top turning point of the RV curve is clearly visible (Figure 6.33). Nevertheless, the data are not sufficient to obtain an orbit. Assuming the orbit is not very eccentric, a rough estimate yields that the orbital period should be at least twice as long as the period of time covered by the RV data, i.e., $P \gtrsim 7.7$ years.

### HD 119027

HD 119027 (LZ Hya) has a visual magnitude of $V = 9.92 \pm 0.03$ (Høg et al. 2000). Its spectral type was given as A3 Sr Eu by Renson & Manfroid (2009). From the *Gaia* parallax of $\pi = 3.0158 \pm 0.0653$ mas (Gaia Collaboration 2018), the distance to the star can be calculated to $d = 332 \pm 7$ pc.

This star was discovered to oscillate with a period of 8.63 min and an amplitude of 1.8 mmag by Martinez & Kurtz (1991), who also noted that their Johnson $B$ photometric observations suggested the presence of amplitude modulations on a time scale of $\approx 1$ day. With additional 18 nights of observations, Martinez et al. (1993) concluded that HD 119027 pulsates with at least five frequencies in the vicinity of 1.9 mHz (principal frequency $\nu_1 = 1.91357$ mHz corresponds to a period of 8.71 min), and these five frequencies are equally spaced by about 26 $\mu$Hz. In conclusion, Martinez & Kurtz (1994a) list an oscillation period of 8.7 min and a peak-to-peak amplitude of 2.0 mmag for this star.

The 13 obtained RV measurements displayed in Figure 6.34 comprise a time span of 1405 days and rise steadily by about 2800 m s$^{-1}$, pointing to the binary nature of this star. The RV curve also indicates a slight curvature, but this is not enough to get an estimate of the orbital period, which must considerably exceed the time the star has been monitored.

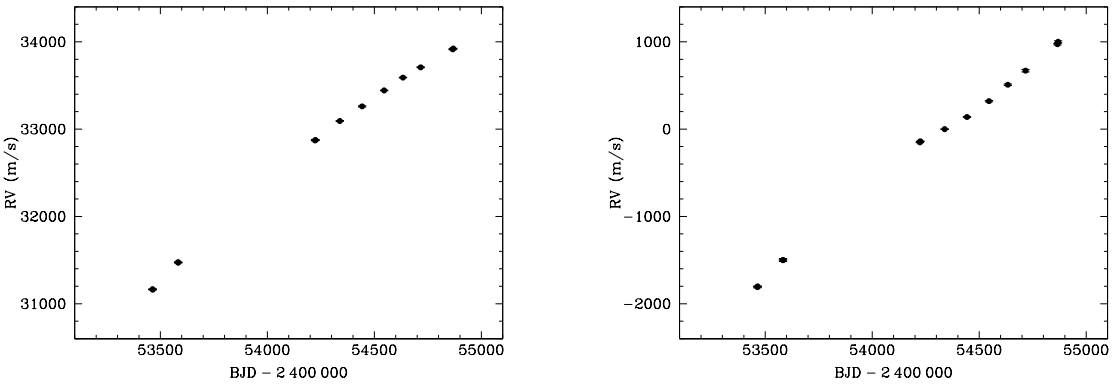


**Figure 6.34:** RV measurements for HD 119027 obtained with the HARPS CCF technique (*left panel*) and the HARPS-TERRA software tool (*right panel*).

### HD 144897

HD 144897 (HIP 79197) is a B8 Eu Cr star (Renson & Manfroid 2009) and listed with a visual magnitude of $V = 8.59$ in the Simbad database. According to the *Gaia* parallax of $\pi = 3.5682 \pm 0.0634$ mas (Gaia Collaboration 2018), the star is located at a distance of $d = 280 \pm 5$ pc.

I took 14 RV measurements spanning 1405 days. These are shown in Figure 6.35. The RV curve is rather flat in the beginning and ends in a rapid increase. For the HARPS CCF data, the change from minimum to maximum is 17 350 m s$^{-1}$, while it is only 11 490 m s$^{-1}$ for the HARPS-TERRA data. This might be an indication of contamination from the secondary star; in other words, this could be an SB2 system. Anyway, the binary orbit has to be eccentric with a very long period.

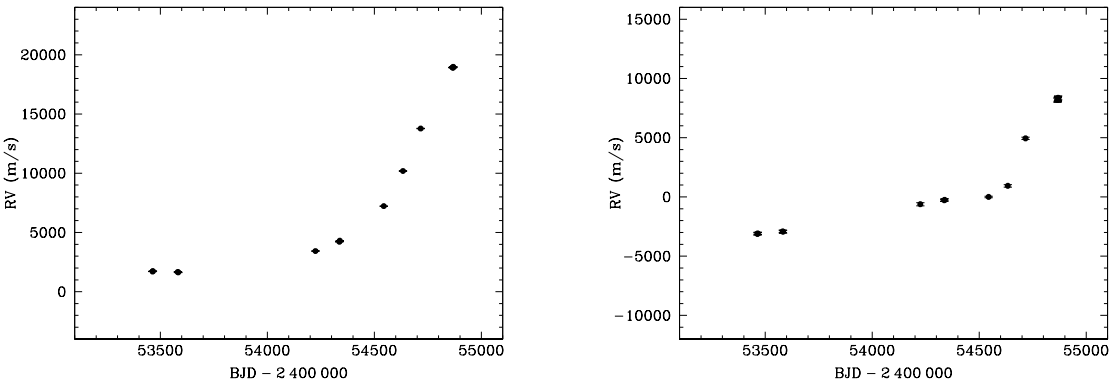


**Figure 6.35:** RV measurements for HD 144897 obtained with the HARPS CCF technique (*left panel*) and the HARPS-TERRA software tool (*right panel*).

### HR 6958

HR 6958 (HD 170973, HIP 90858, MV Ser) was classified as an A0 Si Cr Sr star (Renson & Manfroid 2009) and has a visual magnitude of $V = 6.407 \pm 0.009$ (Høg et al. 2000). The *Gaia* parallax of $\pi = 3.9773 \pm 0.0633$ mas (Gaia Collaboration 2018) results in a distance to the star of $d = 251 \pm 4$ pc.

The data set consists of 19 RV points, which were gathered in 10 nights and distributed over 1253 days (Figure 6.36). The RV values increase nearly linearly by $\sim$3400 m s$^{-1}$ (HARPS CCF data) and $\sim$3200 m s$^{-1}$ (HARPS-TERRA data). The orbit of the stellar companion is thus not yet determinable.

### HD 208217

HD 208217 (HIP 108340, BD Ind) is an A0 Sr Eu Cr star (Renson & Manfroid 2009) with a visual magnitude of $V = 7.19 \pm 0.01$ (Høg et al. 2000). Using the *Gaia* parallax of $\pi = 8.6812 \pm 0.1407$ mas (Gaia Collaboration 2018), the distance to the star is $d = 115.2 \pm 1.9$ pc. The stellar mass provided by Kochukhov & Bagnulo

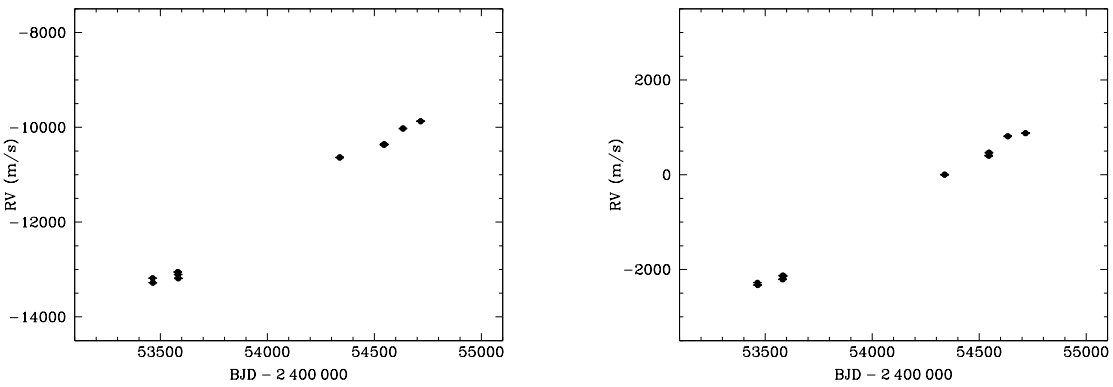


**Figure 6.36:** RV measurements for HR 6958 obtained with the HARPS CCF technique (*left panel*) and the HARPS-TERRA software tool (*right panel*).

(2006) is $1.93 \pm 0.10\ M_{\odot}$. These authors also obtained an effective temperature of $\log(T_{\rm eff}/{\rm K}) = 3.904 \pm 0.011$. This star is a non-oscillationg Ap star.

The star has been monitored for 642 days, and the eight RV measurements show a drop by $\sim 6470\ {\rm m\,s^{-1}}$ and $\sim 5750\ {\rm m\,s^{-1}}$ for the HARPS CCF and HARPS-TERRA data, respectively (Figure 6.37), demonstrating that the star is a binary. Due to the bad time sampling of the data that are clustered around three areas, I cannot make any conclusion whether the orbital period is longer or shorter than the observed time span.

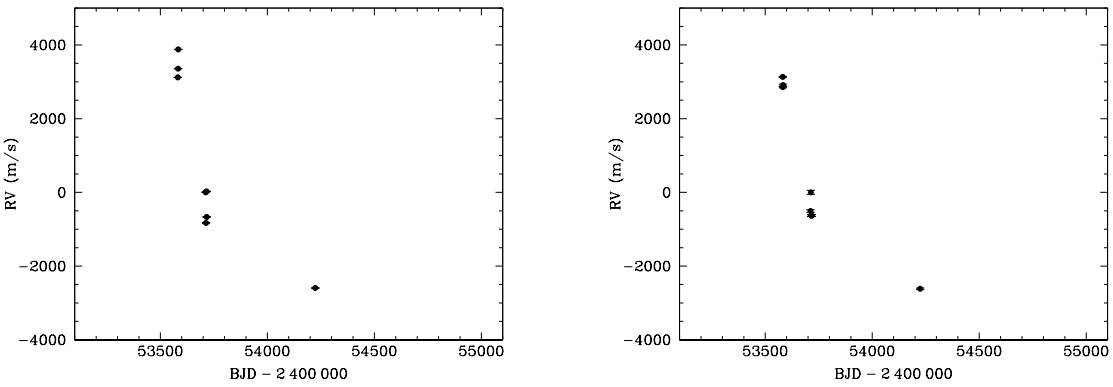


**Figure 6.37:** RV measurements for HD 208217 obtained with the HARPS CCF technique (*left panel*) and the HARPS-TERRA software tool (*right panel*).

### HR 8949

HR 8949 (HD 221760, HIP 116389, iot Phe) is a bright star ($V = 4.71$, Ducati 2002). Its spectral type is cataloged as A2 Sr Cr Eu (Renson & Manfroid 2009). The *Gaia* parallax of $\pi = 12.8425 \pm 0.3922$ mas (Gaia Collaboration 2018) yields a distance of $d = 77.9 \pm 2.4$ pc from the Sun.

I have obtained three consecutive spectra in 19 nights for this star. The resulting 57 RV values span a timeframe of 1284 days and are illustrated in Figure 6.38. However, for the analysis with the HARPS-TERRA software, two spectra were rejected because their S/N was too low to be used with this program. The RV curve is declining with huge maximum-to-minimum variations of about 11 840 m s$^{-1}$ (10 980 m s$^{-1}$) for the HARPS CCF (HARPS-TERRA) data; hence, it is obvious that the star has a binary companion in a very long-period orbit. Although there is a little bit of curvature present, the observed fraction of the orbit is insufficient to calculate any parameters.

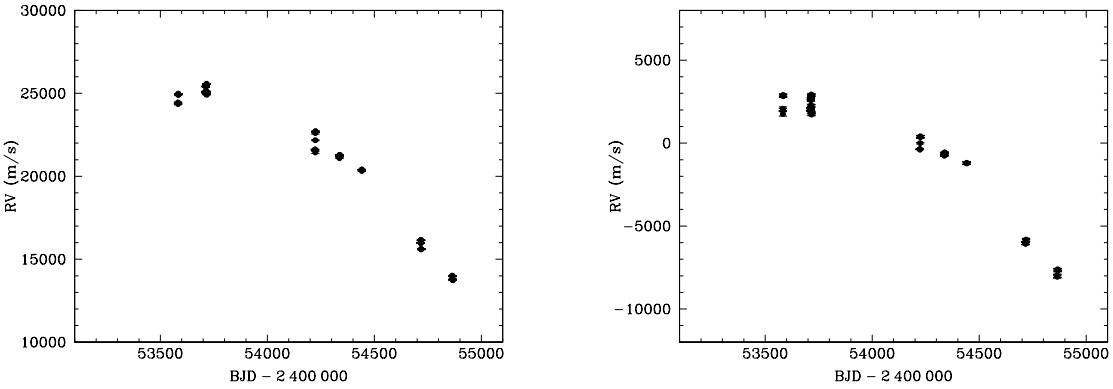


**Figure 6.38:** RV measurements for HR 8949 obtained with the HARPS CCF technique (*left panel*) and the HARPS-TERRA software tool (*right panel*).

### 6.2.3 Rotational modulation

In the following, I will show three examples, where rotational modulation causes RV variations. Depending on which of the two methods for calculating the RVs is used, the detected period can be different from the rotation period.

#### HR 1217

HR 1217 (HD 24712, HIP 18339, DO Eri) is classified as A9 Sr Eu Cr star in the catalog of Renson & Manfroid (2009), and its visual magnitude is $V = 6.00$ (Ducati 2002). According to the *Gaia* parallax of $\pi = 20.6216 \pm 0.0782$ mas (Gaia Collaboration 2018), the distance to the star is $d = 48.49 \pm 0.18$ pc. The stellar mass and the effective temperature from Kochukhov & Bagnulo (2006) are $1.55 \pm 0.03\ M_\odot$ and $\log(T_{\rm eff}/{\rm K}) = 3.857 \pm 0.012$, respectively.

High-speed photometric observations resulted in the discovery of rapid brightness variations with periods around 6.14 min (Kurtz 1982). After collecting more data, Kurtz et al. (2005) found $\nu = 2.7209$ mHz (6.125 min) for the pulsation cycle with the highest amplitude. In their analysis, they also deduced the rotation period of the star, $P_{\rm rot} = 12.4572$ days. Using polarimetric observations, Bagnulo et al. (1995) derived the magnetic period of this star to be $P_{\rm mag} = 12.4610 \pm 0.0011$ days, which was later confirmed by Bychkov et al. (2005), who obtained $P_{\rm mag} = 12.4617$ days. There is a slight discrepancy in the rotation period depending whether photometric or magnetic measurements are used, leading to some controversy. Kurtz et al. (2005) suggested that zero-point shifts between magnetic data resulting from different spectral lines might be the reason for that.

For this star, 61 RV measurements have been taken in 21 nights covering 1287 days (Figure 6.39, middle panels). Both the HARPS CCF and HARPS-TERRA RV data show a variability with a similar period, as can be seen in the periodograms (Figure 6.39, top panels). Sine fits to the data sets yield periods of $12.4527 \pm 0.0018$ and $12.4765 \pm 0.0025$ days with amplitudes of $363.3 \pm 10.2$ and $135.1 \pm 10.6$ m s$^{-1}$, respectively (see Table 6.32). The phase-folded RVs with the corresponding sine wave are displayed in the bottom panels of Figure 6.39.

The derived RV periods are very close to the abovementioned rotation periods. In particular, the period determined from the HARPS CCF data seems to favor the rotation period from Kurtz et al. (2005). The RV amplitudes, on the other hand, differ by almost a factor of three.

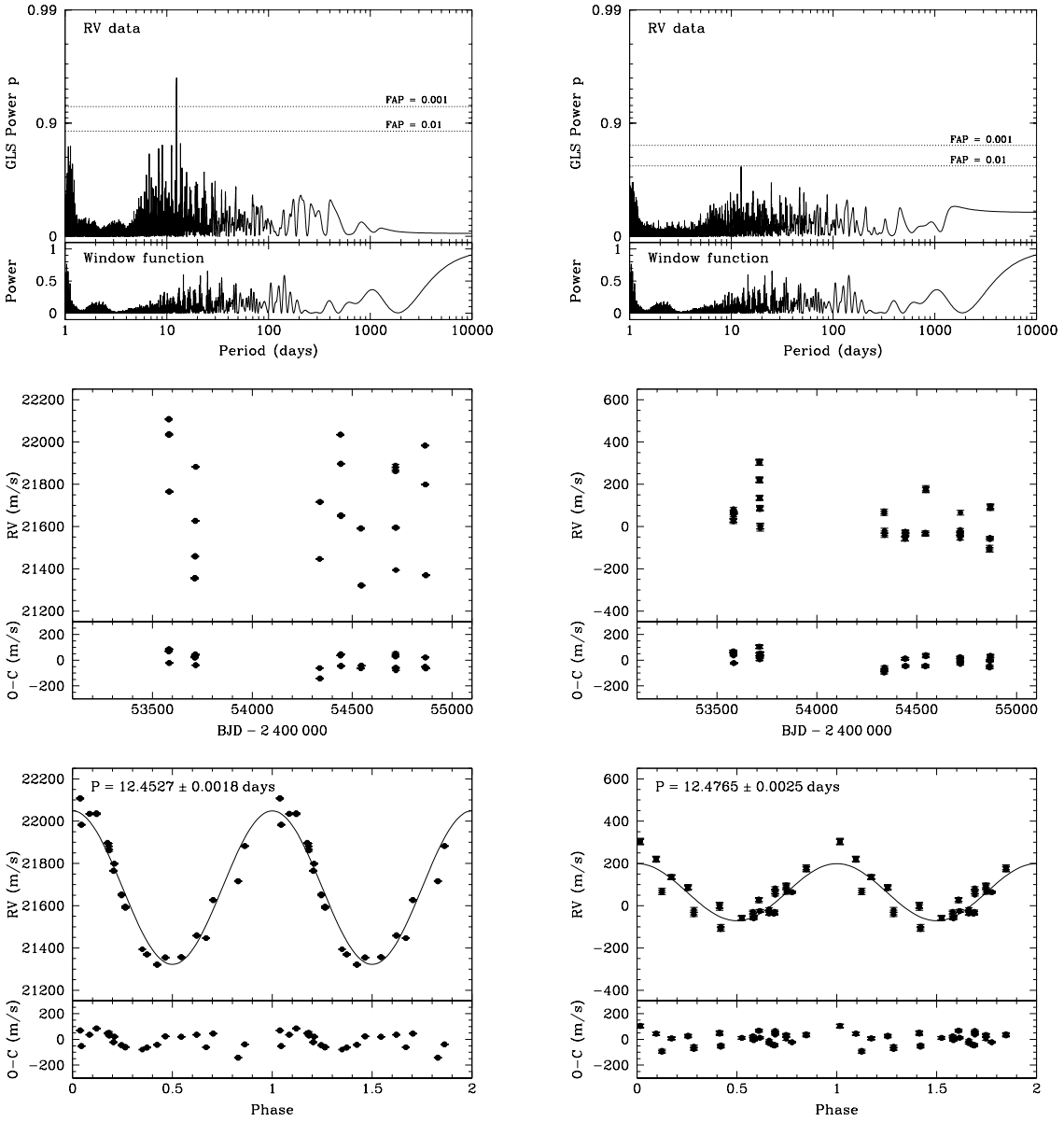


**Figure 6.39:** Results for HR 1217 analyzing the RV data obtained with the HARPS CCF technique (*left panels*) and the HARPS-TERRA software tool (*right panels*), respectively. *Top panels*: GLS periodograms of the RV data. The dotted lines indicate two levels of the FAP. The lower parts display the window function of the observations. *Middle panels*: RV measurements and residuals after subtracting the best-fitting sine function. *Bottom panels*: RV measurements phased to the given period. Phase zero corresponds to the time of maximum RV. The solid line represents the sine fit. Data points are repeated for the second cycle. Again, the RV residuals are shown below.

**Table 6.32:** Parameters of a sine fit to the RV data of HR 1217.

| Parameter | | HARPS CCF | HARPS-TERRA |
|---|---|---|---|
| $P$ | (days) | $12.4527 \pm 0.0018$ | $12.4765 \pm 0.0025$ |
| $K$ | ($\mathrm{m\,s^{-1}}$) | $363.3 \pm 10.2$ | $135.1 \pm 10.6$ |
| $T_0$ | (BJD $-$ 2 400 000) | $54\,179.0934 \pm 0.0560$ | $53\,973.4837 \pm 0.1223$ |
| $\gamma, RV_0$ | ($\mathrm{m\,s^{-1}}$) | $21\,685.4 \pm 8.3$ | $63.9 \pm 7.1$ |
| $N_{\mathrm{obs}}$ | | 61 | 61 |
| $\sigma_{\mathrm{O-C}}$ | ($\mathrm{m\,s^{-1}}$) | 58.3 | 47.2 |

## HD 126515

HD 126515 (HIP 70553, FF Vir) is an A2 Cr Sr Eu star (Renson & Manfroid 2009) with a visual magnitude of $V = 7.07$ (Ducati 2002). Using the *Gaia* parallax of $\pi = 7.5682 \pm 0.0871$ mas (Gaia Collaboration 2018), the star is located at a distance of $d = 132.1 \pm 1.5$ pc. The star has a mass of $2.32 \pm 0.11\ M_{\odot}$ and an effective temperature of $\log(T_{\mathrm{eff}}/\mathrm{K}) = 4.007 \pm 0.013$ (Kochukhov & Bagnulo 2006). This star belongs to the non-oscillating Ap stars.

The measurements of the mean magnetic field modulus yielded a period of $P_{\mathrm{mag}} = 129.95$ days (Mathys & Hubrig 1997). The phase curve of the effective (longitudinal) magnetic field is best fit by a double sine wave (Bychkov et al. 2005).

Spanning a timeframe of 1404 days, the star was monitored during 16 nights, in which always two consecutive spectra have been recorded. The resulting 32 RV points are illustrated in the middle panels of Figure 6.40. The GLS periodograms of the HARPS CCF and HARPS-TERRA RV data are displayed in the top panels of Figure 6.40. The highest peaks in these periodograms are visible at different periods. Fitting a sine function to the data results in the following periods: $130.60 \pm 0.15$ days for the HARPS CCF data and $64.989 \pm 0.035$ days for the HARPS-TERRA data. The amplitudes of the signals are $407.0 \pm 9.9$ and $102.2 \pm 4.1\ \mathrm{m\,s^{-1}}$, respectively, hence again several times (factor 4) lower for the HARPS-TERRA data. All parameters of these fits are given in Table 6.33. The phase-folded RV curves with the adopted sine functions are shown in the bottom panels of Figure 6.40.

In this case, we see the rotation period in the HARPS CCF data and half the rotation period in the HARPS-TERRA data.

**Table 6.33:** Parameters of a sine fit to the RV data of HD 126515.

| Parameter | | HARPS CCF | HARPS-TERRA |
|---|---|---|---|
| $P$ | (days) | $130.60 \pm 0.15$ | $64.989 \pm 0.035$ |
| $K$ | ($\mathrm{m\,s^{-1}}$) | $407.0 \pm 9.9$ | $102.2 \pm 4.1$ |
| $T_0$ | (BJD $-$ 2 400 000) | $54\,362.98 \pm 0.48$ | $54\,292.717 \pm 0.251$ |
| $\gamma, RV_0$ | ($\mathrm{m\,s^{-1}}$) | $-4076.8 \pm 7.7$ | $-57.1 \pm 3.3$ |
| $N_{\mathrm{obs}}$ | | 32 | 32 |
| $\sigma_{\mathrm{O-C}}$ | ($\mathrm{m\,s^{-1}}$) | 37.6 | 16.5 |

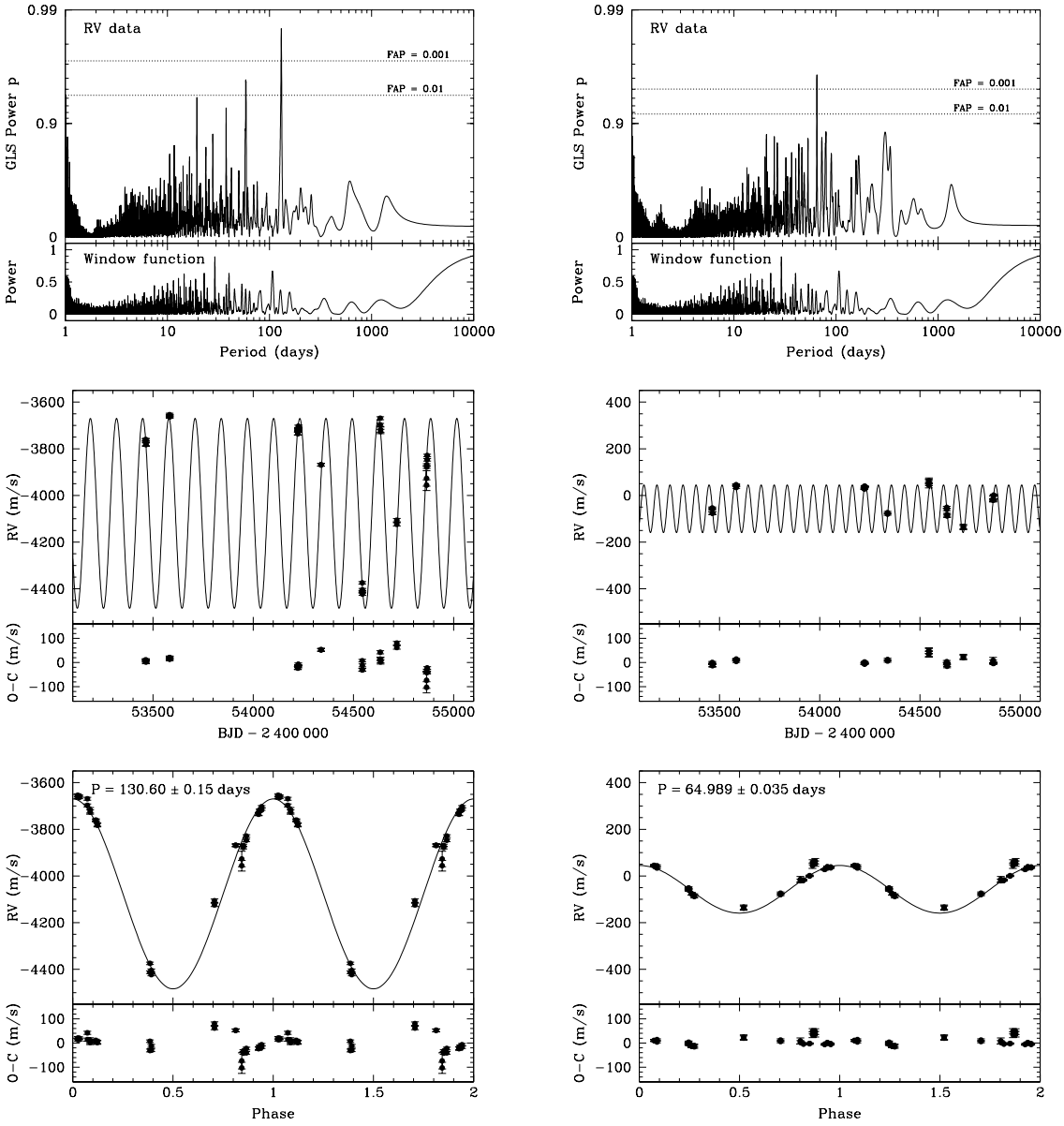


**Figure 6.40:** Results for HD 126515 analyzing the RV data obtained with the HARPS CCF technique (*left panels*) and the HARPS-TERRA software tool (*right panels*), respectively. *Top panels*: GLS periodograms of the RV data. The dotted lines indicate two levels of the FAP. The lower parts display the window function of the observations. *Middle panels*: RV measurements and best-fitting sine function (solid line). The RV residuals after subtracting the sine fit are shown below. *Bottom panels*: RV measurements phased to the given period. Phase zero corresponds to the time of maximum RV. The solid line represents the sine fit. Data points are repeated for the second cycle. Again, the RV residuals are shown below.

### HD 188041

HD 188041 (HIP 97871, HR 7575, V1291 Aql) is listed as A6 Sr Cr Eu star (Renson & Manfroid 2009) and has a visual magnitude of $V = 5.619 \pm 0.010$ (Høg et al. 2000). The distance to the star is $d = 85.3 \pm 0.7$ pc, as calculated from the *Gaia* parallax of $\pi = 11.7248 \pm 0.1011$ mas (Gaia Collaboration 2018). Kochukhov & Bagnulo (2006) provided a stellar mass of $2.20 \pm 0.07\ M_\odot$ and an effective temperature of $\log(T_{\rm eff}/{\rm K}) = 3.926 \pm 0.010$.

Hensberge (1993) determined a photometric period of $223.9 \pm 0.2$ days. A similar period (223.826 days) was found by Bychkov et al. (2005) when analyzing the available effective (longitudinal) magnetic field measurements.

I have acquired a sequence of three RV measurements in 13 nights spread over 1253 days (Figure 6.41, middle panels). The GLS periodograms of the HARPS CCF and HARPS-TERRA RV data are presented in the top panels of Figure 6.41. The highest peaks in these periodograms are again located at different periods. Calculating the best-fit sine functions to the data gives periods of $35.170 \pm 0.015$ and $224.42 \pm 0.22$ days with amplitudes of $15.95 \pm 0.66$ and $22.56 \pm 0.40$ m s$^{-1}$ for the HARPS CCF and HARPS-TERRA data, respectively. Table 6.34 summarizes the fitting parameters. The RVs data and these fits are presented in Figure 6.41 as a time series (middle panels) and phased to the corresponding period (bottom panels).

In contrast to the previous examples, the HARPS-TERRA data now show the slightly larger amplitude, and the RV period is consistent with the rotation period. The HARPS CCF data, on the other hand, reveal a period that cannot be attributed to rotation at all because it is not a harmonic of the rotation period; or in other words, the RV frequency it not an integer multiple of the rotation frequency.

The question arises whether this signal can origin from a companion. If so, this would be with very high probability a planetary-mass body. Assuming a circular orbit, the minimum mass of this companion would be $0.435 \pm 0.020\ M_{\rm Jup}$ when using the stellar mass of $2.20 \pm 0.07\ M_\odot$ from Kochukhov & Bagnulo (2006). The orbital separation would amount to $0.273 \pm 0.003$ AU.

**Table 6.34:** Parameters of a sine fit to the RV data of HD 188041.

| Parameter | | HARPS CCF | HARPS-TERRA |
|---|---|---|---|
| $P$ | (days) | $35.170 \pm 0.015$ | $224.42 \pm 0.22$ |
| $K$ | (m s$^{-1}$) | $15.95 \pm 0.66$ | $22.56 \pm 0.40$ |
| $T_0$ | (BJD $-$ 2 400 000) | $54\,308.392 \pm 0.158$ | $53\,977.89 \pm 0.58$ |
| $\gamma, RV_0$ | (m s$^{-1}$) | $-21\,766.22 \pm 0.40$ | $-0.36 \pm 0.28$ |
| $N_{\rm obs}$ | | 39 | 39 |
| $\sigma_{\rm O-C}$ | (m s$^{-1}$) | 2.28 | 1.57 |
| $\chi^2_{\rm red}$ | | 2.57 | 0.76 |

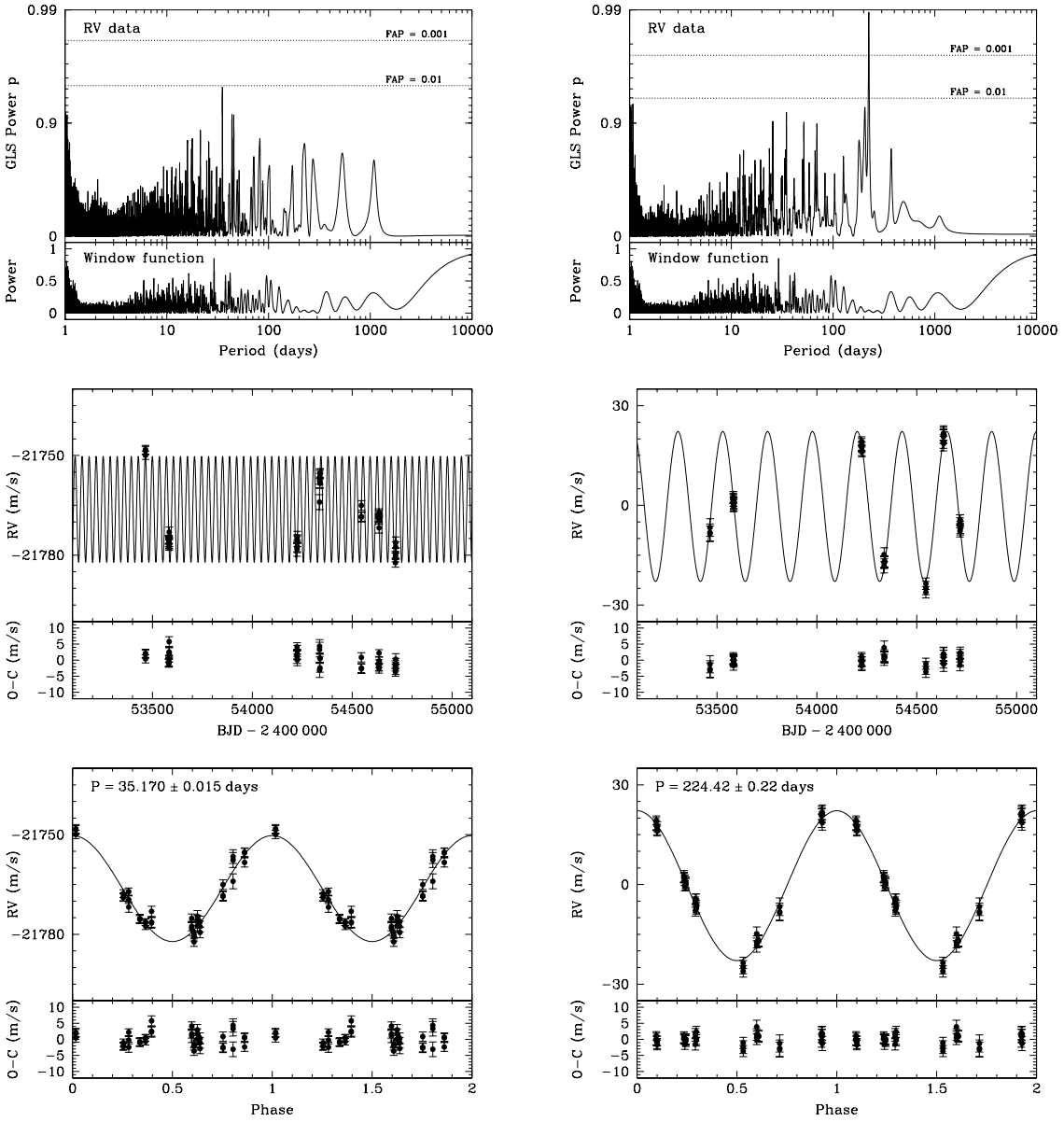


**Figure 6.41:** Results for HD 188041 analyzing the RV data obtained with the HARPS CCF technique (*left panels*) and the HARPS-TERRA software tool (*right panels*), respectively. *Top panels*: GLS periodograms of the RV data. The dotted lines indicate two levels of the FAP. The lower parts display the window function of the observations. *Middle panels*: RV measurements and best-fitting sine function (solid line). The RV residuals after subtracting the sine fit are shown below. *Bottom panels*: RV measurements phased to the given period. Phase zero corresponds to the time of maximum RV. The solid line represents the sine fit. Data points are repeated for the second cycle. Again, the RV residuals are shown below.

### 6.2.4 Concluding remarks

Surprisingly, no extrasolar planet could be detected within the Ap-star sample, despite the fact that theories predicted a high planet frequency around stars of that mass regime.

Nevertheless, monitoring these kind of stars was very fruitful because it turned out that many of these are part of a binary system. In total, I have discovered 17 spectroscopic binaries, which yields a fraction of 27%. Compared to solar-like and slightly higher-mass stars (F stars), this fraction is about 70% higher. But the high binarity rate is not unusual for these stars. Carrier et al. (2002), for example, carried out a spectroscopic survey of cool magnetic Ap stars at the Observatoire de Haute-Provence. They found 34 binaries among the 113 stars of their sample that were qualified for a statistical analysis, yielding a rate of 30%. This is identical to what I find in my survey. Additionally, Carrier et al. (2002) also took into account their detection biases. Applying a simulation, they estimated their detection rate to be 69%, which translates into a corrected binary fraction of about 43%.

When looking into the binarity of Ap stars in more detail, it becomes even more interesting. Half of my program stars consists of roAp stars, the other half of noAp stars. Inspecting the multiplicity of both parts separately, there are huge differences. On the one hand, I could find 14 binaries (45%) among the noAp stars, but on the other hand, I could only track down three (10%) binaries among the roAp stars. According to a study by Hubrig et al. (2000), there is indeed no roAp star known being a member of a binary system, while binarity seems to be quite common for noAp stars. However, the three brightest roAp stars $\alpha$ Cir (HD 128898), $\beta$ CrB (HD 137909) and $\gamma$ Equ (HD 201601) do have optical – and maybe also physical – stellar companions. But these are in wide orbits, and only the orbit of $\beta$ CrB is spectroscopically constrained (Neubauer 1944; Oetken & Orwert 1984).

The discrepancy of binarity between noAp and roAp stars is not well understood. Hubrig et al. (2000) suggested that pulsations might be repressed or reduced due to tidal interactions. To prove this hypothesis, it is either necessary to show that all noAp stars are close binaries or that all roAp stars are single stars or wide visual binaries, as pointed out by Schöller et al. (2012). Within this doctoral work, however, I could find three binaries around roAp stars, one of them (HD 42659) being the first confirmed spectroscopic binary of this class of stars in a relatively tight orbit (Hartmann & Hatzes 2015). This discovery contradicts the above hypothesis and demonstrates that the absence of a binary companion is not a necessary condition for an Ap star to show rapid oscillations. In other words, tidal interactions in binaries do not necessarily inhibit pulsations in Ap stars.

Beside the RV variations due to binaries, almost all other Ap stars show also large RV variations that can be most likely associated with the rotation period of the star and its harmonics. The amplitudes of these variations are of the order of several hundreds of $\mathrm{m\,s^{-1}}$, hence comparable to or larger than the signals of massive planetary companions. This emphasises the difficulty to detect additional planetary signatures with the sparse sampling of my HARPS RV data. But the

highly oversubscribed observing time at ESO prevented me to get a better time sampling. To find any planet around such stars would require a very high number of RV measurements with a dense time coverage to model first the signals of the rotation period and its harmonics and to search then for further planetary signals.

As demonstrated in section 6.2.3, the two methods to calculate the RVs do not always give the same or similar results in the sense that the RV periods and/or amplitudes are different. This arises from the fact that each of these methods is differently sensitive to the spectral lines of various chemical elements originating at different heights of the stellar atmosphere. The provided binary mask for the HARPS CCF method mainly consists of Fe lines, whereas the HARPS-TERRA tool is most sensitive to the strongest lines of the particular star (e.g., Cr, Sr, Eu), which predominantly occur in so-called abundance spots that are connected to the stellar magnetic field, especially to the magnetic poles. In summary, the examples of section 6.2.3 can be divided into three categories:

(i) $P_{\mathrm{RV_{CCF}}} = P_{\mathrm{rot}} = P_{\mathrm{RV_{TERRA}}}$

The stellar spin and magnetic field axes are probably in such a configuration that – with respect to the line of sight – only one magnetic pole, thus one abundance spot, is visible. As a consequence, the RVs are modulated with the stellar rotation period.

(ii) $P_{\mathrm{RV_{CCF}}} = P_{\mathrm{rot}} = 2\,P_{\mathrm{RV_{TERRA}}}$

In this case, the stellar configuration has to be in such a way that both magnetic poles are visible from Earth, each one linked with an abundance spot and seen for about half a rotation cycle.

(iii) $P_{\mathrm{RV_{TERRA}}} = P_{\mathrm{rot}} \neq n\,P_{\mathrm{RV_{CCF}}}, \quad n \in \mathbb{N}$

This speaks again for a situation, where only one magnetic pole, i.e., one abundance spot, is facing the observer on Earth. The fact that a period different from the rotation period and its harmonics is present in the HARPS CCF data might provide evidence that the origin of this signature could come from a companion.

A physical companion should induce the same RV variations, no matter what spectral lines were used for the RV calculation with which method. This is the case for the spectroscopic binaries, except for the SB2 systems, for which HARPS-TERRA cannot determine proper RVs. But these RV signals have huge amplitudes; it might not hold if the dominant signature comes from rotational modulation and a low-amplitude planetary signal is also hidden in the RV data.

HD 188041 might be such an example. If a companion is the cause of the 35-day RV variations seen in the HARPS CCF data, then this signal should be also seen in the HARPS-TERRA data. There is indeed a peak in the periodogram at this period (see upper right panel of Fig 6.41), but with an FAP below 1%. It might well be that we have a case, where both a signal from rotation and from a companion is

present in the data. This is a promising target for further monitoring. Should it really have a companion, the application of these two RV methods would provide a new tool for Ap stars to distinguish between signals arising from rotation or planetary companions.

# 7 Outlook

In the future, I will continue monitoring the F stars from this survey that show an interesting RV behavior to gather more RV measurements to confirm or refute additional planets. Dr. Michaela Döllinger and I have initiated a joint project within the DFG Priority Programme 1992 *"Exploring the Diversity of Extrasolar Planets"* to investigate the planet occurrence rates of a combined sample of intermediate-mass stars with a similar mass distribution (F stars and K giants) in more detail and to understand their differences.

We assume that there is a number of false positives among the published planets around K giants. First, our long-term RV data for some giants with large radii reveal hints for a new phenomenon shown by amplitude variations, which can mimic a planet signal over several years. About 30% of the K giants, for which a planet is published, have radii larger than 20 $R_{\odot}$. It would significantly decrease the planet frequency if all of these planets turned out to be false positives. But how the RV variability depends on the stellar radius and if there is a critical radius where things start getting interesting needs to be examined. Second, the rotation periods are comparable to the orbital periods of most known planets around giant stars, and having a critical look at those stars is thus important to distinguish between reflex motion or stellar phenomena as the origin of the RV variations.

Furthermore, we are going to explore if the known planet–metallicity relation for solar-like stars is also valid for F stars and K giants. So far, we have no knowledge whether this relation applies also for MS stars more massive than the Sun. On top of that, the results for evolved stars are inconclusive. Subgiants show a weaker relation, whereas a relation is only seen for giants above 1.5 $M_{\odot}$ but not for giants below that threshold. Therefore, I will carry out a homogeneous spectral analysis to determine the stellar parameters and chemical abundances for my F-star sample.

In a next step, we will also develope stringent criteria to classify the published exoplanets into secure planets and some categories of less convincing planet candidates. This roadmap will reveal a catalog of robust planet detections around giant stars, leading to reliable input data for theoretical investigations.

# Bibliography

Abt, H. A. 1970, ApJS, 19, 387

Abt, H. A. 1985, ApJS, 59, 95

Abt, H. A. & Snowden, M. S. 1973, ApJS, 25, 137

Adams, W. S., Joy, A. H., Sanford, R. F., & Stromberg, G. 1929, ApJ, 70

Alentiev, D., Kochukhov, O., Ryabchikova, T., et al. 2012, MNRAS, 421, L82

Anderson, K. S. & Kraft, R. P. 1972, ApJ, 172, 631

Anglada-Escudé, G. & Butler, R. P. 2012, ApJS, 200, 15

Appenzeller, I. 1967, PASP, 79, 102

Arzoumanian, Z., Joshi, K., Rasio, F. A., & Thorsett, S. E. 1996, in Astronomical Society of the Pacific Conference Series, Vol. 105, IAU Colloq. 160: Pulsars: Problems and Progress, ed. S. Johnston, M. A. Walker, & M. Bailes, 525–530

Babcock, H. W. 1958, ApJS, 3, 141

Bagnulo, S., Landi Degl'Innocenti, E., Landolfi, M., & Leroy, J. L. 1995, A&A, 295, 459

Balachandran, S. 1990, ApJ, 354, 310

Balega, I. I., Balega, Y. Y., Hofmann, K.-H., et al. 2002, A&A, 385, 87

Barning, F. J. M. 1963, Bull. Astron. Inst. Netherlands, 17, 22

Barry, D. C. 1970, ApJS, 19, 281

Beavers, W. I. & Eitter, J. J. 1986, ApJS, 62, 147

Beavers, W. I. & Eitter, J. J. 1988, in BAAS, Vol. 20, Bulletin of the American Astronomical Society, 737

Boesgaard, A. M. & Friel, E. D. 1990, ApJ, 351, 467

Boesgaard, A. M. & Tripicco, M. J. 1986, ApJ, 303, 724

Bonfils, X., Forveille, T., Delfosse, X., et al. 2005, A&A, 443, L15

Bonsack, W. K. 1976, ApJ, 209, 160

Borgniet, S., Boisse, I., Lagrange, A.-M., et al. 2014, A&A, 561, A65

Borgniet, S., Lagrange, A.-M., Meunier, N., & Galland, F. 2017, A&A, 599, A57

Bowler, B. P., Johnson, J. A., Marcy, G. W., et al. 2010, ApJ, 709, 396

Butler, R. P., Johnson, J. A., Marcy, G. W., et al. 2006, PASP, 118, 1685

Bychkov, V. D., Bychkova, L. V., & Madej, J. 2005, A&A, 430, 1143

Carrier, F., North, P., Udry, S., & Babel, J. 2002, A&A, 394, 151

Cenarro, A. J., Peletier, R. F., Sánchez-Blázquez, P., et al. 2007, MNRAS, 374, 664

Cowley, A. & Fraquelli, D. 1974, PASP, 86, 70

Cumming, A., Marcy, G. W., & Butler, R. P. 1999, ApJ, 526, 890

da Silva, L., Girardi, L., Pasquini, L., et al. 2006, A&A, 458, 609

Döllinger, M. P., Hatzes, A. P., Pasquini, L., et al. 2007, A&A, 472, 649

Döllinger, M. P., Hatzes, A. P., Pasquini, L., et al. 2009a, A&A, 499, 935

Döllinger, M. P., Hatzes, A. P., Pasquini, L., Guenther, E. W., & Hartmann, M. 2009b, A&A, 505, 1311

Dommanget, J. & Nys, O. 2002, VizieR Online Data Catalog, 1274, 0

Ducati, J. R. 2002, VizieR Online Data Catalog, 2237

Duquennoy, A. & Mayor, M. 1991, A&A, 248, 485

Dworetsky, M. M. 1982, The Observatory, 102, 138

Edwards, T. W. 1976, AJ, 81, 245

Elkin, V. G., Riley, J. D., Cunha, M. S., Kurtz, D. W., & Mathys, G. 2005, MNRAS, 358, 665

Endl, M., Kürster, M., Els, S., et al. 2002, A&A, 392, 671

Endl, M., Cochran, W. D., Kürster, M., et al. 2006, ApJ, 649, 436

ESA, ed. 1997, ESA Special Publication, Vol. 1200, The HIPPARCOS and TYCHO catalogues. Astrometric and photometric star catalogues derived from the ESA HIPPARCOS Space Astrometry Mission

Esposito, M. 2009, PhD thesis, Friedrich-Schiller-Universität Jena

Fabricius, C. & Makarov, V. V. 2000, A&A, 356, 141

Finsen, W. S. 1968, Republic Observatory Johannesburg Circular, 127, 170

Fischer, D. A. & Valenti, J. 2005, ApJ, 622, 1102

Frink, S., Quirrenbach, A., Fischer, D., Röser, S., & Schilbach, E. 2001, PASP, 113, 173

Frink, S., Mitchell, D. S., Quirrenbach, A., et al. 2002, ApJ, 576, 478

Fuhrmann, K. 2008, MNRAS, 384, 173

Gaia Collaboration. 2018, VizieR Online Data Catalog, 1345

Gaia Collaboration, Brown, A. G. A., Vallenari, A., et al. 2016, A&A, 595, A2

Galland, F., Lagrange, A.-M., Udry, S., et al. 2005a, A&A, 443, 337

Galland, F., Lagrange, A.-M., Udry, S., et al. 2005b, A&A, 444, L21

Galland, F., Lagrange, A.-M., Udry, S., et al. 2006, A&A, 452, 709

Gettel, S., Wolszczan, A., Niedzielski, A., et al. 2012a, ApJ, 745, 28

Gettel, S., Wolszczan, A., Niedzielski, A., et al. 2012b, ApJ, 756, 53

Girardi, L., Bressan, A., Bertelli, G., & Chiosi, C. 2000, A&AS, 141, 371

Goldin, A. & Makarov, V. V. 2007, ApJS, 173, 137

Gratton, R. G., Carretta, E., & Castelli, F. 1996, A&A, 314, 191

Gray, R. O., Napier, M. G., & Winkler, L. I. 2001, AJ, 121, 2148

Gray, R. O., Corbally, C. J., Garrison, R. F., McFadden, M. T., & Robinson, P. E. 2003, AJ, 126, 2048

Griffin, R. F. 2007, The Observatory, 127, 113

Griffin, R. F. 2010, The Observatory, 130, 17

Griffin, R. F. 2011, The Observatory, 131, 294

Griffin, R. F. 2014, The Observatory, 134, 245

Griffin, R. F. & Suchkov, A. A. 2003, ApJS, 147, 103

Griffin, R. F., Mayor, M., Udry, S., & Tomkin, J. 1999, The Observatory, 119, 213

Guenther, E. W., Hartmann, M., Esposito, M., et al. 2009, A&A, 507, 1659

Halbwachs, J.-L., Mayor, M., & Udry, S. 2012, MNRAS, 422, 14

Han, I., Lee, B. C., Kim, K. M., et al. 2010, A&A, 509, A24

Harlan, E. A. 1969, AJ, 74, 916

Harlan, E. A. & Taylor, D. C. 1970, AJ, 75, 165

Hartmann, M. & Hatzes, A. P. 2015, A&A, 582, A84

Hartmann, M., Guenther, E. W., & Hatzes, A. P. 2010, ApJ, 717, 348

Hatzes, A. P., Guenther, E. W., Endl, M., et al. 2005, A&A, 437, 743

Hatzes, A. P., Cochran, W. D., Endl, M., et al. 2006, A&A, 457, 335

Hensberge, H. 1993, in Astronomical Society of the Pacific Conference Series, Vol. 44, IAU Colloq. 138: Peculiar versus Normal Phenomena in A-type and Related Stars, ed. M. M. Dworetsky, F. Castelli, & R. Faraggiana, 547

Hockey, M. S. 1969, MNRAS, 142, 543

Høg, E., Fabricius, C., Makarov, V. V., et al. 2000, A&A, 355, L27

Holmberg, J., Nordström, B., & Andersen, J. 2007, A&A, 475, 519

Houk, N. & Swift, C. 1999, in Michigan Spectral Survey, Ann Arbor, Dep. Astron., Univ. Michigan, Vol. 5, p. 0 (1999), Vol. 5, 0

Hubrig, S., Kharchenko, N., Mathys, G., & North, P. 2000, A&A, 355, 1031

Ida, S. & Lin, D. N. C. 2005, ApJ, 626, 1045

Jefferys, W. H., Fitzpatrick, M. J., & McArthur, B. E. 1988, Celestial Mechanics, 41, 39

Johnson, J. A., Butler, R. P., Marcy, G. W., et al. 2007, ApJ, 670, 833

Johnson, J. A., Howard, A. W., Bowler, B. P., et al. 2010a, PASP, 122, 701

Johnson, J. A., Aller, K. M., Howard, A. W., & Crepp, J. R. 2010b, PASP, 122, 905

Joner, M. D., Taylor, B. J., Laney, C. D., & van Wyk, F. 2006, AJ, 132, 111

Jones, M. I., Jenkins, J. S., Rojo, P., & Melo, C. H. F. 2011, A&A, 536, A71

Jones, M. I., Jenkins, J. S., Rojo, P., Melo, C. H. F., & Bluhm, P. 2013, A&A, 556, A78

Jones, M. I., Jenkins, J. S., Bluhm, P., Rojo, P., & Melo, C. H. F. 2014, A&A, 566, A113

Jones, M. I., Jenkins, J. S., Rojo, P., Melo, C. H. F., & Bluhm, P. 2015a, A&A, 573, A3

Jones, M. I., Jenkins, J. S., Rojo, P., Olivares, F., & Melo, C. H. F. 2015b, A&A, 580, A14

Kane, S. R., Barclay, T., Hartmann, M., et al. 2015, ApJ, 815, 32

Kennedy, G. M. & Kenyon, S. J. 2008, ApJ, 673, 502

Kochukhov, O. & Bagnulo, S. 2006, A&A, 450, 763

Konacki, M. & Wolszczan, A. 2003, ApJ, 591, L147

Kornet, K., Wolf, S., & Różyczka, M. 2006, A&A, 458, 661

Korzennik, S. G., Brown, T. M., Fischer, D. A., Nisenson, P., & Noyes, R. W. 2000, ApJ, 533, L147

Kürster, M., Schmitt, J. H. M. M., Cutispoto, G., & Dennerl, K. 1997, A&A, 320, 831

Kurtz, D. W. 1982, MNRAS, 200, 807

Kurtz, D. W., Cameron, C., Cunha, M. S., et al. 2005, MNRAS, 358, 651

Kurtz, D. W., Elkin, V. G., Cunha, M. S., et al. 2006, MNRAS, 372, 286

Lee, B.-C., Han, I., Park, M.-G., Mkrtichian, D. E., & Kim, K.-M. 2012a, A&A, 546, A5

Lee, B.-C., Mkrtichian, D. E., Han, I., Park, M.-G., & Kim, K.-M. 2012b, A&A, 548, A118

Lee, B.-C., Han, I., & Park, M.-G. 2013, A&A, 549, A2

Lomb, N. R. 1976, Ap&SS, 39, 447

Lovis, C. & Mayor, M. 2007, A&A, 472, 657

Lu, P. K., Demarque, P., van Altena, W., McAlister, H., & Hartkopf, W. 1987, AJ, 94, 1318

Marcy, G. W. & Butler, R. P. 1992, PASP, 104, 270

Martinez, P. & Kurtz, D. W. 1991, Information Bulletin on Variable Stars, 3611

Martinez, P. & Kurtz, D. W. 1994a, MNRAS, 271, 118

Martinez, P. & Kurtz, D. W. 1994b, MNRAS, 271, 129

Martinez, P., Kurtz, D. W., & Meintjes, P. J. 1993, MNRAS, 260, 9

Mason, B. D., Hartkopf, W. I., Wycoff, G. L., et al. 2001, AJ, 122, 1586

Mathys, G. & Hubrig, S. 1997, A&AS, 124, 475

Mayor, M., Pepe, F., Queloz, D., et al. 2003, The Messenger, 114, 20

McAlister, H. A., Hartkopf, W. I., & Mason, B. D. 1992, AJ, 104, 1961

Mitchell, D. S., Reffert, S., Trifonov, T., Quirrenbach, A., & Fischer, D. A. 2013, A&A, 555, A87

Morbey, C. L. & Brosterhus, E. B. 1974, PASP, 86, 455

Muterspaugh, M. W., Lane, B. F., Kulkarni, S. R., et al. 2010, AJ, 140, 1657

Nelson, M. J. & Kreidl, T. J. 1993, AJ, 105, 1903

Neubauer, F. J. 1944, ApJ, 99, 134

Niedzielski, A., Konacki, M., Wolszczan, A., et al. 2007, ApJ, 669, 1354

Niedzielski, A., Goździewski, K., Wolszczan, A., et al. 2009a, ApJ, 693, 276

Niedzielski, A., Nowak, G., Adamów, M., & Wolszczan, A. 2009b, ApJ, 707, 768

Nordström, B., Stefanik, R. P., Latham, D. W., & Andersen, J. 1997, A&AS, 126, 21

Nordström, B., Mayor, M., Andersen, J., et al. 2004, A&A, 418, 989

Oetken, L. & Orwert, R. 1984, Astronomische Nachrichten, 305, 317

Oja, T. 1987, A&AS, 71, 561

Oja, T. 1991, A&AS, 89, 415

Pannunzio, R. & Delgrosso, A. 1980, A&AS, 39, 423

Pepe, F., Mayor, M., Galland, F., et al. 2002, A&A, 388, 632

Plaskett, J. S., Harper, W. E., Young, R. K., & Plaskett, H. H. 1921, Publications of the Dominion Astrophysical Observatory Victoria, 2

Queloz, D. 1995, in IAU Symposium, Vol. 167, New Developments in Array Technology and Applications, ed. A. G. D. Philip, K. Janes, & A. R. Upgren, 221

Rakos, K. D., Albrecht, R., Jenkner, H., et al. 1982, A&AS, 47, 221

Reffert, S., Quirrenbach, A., Mitchell, D. S., et al. 2006, ApJ, 652, 661

Reffert, S., Bergmann, C., Quirrenbach, A., Trifonov, T., & Künstler, A. 2015, A&A, 574, A116

Reiners, A., Ribas, I., Zechmeister, M., et al. 2018, A&A, 609, L5

Renson, P. & Manfroid, J. 2009, A&A, 498, 961

Santos, N. C., Israelian, G., & Mayor, M. 2004, A&A, 415, 1153

Sarkis, P., Henning, T., Kürster, M., et al. 2018, AJ, 155, 257

Sato, B., Ando, H., Kambe, E., et al. 2003, ApJ, 597, L157

Sato, B., Izumiura, H., Toyota, E., et al. 2007, ApJ, 661, 527

Sato, B., Izumiura, H., Toyota, E., et al. 2008a, PASJ, 60, 539

Sato, B., Toyota, E., Omiya, M., et al. 2008b, PASJ, 60, 1317

Sato, B., Omiya, M., Liu, Y., et al. 2010, PASJ, 62, 1063

Sato, B., Omiya, M., Harakawa, H., et al. 2012, PASJ, 64, 135

Scargle, J. D. 1982, ApJ, 263, 835

Schneider, J., Dedieu, C., Le Sidaner, P., Savalle, R., & Zolotukhin, I. 2011, A&A, 532, A79

Schöller, M., Correia, S., Hubrig, S., & Kurtz, D. W. 2012, A&A, 545, A38

Setiawan, J., Pasquini, L., da Silva, L., von der Lühe, O., & Hatzes, A. 2003, A&A, 397, 1151

Setiawan, J., Rodmann, J., da Silva, L., et al. 2005, A&A, 437, L31

Shatsky, N. 2001, A&A, 380, 238

Sigurdsson, S., Richer, H. B., Hansen, B. M., Stairs, I. H., & Thorsett, S. E. 2003, Science, 301, 193

Smalley, B., Niemczura, E., Murphy, S. J., et al. 2015, MNRAS, 452, 3334

Starikova, G. A. 1981, Soviet Astronomy Letters, 7, 235

Takeda, G., Ford, E. B., Sills, A., et al. 2007, ApJS, 168, 297

Thorsett, S. E., Arzoumanian, Z., Camilo, F., & Lyne, A. G. 1999, ApJ, 523, 763

Trifonov, T., Reffert, S., Tan, X., Lee, M. H., & Quirrenbach, A. 2014, A&A, 568, A64

Tsantaki, M., Sousa, S. G., Santos, N. C., et al. 2014, A&A, 570, A80

Valenti, J. A. & Fischer, D. A. 2005, ApJS, 159, 141

van Dessel, E. L. 1972, A&A, 21, 155

van Leeuwen, F. 2007, A&A, 474, 653

Wade, G. A., North, P., Mathys, G., & Hubrig, S. 1996, A&A, 314, 491

Wade, G. A., Debernardi, Y., Mathys, G., et al. 2000, A&A, 361, 991

Willmarth, D. W., Fekel, F. C., Abt, H. A., & Pourbaix, D. 2016, AJ, 152, 46

Wolszczan, A. 1994, Science, 264, 538

Wolszczan, A. 1997, in Astronomical Society of the Pacific Conference Series, Vol. 119, Planets Beyond the Solar System and the Next Generation of Space Missions, ed. D. Soderblom, 135

Wolszczan, A. & Frail, D. A. 1992, Nature, 355, 145

Wolszczan, A., Doroshenko, O., Konacki, M., et al. 2000, ApJ, 528, 907

Zechmeister, M. & Kürster, M. 2009, A&A, 496, 577

Zickgraf, F.-J., Engels, D., Hagen, H.-J., Reimers, D., & Voges, W. 2003, A&A, 406, 535

# Appendix A: Target lists

**Table A.1:** Sample of the observed F stars and their basic physical parameters. Column 1 lists the star names and column 2 the visual magnitudes derived by Holmberg et al. (2007), except for the visual binaries HD 97855 and HD 216172, for which the magnitudes were taken from Simbad. The spectral types in column 3 were also taken from Simbad as of March 2019. Columns 4–7 provide the effective temperatures, metallicities, masses and ages of the target stars obtained from Holmberg et al. (2007).

| Star | $V$ (mag) | Spectral type | $\log(T_{\rm eff}/{\rm K})$ | [Fe/H] (dex) | $M$ ($M_\odot$) | Age (Gyr) |
|---|---|---|---|---|---|---|
| HD 3268 | 6.410 | F7V | 3.788 | −0.22 | 1.10 | 3.7 |
| HD 3440 | 6.382 | F9V | 3.771 | −0.39 | 0.98 | 8.1 |
| HD 4295 | 6.387 | F3V | 3.813 | −0.23 | 1.25 | 2.4 |
| HD 4568 | 6.515 | F8V | 3.795 | 0.08 | 1.47 | 2.2 |
| HD 6479 | 6.360 | F5V | 3.824 | −0.25 | 1.32 | 2.0 |
| HD 6480 | 7.260 | F5/7(V) | 3.792 | −0.28 | 1.06 | 3.3 |
| HD 8671 | 6.000 | F7V | 3.793 | −0.13 | 1.37 | 2.7 |
| HD 8673 | 6.310 | F7V | 3.800 | −0.01 | 1.28 | 2.5 |
| HD 10874 | 6.320 | F6V | 3.807 | −0.20 | 1.47 | 2.1 |
| HD 11803 | 6.020 | F9V | 3.783 | −0.07 | 1.31 | 2.9 |
| HD 13201 | 6.360 | F5V | 3.806 | −0.21 | 1.23 | 2.7 |
| HD 13555 | 5.231 | F5V | 3.803 | −0.26 | 1.35 | 2.5 |
| HD 15228 | 6.451 | F5V | 3.803 | −0.22 | 1.17 | 2.8 |
| HD 16176 | 5.870 | F5V | 3.797 | −0.05 | 1.61 | 1.8 |
| HD 16220 | 6.230 | F8V | 3.795 | −0.16 | 1.46 | 2.2 |
| HD 16232 | 7.091 | F6V | 3.791 | −0.09 | 1.11 | 1.4 |
| HD 16895 | 4.115 | F8V | 3.794 | −0.12 | 1.15 | 3.1 |
| HD 17948 | 5.579 | F5V | 3.808 | −0.36 | 1.17 | 3.0 |
| HD 20193 | 6.290 | F4Vwv | 3.827 | −0.49 | 1.48 | 1.9 |
| HD 20675 | 5.930 | F6V | 3.811 | 0.06 | 1.52 | 1.8 |
| HD 21794 | 6.340 | F7V | 3.785 | −0.20 | | 2.0 |
| HD 25948 | 6.160 | F5V | 3.815 | 0.05 | 1.48 | 1.8 |
| HD 25998 | 5.470 | F8V | 3.792 | 0.02 | 1.22 | 2.6 |
| HD 26345 | 6.601 | F6V | 3.818 | 0.08 | 1.35 | 0.5 |
| HD 27901 | 5.970 | F4V | 3.832 | 0.08 | 1.59 | 1.3 |
| HD 30652 | 3.183 | F6V | 3.807 | −0.03 | 1.25 | 1.4 |
| HD 30736 | 6.680 | F7V | 3.782 | 0.14 | 1.49 | 2.2 |
| HD 31662 | 6.050 | F4V | 3.820 | 0.19 | 1.46 | 0.8 |
| HD 31675 | 6.191 | F6V: | 3.790 | −0.21 | 1.08 | 3.9 |
| HD 31845 | 6.750 | F5V | 3.813 | 0.10 | 1.25 | 0.3 |
| HD 33185 | 6.674 | F8V | 3.790 | 0.00 | 1.37 | 2.7 |
| HD 33564 | 5.081 | F6 | 3.796 | −0.06 | 1.25 | 3.0 |
| HD 35296 | 4.980 | G1 | 3.784 | −0.15 | 1.06 | 3.6 |
| HD 36066 | 6.400 | F8V | 3.774 | −0.02 | 1.22 | 4.4 |
| HD 40832 | 6.240 | F4V | 3.811 | −0.04 | 1.45 | 2.0 |
| HD 43042 | 5.200 | F5.5IV-V | 3.810 | 0.00 | 1.28 | 1.2 |
| HD 46136A | 6.266 | F7III | 3.781 | −0.09 | 1.43 | 2.3 |
| HD 46136B | 6.913 | F5IV | | | | |
| HD 51530 | 6.203 | F7V | 3.782 | −0.39 | 1.21 | 3.7 |
| HD 55130 | 6.430 | F8V | 3.793 | −0.02 | 1.32 | 2.7 |

**Table A.1:** Continued.

| Star | $V$ (mag) | Spectral type | $\log(T_{\rm eff}/{\rm K})$ | [Fe/H] (dex) | $M$ ($M_\odot$) | Age (Gyr) |
|---|---|---|---|---|---|---|
| HD 57006 | 5.915 | F8IV | 3.790 | 0.02 | 1.66 | 1.7 |
| HD 58855 | 5.360 | F6V | 3.800 | −0.28 | 1.11 | 2.8 |
| HD 63332 | 6.020 | F6V | 3.797 | −0.12 | 1.19 | 3.1 |
| HD 66348 | 6.747 | F8V | 3.789 | 0.01 | 1.21 | 3.1 |
| HD 69897 | 5.140 | F6V | 3.797 | −0.25 | 1.11 | 3.1 |
| HD 71030 | 6.140 | F5IIIm? | 3.811 | −0.18 | 1.37 | 2.3 |
| HD 74243 | 6.330 | F7V | 3.812 | 0.02 | 1.62 | 1.6 |
| HD 75332 | 6.250 | F7Vs | 3.791 | 0.02 | 1.22 | 2.2 |
| HD 76333 | 6.745 | F3V | 3.826 | −0.20 | 1.58 | 1.7 |
| HD 79929 | 6.773 | F6V | 3.817 | −0.31 | 1.29 | 2.3 |
| HD 80654 | 6.669 | F8V | 3.800 | 0.02 | 1.29 | 2.4 |
| HD 82189 | 5.774 | F7V | 3.795 | 0.15 | 1.64 | 1.7 |
| HD 83951 | 6.140 | F3V | 3.830 | −0.09 | 1.56 | 1.7 |
| HD 84183 | 7.011 | F8V | 3.784 | 0.11 | 1.49 | 2.2 |
| HD 87141 | 5.740 | F5V | 3.799 | 0.06 | 1.59 | 1.8 |
| HD 88737 | 6.020 | F9V | 3.782 | 0.10 | 1.55 | 2.1 |
| HD 89744 | 5.760 | F7V | 3.794 | 0.18 | 1.50 | 2.1 |
| HD 89995 | 6.550 | F6V | 3.803 | −0.31 | 1.33 | 2.5 |
| HD 90508 | 6.435 | F9-V | 3.758 | −0.40 | 0.85 | 12.2 |
| HD 90839 | 4.840 | F8V | 3.786 | −0.16 | 1.09 | 2.7 |
| HD 91752 | 6.280 | F3V | 3.809 | −0.30 | 1.31 | 2.5 |
| HD 92196 | 6.604 | F5V | 3.817 | −0.22 | 1.32 | 2.2 |
| HD 95216 | 6.530 | F5V | 3.811 | −0.09 | 1.31 | 2.2 |
| HD 95241 | 6.032 | F9V | 3.769 | −0.23 | 1.35 | 3.4 |
| HD 97855A | 6.489 | F6VgF6mF3 | 3.797 | −0.44 | 1.09 | 3.6 |
| HD 97855B | 7.95 | G0V | | | | |
| HD 99373 | 6.320 | F5.5IV-V | 3.804 | −0.14 | 1.47 | 2.1 |
| HD 99984 | 5.940 | F4V | 3.786 | −0.23 | 1.45 | 2.0 |
| HD 100563 | 5.770 | F5.5V | 3.809 | 0.06 | 1.30 | 0.4 |
| HD 101606 | 5.744 | F5 | 3.795 | −0.55 | 1.24 | 3.4 |
| HD 102870 | 3.600 | F9V | 3.786 | 0.11 | 1.30 | 2.7 |
| HD 102988 | 7.047 | F6V | 3.796 | −0.25 | 1.16 | 3.2 |
| HD 103799 | 6.620 | F6V | 3.790 | −0.34 | 1.12 | 4.6 |
| HD 104904 | 6.275 | F6V | 3.772 | −0.25 | | 1.9 |
| HD 107113 | 6.333 | F4V | 3.804 | −0.52 | 1.09 | 3.3 |
| HD 107213 | 6.362 | F8Va | 3.790 | 0.09 | 1.43 | 2.4 |
| HD 108845 | 6.210 | F7V | 3.786 | −0.05 | 1.38 | 2.7 |
| HD 108954 | 6.210 | F9V | 3.779 | −0.13 | 1.04 | 0.3 |
| HD 111456 | 5.850 | F6V | 3.796 | −0.19 | 1.13 | 2.8 |
| HD 113022 | 6.200 | F6Vs | 3.814 | 0.15 | 1.45 | 1.5 |
| HD 113337 | 6.000 | F6V | 3.818 | 0.06 | 1.40 | 1.5 |
| HD 114710 | 4.260 | F9.5V | 3.776 | −0.06 | 1.04 | 2.9 |
| HD 114905 | 6.828 | F7V | 3.796 | −0.21 | 1.34 | 2.6 |
| HD 119124 | 6.320 | F7.7V | 3.784 | −0.21 | 1.04 | 2.6 |
| HD 119288 | 6.162 | F2V | 3.814 | −0.22 | 1.24 | 2.2 |
| HD 120510 | 6.670 | F8V | 3.804 | 0.02 | 1.43 | 2.2 |
| HD 122797 | 6.240 | F4V | 3.819 | −0.19 | 1.55 | 1.8 |
| HD 123033 | 6.959 | F6V | 3.800 | −0.10 | 1.18 | 2.4 |
| HD 123845 | 6.872 | F7V | 3.807 | −0.18 | 1.29 | 2.5 |

**Table A.1:** Continued.

| Star | $V$ (mag) | Spectral type | $\log(T_{\rm eff}/{\rm K})$ | [Fe/H] (dex) | $M$ ($M_\odot$) | Age (Gyr) |
|---|---|---|---|---|---|---|
| HD 126141 | 6.220 | F5V | 3.824 | 0.00 | 1.33 | |
| HD 126660 | 4.060 | F7V | 3.789 | −0.14 | 1.18 | 3.1 |
| HD 128167 | 4.472 | F4VkF2mF1 | 3.825 | −0.36 | 1.22 | 0.9 |
| HD 130173 | 6.882 | F3V | 3.811 | −0.37 | 1.52 | 1.9 |
| HD 130604 | 6.818 | F6V+F6V | 3.807 | −0.09 | 1.34 | 2.3 |
| HD 132254 | 5.620 | F8-V | 3.790 | 0.02 | 1.23 | 2.9 |
| HD 133002 | 5.639 | F9V | 3.735 | −0.45 | 1.43 | |
| HD 134044 | 6.350 | F8V | 3.782 | −0.12 | 1.06 | 4.1 |
| HD 139389 | 6.470 | F5V: | 3.809 | −0.23 | 1.18 | 1.9 |
| HD 139798 | 5.750 | F2V | 3.830 | −0.31 | 1.37 | 1.8 |
| HD 142373 | 4.610 | F8VFe-2Hdel-1 | 3.764 | −0.50 | 1.00 | 8.0 |
| HD 145228 | 7.046 | F0V | 3.837 | −0.19 | 1.57 | 1.6 |
| HD 151044 | 6.460 | F8V | 3.779 | −0.17 | 1.01 | 5.5 |
| HD 151939 | 6.988 | F6V | 3.799 | −0.03 | 1.61 | 1.7 |
| HD 152303 | 5.997 | F4V | 3.810 | −0.21 | 1.27 | 2.4 |
| HD 153376 | 6.900 | F8V | 3.776 | 0.12 | 1.40 | 2.9 |
| HD 153897 | 6.550 | F5V | 3.817 | −0.09 | 1.29 | 1.7 |
| HD 157373 | 6.358 | F4V | 3.807 | −0.47 | 1.18 | 3.0 |
| HD 157466 | 6.880 | F8V | 3.778 | −0.48 | 0.94 | 3.9 |
| HD 159332 | 5.640 | F4V | 3.791 | −0.19 | 1.36 | 2.6 |
| HD 160933 | 6.345 | F9IV-V | 3.762 | −0.33 | 1.13 | 5.3 |
| HD 162826 | 6.460 | F8V | 3.785 | 0.04 | 1.20 | 3.5 |
| HD 165281 | 6.793 | F5V | 3.790 | −0.07 | 1.20 | 3.2 |
| HD 165567 | 6.520 | F7V | 3.796 | −0.02 | 1.37 | 2.5 |
| HD 167588 | 6.560 | F8V | 3.769 | −0.33 | 1.06 | 6.3 |
| HD 168151 | 5.030 | F5V | 3.813 | −0.22 | 1.28 | 2.5 |
| HD 173494 | 6.303 | F6V | 3.817 | −0.03 | 1.38 | 1.8 |
| HD 173667 | 4.190 | F5.5IV-V | 3.799 | −0.15 | 1.39 | 2.4 |
| HD 176051 | 5.218 | F9V+K1V | 3.766 | −0.19 | 0.98 | 8.1 |
| HD 176303 | 5.220 | F8V | 3.786 | 0.04 | | 1.5 |
| HD 179422 | 6.360 | F5V | 3.813 | −0.02 | 1.35 | 1.9 |
| HD 182101 | 6.350 | F6V | 3.799 | −0.31 | 1.14 | 3.4 |
| HD 182807 | 6.190 | F8 | 3.787 | −0.14 | 1.12 | 4.1 |
| HD 184151 | 6.874 | F5V | 3.803 | −0.36 | 1.44 | 2.1 |
| HD 184960 | 5.740 | F7V | 3.795 | −0.22 | 1.13 | 3.5 |
| HD 185395 | 4.490 | F3+V | 3.823 | −0.04 | 1.38 | 1.3 |
| HD 187013 | 5.006 | F5.5IV-V | 3.798 | −0.11 | 1.24 | 3.1 |
| HD 187691 | 5.126 | F8V | 3.784 | 0.10 | 1.23 | 3.1 |
| HD 191195 | 5.850 | F5V | 3.815 | −0.07 | 1.38 | 2.2 |
| HD 192455 | 5.750 | F5V | 3.795 | 0.20 | 1.66 | 1.7 |
| HD 192985 | 5.910 | F5V: | 3.816 | 0.03 | 1.36 | 1.6 |
| HD 194012 | 6.165 | F7V | 3.792 | −0.19 | 1.09 | 2.8 |
| HD 197963 | 5.156 | F8 | 3.789 | −0.06 | 1.42 | 2.4 |
| HD 200790 | 5.960 | F8V | 3.787 | −0.01 | 1.33 | 2.8 |
| HD 201545 | 6.968 | F8V | 3.796 | −0.13 | 1.16 | 3.0 |
| HD 204121 | 6.120 | F5V | 3.807 | 0.00 | 1.46 | 2.0 |
| HD 204277 | 6.728 | F8V | 3.787 | −0.16 | 1.07 | 3.6 |
| HD 205420 | 6.470 | F7V | 3.794 | 0.04 | 1.61 | 1.8 |
| HD 209369 | 5.037 | F5V | 3.799 | −0.26 | 1.55 | 1.9 |

**Table A.1:** Continued.

| Star | $V$ (mag) | Spectral type | $\log(T_{\rm eff}/{\rm K})$ | [Fe/H] (dex) | $M$ ($M_\odot$) | Age (Gyr) |
|---|---|---|---|---|---|---|
| HD 210855 | 5.240 | F8V | 3.791 | 0.08 | 1.58 | 1.9 |
| HD 211976 | 6.180 | F5V | 3.805 | −0.20 | 1.18 | 2.5 |
| HD 212395 | 6.203 | F7IV | 3.784 | −0.25 | 1.09 | 5.5 |
| HD 212754 | 5.760 | F7V | 3.794 | 0.10 | 1.47 | 2.2 |
| HD 215648 | 4.190 | F6V | 3.790 | −0.24 | 1.17 | 3.1 |
| HD 216172A | 6.86 | F4V | 3.812 | −0.02 | 1.61 | 1.7 |
| HD 216172B | 6.97 | F5V | | | | |
| HD 218235 | 6.130 | F6Vs | 3.816 | 0.29 | 1.52 | 1.2 |
| HD 218261 | 6.300 | F6V | 3.784 | −0.02 | 1.13 | 3.5 |
| HD 218470 | 5.701 | F5V | 3.809 | −0.18 | 1.32 | 2.5 |
| HD 219487 | 6.600 | F5V | 3.816 | −0.18 | 1.25 | 1.9 |
| HD 219623 | 5.578 | F8V | 3.783 | −0.09 | 1.07 | 3.8 |
| HD 220117 | 5.770 | F5V | 3.810 | 0.09 | 1.53 | 1.8 |
| HD 220242 | 6.583 | F5V | 3.833 | −0.06 | 1.60 | 1.5 |
| HD 221830 | 6.851 | G2 | 3.757 | −0.45 | 0.85 | 12.6 |
| HD 221970 | 6.350 | F6V | 3.807 | 0.10 | 1.75 | 1.4 |
| HD 222368 | 4.131 | F7V | 3.792 | −0.08 | 1.25 | 3.1 |

**Table A.2:** Sample of the monitored Ap stars and their basic physical parameters. Columns 1 and 2 give the HD and HR numbers or an alternative star name. Columns 3 and 4 provide the visual magnitudes taken from the SIMBAD database and the spectral types from the catalog of Renson & Manfroid (2009). Columns 5 and 6 list the effective temperatures and stellar masses from Kochukhov & Bagnulo (2006), if available. The last column indicates if a star belongs to the roAp stars.

| HD | HR/name | $V$ | Spectral type | $\log(T_{\rm eff}/{\rm K})$ | $M/M_\odot$ | roAp |
|---|---|---|---|---|---|---|
| 965 | | 8.57 | A8 Sr Eu Cr | | | |
| 3980 | 183 | 5.70 | A7 Sr Eu Cr | $3.917 \pm 0.011$ | $1.91 \pm 0.03$ | |
| 6532 | | 8.40 | A3 Sr Cr | | | yes |
| 9289 | | 9.38 | A3 Sr Eu Cr | | | yes |
| 12932 | | 10.17 | A4 Sr Eu | | | yes |
| 19918 | | 9.35 | A5 Sr Eu Cr | | | yes |
| 24712 | 1217 | 6.00 | A9 Sr Eu Cr | $3.857 \pm 0.012$ | $1.55 \pm 0.03$ | yes |
| 42659 | | 6.75 | A3 Sr Cr Eu | $3.900 \pm 0.011$ | $2.10 \pm 0.10$ | yes |
| 46462 | | 7.56 | B9 Si | | | |
| 50169 | | 8.98 | A3 Sr Eu Cr | | | |
| 50304 | | 7.56 | A0 Eu Cr | | | |
| 53116 | | 8.90 | A0 Sr Eu | | | |
| 55719 | 2727 | 5.31 | A3 Sr Cr Eu | $3.960 \pm 0.014$ | $2.49 \pm 0.07$ | |
| 59435 | | 7.94 | A4 Sr Cr Eu | | | |
| 60435 | | 8.89 | A3 Sr Eu | $3.910 \pm 0.011$ | $1.82 \pm 0.12$ | yes |
| 66255 | 3151 | 6.11 | A0 Si | | | |
| 72968 | 3398 | 5.72 | A2 Sr Cr Eu | $3.992 \pm 0.013$ | $2.30 \pm 0.06$ | |
| 74521 | 49 Cnc | 5.66 | A1 Si Eu Cr | $4.033 \pm 0.016$ | $2.92 \pm 0.12$ | |
| 80316 | | 7.77 | A3 Sr Eu | | | yes |
| 81009 | 3724 | 6.53 | A3 Cr Sr Si | $3.900 \pm 0.011$ | $2.04 \pm 0.09$ | |
| 83368 | 3831 | 6.23 | A8 Sr Cr Eu | $3.877 \pm 0.012$ | $1.76 \pm 0.04$ | yes |

**Table A.2:** Continued.

| HD | HR/name | $V$ | Spectral type | $\log(T_{\rm eff}/{\rm K})$ | $M/M_\odot$ | roAp |
|---|---|---|---|---|---|---|
| 84041 | | 9.36 | A5 Sr Eu | | | yes |
| 86181 | | 9.38 | F0 Sr | | | yes |
| 87488 | | 6.96 | B9 Eu Cr | | | |
| 90569 | 4101 | 6.04 | A0 Sr Cr Si | $4.003 \pm 0.013$ | $2.52 \pm 0.09$ | |
| 92106 | | 7.77 | A0 Sr Eu Cr | | | |
| 93507 | | 8.44 | A0 Si Cr | | | |
| 98457 | | 7.94 | A0 Si | | | |
| 101065 | | 8.03 | F3 Ho | $3.810 \pm 0.013$ | $1.53 \pm 0.09$ | yes |
| 111133 | 4854 | 6.34 | A1 Sr Cr Eu | $3.997 \pm 0.013$ | $2.69 \pm 0.16$ | |
| 116114 | | 7.02 | F0 Sr Cr Eu | $3.870 \pm 0.012$ | $1.92 \pm 0.10$ | yes |
| 116458 | 5049 | 5.65 | A0 Eu Cr | $4.012 \pm 0.013$ | $2.93 \pm 0.10$ | |
| 118022 | 78 Vir | 4.94 | A2 Cr Eu Sr | $3.957 \pm 0.014$ | $2.16 \pm 0.05$ | |
| 119027 | | 9.92 | A3 Sr Eu | | | yes |
| 122970 | | 8.29 | F0 Cr Eu Sr | $3.840 \pm 0.013$ | $1.48 \pm 0.07$ | yes |
| 125248 | 5355 | 5.90 | A1 Eu Cr | $3.992 \pm 0.013$ | $2.27 \pm 0.07$ | |
| 126515 | | 7.07 | A2 Cr Sr Eu | $4.007 \pm 0.013$ | $2.32 \pm 0.11$ | |
| 128898 | $\alpha$ Cir | 3.19 | A9 Sr Eu | $3.885 \pm 0.011$ | $1.71 \pm 0.02$ | yes |
| 129750 | | 7.15 | B9 Si | | | |
| 134214 | | 7.46 | F2 Sr Eu Cr | $3.858 \pm 0.012$ | $1.55 \pm 0.04$ | yes |
| 137949 | 33 Lib | 6.69 | F0 Sr Eu Cr | $3.861 \pm 0.012$ | $1.78 \pm 0.06$ | yes |
| 142070 | | 7.97 | A0 Sr Cr Eu | | | |
| 144059 | | 9.02 | A0 Si | | | |
| 144897 | | 8.59 | B8 Eu Cr | | | |
| 150562 | | 9.91 | A5: Eu Si? | | | yes |
| 154708 | | 8.76 | A2 Sr Eu Cr | $3.829 \pm 0.013$ | $1.43 \pm 0.08$ | yes |
| 159376 | 6545 | 6.48 | B9 Si | | | |
| 161459 | | 10.39 | A2 Eu Sr Cr | | | yes |
| 166473 | | 7.92 | A5 Sr Eu Cr | | | yes |
| 170973 | 6958 | 6.41 | A0 Si Cr Sr | | | |
| 185256 | | 9.96 | F0 Sr Eu | | | yes |
| 188041 | 7575 | 5.62 | A6 Sr Cr Eu | $3.926 \pm 0.010$ | $2.20 \pm 0.07$ | |
| 190290 | | 9.94 | A0 Eu Sr | | | yes |
| 193756 | | 9.18 | A9 Sr Cr Eu | | | yes |
| 196470 | | 9.71 | A2 Sr Eu | | | yes |
| 201601 | $\gamma$ Equ | 4.68 | A9 Sr Eu | $3.882 \pm 0.011$ | $1.74 \pm 0.03$ | yes |
| 203932 | | 8.81 | A5 Sr Eu | | | yes |
| 208217 | | 7.19 | A0 Sr Eu Cr | $3.904 \pm 0.011$ | $1.93 \pm 0.10$ | |
| 213637 | | 9.58 | F1 Eu Sr | | | yes |
| 217522 | | 7.52 | A5 Sr Eu Cr | $3.816 \pm 0.013$ | $1.49 \pm 0.06$ | yes |
| 218495 | | 9.38 | A2 Eu Sr | | | yes |
| 221760 | 8949 | 4.71 | A2 Sr Cr Eu | | | |

# Danksagung

Mein Dank gilt zunächst Prof. Dr. Artie Hatzes, der als Direktor der Thüringer Landessternwarte seit dem Jahr 2000 durch seine Kenntnisse und Erfahrungen dafür gesorgt hat, das interessante Forschungsgebiet der extrasolaren Planeten auch in Tautenburg zu etablieren. Als Betreuer meiner Doktorarbeit ließ er mir viele Freiheiten bei der Bearbeitung dieses faszinierenden Themas. Seine erfolgreichen Beobachtungsanträge sorgten für etliche Beobachtungskampagnen in Chile und Texas, die mir die Aufnahme einer Vielzahl spektroskopischer Daten ermöglichten und als Basis dieser Arbeit dienten. Weiterhin möchte ich seine Geduld loben, die er mir in Bezug auf die Fertigstellung dieser Arbeit entgegengebracht hat.

Ein besonderer Dank gebührt meiner langjährigen Kollegin Dr. Michaela Döllinger, die in entscheidenden Momenten, zum Beispiel beim Schreiben der Diskussion, die „Initialzündung“ lieferte und hin und wieder mit moderatem Anschieben half, die Arbeit zu einem Ende zu führen. Auch die Sessions in der Bibliothek haben ihren Beitrag dazu geleistet.

Für die Unterstützung während der zahlreichen und manchmal langen Beobachtungsnächte in Tautenburg – sicherlich einige hundert im Laufe der Jahre – danke ich den Nachtassistenten Uwe Laux, Frank Ludwig und Christian Högner, der auch immer für eine ausreichende Versorgung mit Tee sorgte. In diesem Zusammenhang möchte ich ebenfalls den Werkstätten und Systemadministratoren meinen Dank aussprechen, dass sie sich stets für das Funktionieren der Beobachtungstechnik gekümmert haben. Danken möchte ich auch allen anderen Mitarbeiterinnen und Mitarbeitern der Thüringer Landessternwarte für die gute Zusammenarbeit in angenehmer Arbeitsatmosphäre.

Vor einigen Jahren habe ich einen neuen Sport ausprobiert, bei dem ich vom Stress der Arbeit abschalten und nette neue Leute kennenlernen konnte. Für die schönen Spiele in gemütlicher Runde im Paradies, aber auch die anstrengenden Ligaspieltage danke ich allen Nebenboulern.

Außerdem danke ich allen Musikerinnen und Musikern, die mich während meiner Promotion mit ihren Melodien, Rhythmen und Klängen begleitet und auf vielen Konzerten begeistert haben.

Zum Schluß sei ganz besonders meinen Eltern gedankt, die mich die gesamte Zeit in jeder Hinsicht großartig unterstützt und daher ebenfalls eine Aktie am Gelingen dieser Arbeit haben, die sie nun endlich in ihren Händen halten können.

# Ehrenwörtliche Erklärung

Ich erkläre hiermit ehrenwörtlich, dass ich die vorliegende Arbeit selbständig, ohne unzulässige Hilfe Dritter und ohne Benutzung anderer als der angegebenen Hilfsmittel und Literatur angefertigt habe. Die aus anderen Quellen direkt oder indirekt übernommenen Daten und Konzepte sind unter Angabe der Quelle gekennzeichnet.

Insbesondere habe ich für die Erstellung der vorliegenden Arbeit nicht die entgeltliche Hilfe von Vermittlungs- bzw. Beratungsdiensten (Promotionsberater oder andere Personen) in Anspruch genommen. Niemand hat von mir unmittelbar oder mittelbar geldwerte Leistungen für Arbeiten erhalten, die im Zusammenhang mit dem Inhalt der vorgelegten Dissertation stehen.

Die Arbeit wurde bisher weder im In- noch im Ausland in gleicher oder ähnlicher Form einer anderen Prüfungsbehörde vorgelegt.

Die geltende Promotionsordnung der Physikalisch-Astronomischen Fakultät ist mir bekannt.

Ich versichere ehrenwörtlich, dass ich nach bestem Wissen die reine Wahrheit gesagt und nichts verschwiegen habe.

Tautenburg, den 25.03.2019

Michael Hartmann